राष्ट्रीय रासायनिक प्रयोगशाला
(वैज्ञानिक तथा औद्योगिक अनुसंधान परिषद)
डॉ. होमी भाभा मार्ग पुणे - 411 008. भारत
NATIONAL CHEMICAL LABORATORY
(Council of Scientific & Industrial Research)
Dr. Homi Bhabha Road, Pune - 411 008. India.

Certificate of the Guide

This is to certify that work presented in the thesis entitled " **Hybrid nanomaterials tailored for therapeutics, imaging and sensing applications** " by **Pooja Singh**, submitted for the degree of **Doctor of Philosophy in Biological Sciences** was carried out under our supervision at the Biochemical Sciences Division, National Chemical Laboratory, Pune, 411008, India. All the materials from other sources have been duly acknowledged in the thesis.

Dr. Absar Ahmad
(Research Guide)

Dr. Asmita Prabhune
(Research Co-Guide)

August, 2016
Biochemical Sciences Division
CSIR-National Chemical Laboratory,
Pune-411008

Communication Channels
NCL Level DID : 2590
NCL Board No. : +91-20-25902000
EPABX : +91-20-25893300
+91-20-25893400
FAX
Director's Office : +91-20-25902601
COA's Office : +91-20-25902660
COS&P's Office : +91-20-25902664
WEBSITE
www.ncl-india.org

राष्ट्रीय रासायनिक प्रयोगशाला
(वैज्ञानिक तथा औद्योगिक अनुसंधान परिषद)
डॉ. होमी भाभा मार्ग पुणे - 411 008. भारत
NATIONAL CHEMICAL LABORATORY
(Council of Scientific & Industrial Research)
Dr. Homi Bhabha Road, Pune - 411 008. India.

Certificate

This is to certify that work incorporated in this PhD thesis entitled " **Hybrid nanomaterials tailored for therapeutics, imaging and sensing applications** " submitted by Ms **Pooja Singh** to Academy of Scientific and Innovative Research (AcSIR) in fulfillment of the requirements for the award of the Degree of Doctor of Philosophy, embodies original research work under our supervision/ guidance. We further certify that this work has not been submitted to any other University or Institution in part or full for the award of any degree or diploma. Research material obtained from other sources has been duly acknowledged in the thesis. Any text, illustration, table etc, used in the thesis from other sources have been duly cited and acknowledged.

Pooja Singh	Dr. Asmita Prabhune	Dr. Absar Ahmad
(Student)	(Co-supervisor)	(Supervisor)

Communication Channels
NCL Level DID : 2590
NCL Board No. : +91-20-25902000
EPABX : +91-20-25893300
+91-20-25893400
FAX
Director's Office : +91-20-25902601
COA's Office : +91-20-25902660
COS&P's Office : +91-20-25902664
WEBSITE
www.ncl-india.org

Declaration by the Candidate

I hereby declare that the work incorporated in this thesis entitled "**Hybrid nanomaterials tailored for therapeutics, imaging and sensing applications**". submitted by me for the degree of Doctor of Philosophy to the AcSIR is the record of the work I have carried out at the Biochemical Sciences Division, CSIR-National Chemical Laboratory, Pune, India, under the supervision of Dr. Absar Ahmad and Dr. Asmita Prabhune. The work is original and has not formed the basis of award of any degree or diploma. Such material as has been obtained from other sources has been duly acknowledged in this thesis.

August, 2016

CSIR-National Chemical Laboratory,

Pune-411 008.

Pooja Singh

(Research Student)

Thesis

Thesis Submitted to AcSIR For the Award of

the Degree of

DOCTOR OF PHILOSOPHY

In **Biology**

By

Pooja Singh

10BB13J26042

Under the guidance of

Dr. Absar Ahmad

(Research guide)

Dr. Asmita Prabhune

(Research co-guide)

National Chemical laboratory

Dr. Homi Bhabha Road

Pune 411008

Declaration by the Candidate

I hereby declare that the work incorporated in this thesis entitled "**Hybrid nanomaterials tailored for therapeutics, imaging and sensing applications**". submitted by me for the degree of Doctor of Philosophy to the AcSIR is the record of the work I have carried out at the Biochemical Sciences Division, CSIR-National Chemical Laboratory, Pune, India, under the supervision of Dr. Absar Ahmad and Dr. Asmita Prabhune. The work is original and has not formed the basis of award of any degree or diploma. Such material as has been obtained from other sources has been duly acknowledged in this thesis.

August, 2016

CSIR-National Chemical Laboratory,

Pune-411 008.

Pooja Singh

(Research Student)

ACKNOWLEDGEMENT

Pursuing doctoral research is often thought to be an individual project, however, I now realise is a result of teamwork arising from endless support from many people rather than a one-man-show and I feel absolutely privileged in this regard. My stay at NCL has been quite intellectually demanding, as well as rewarding, apart from being pleasant, mainly due to an endless list of friends and colleagues who helped me in various capacities.

Firstly, I wish to express my gratitude towards my research supervisor Dr. Absar Ahmad and my co-guide Dr. Asmita Prabhune for her continuous support and positive direction to my work. She has always been a cheerful and enthusiastic person. I would also like to thank her for giving me an opportunity to work under her supervision. She always gave me independence to think and has always been positive and supportive about my experiments. A special thanks to her for making the lab environment so friendly and loving. She never let me feel that I am away from home.

I now take this opportunity to thank Dr. Satishchandra Ogale without whose encouragement, directions and technical support i would not have developed an interest in nanotechnology and their applications. He has always been my driving force to achieve more and think out of the box. His invaluable advices and suggestions on experiments, even over coffee meetings were just fantabulous. With his constant mentorship and friendly nature, my PhD work was so easy and fruitful. His views not only on work but work-culture or general life has always been so inspiring. The deep gratitude that I feel for him is beyond the scope of his acknowledgement.

I would also like to thank Dr. Debanjan Guin for his kind help and encouragement and providing a welcoming and pleasant working environment along with constructive criticism and advice throughout my research.

As I mentioned earlier, doctoral research is always a teamwork arising from constant feedback, support and troubleshooting from many people. And a student's colleagues stand out in this matter, with whom one also shares a

personal bond apart from a professional rapport. As my work includes chemistry, physics and biology, the kind of expertise i received from my colleagues was beyond my imagination and a major part of my research takes its current form due to various interactive session with these peers. Though there is endless list of contributors, i would name only a few who had a major impact on my work. And I apologise to anyone who I am unable to mention here, however their help is duly acknowledged. Help extended towards my research by the following collaborators is appreciated; Dr, Suresh for letting me to use DLS and Zetasizer instrument, Dr. Prasad for access to FTIR and Photoluminescence instrument, Dr. Sarkar and Dr. Sanjeev Galande from IISER Pune for Cell culture studies.

I take this opportunity to express my gratitude to Dr. Sourav Pal (Director, NCL), Dr. Vidya Gupta (Head of Biochemical Sciences Division) and Dr. Anil Kumar (Head of Physical and Material chemistry division), for providing the infrastructure and advanced facilities for research and giving me an opportunity to work at CSIR- NCL. I would also like to acknowledge the role of University Grant Commission (UGC), Govt. of India for providing me research fellowship during my PhD study period.

For the PhD degree, we students need to complete a course curriculum that is monitored by Doctoral Advisory Committee. I am thankful to my DAC chairman, Dr. H.V Adikane and members, Dr. Narendra Kadoo, Dr. Dhiman Sarkar for their timely assessment and expert comments that helped in successfully completing my courses and PhD work.

I thank all the journal editors, reviewers of our published articles and the editors, authors who have allowed us to reprint their published material in this thesis.

I deeply acknowledge the help and support from my colleagues and friends from laboratory, Dr. Vivek, Dr Arif, Dr. Harish, Dr. Subas, Dr Dattakumar, Dr. Prasad, Dr. Abhik, Dr. Rohan, Dr. Mandakini, Dhanya, Wahid, Pradeep, Anil, Vishal, Aniruddha, Rounak, Dipti, Meenal, Lily, Shraddha, Umesh, Ketaki, Dr. Kasturi, Dr. Vrushali, Parul, Pushpa, Priti, Mihir, Hrishikesh.

Special thanks to my friend Abhik, Satish B, Wahid and Parul for their tremendous help during the laboratory research work.

I wish to thank my friend out of laboratory in NCL, Ketaki for always being around whenever I needed her. I thank my partner in crime, Jyoti for her unconditional support whenever i needed her, though it was for a shorter period of time. I must acknowledge the great time which i had with my gang of Rishi tau, Somesh Tau, DD, Parth, Uma. I thank my dearest and oldest friend Rini from IISER for her unconditional love and support.

I like to thank my room-mate, Neha, who has always been a caring and understanding one, not just as a room-mate but also as very good friend. Without her I cannot imagine my stay in NCL hostel, I am going to miss all our random talks, evening walks, sunday brunch together, shopping on weekends was so fun and relieving from work.

I wish to thank my loving family, my dad (J R Singh), my mom (Mamta Singh), my loving brother (Ranjit Singh) for their unconditional love, support and comfort. They have always been a pillar of strength and inspiration in my life. I would also like to dedicate my accomplishments to the biggest strength in life, my best friend and loving husband, Gautam Kishore. His patience kept me going through this journey especially during the final stages of my thesis. Hats off to his patience and bearing attitude.

Finally, I thank the almighty God for making my life so special and being me with all the way.

List of Abbreviations

Abbreviations	Name
NPs	Nanoparticles
QD	Quantum dots
CdTe	Cadmium telluride
QY	Quantum yield
PL	Photoluminescence
SL	Sophorolipid
NMR	Nuclear magnetic resonance
MPA	Mercaptopropionic acid
DLS	Dynamic light scattering
TEM	Transmission electron microscopy
UV	Ultraviolet
FE SEM	Field emission scanning electron microscopy
LCMS	Liquid chromatography- Mass spectrometry
FTIR	Fourier Transform Infrared spectroscopy
Zeta	Zeta potential
C. bombicola	Candida bombicola
HR TEM	High resolution transmission electron microscopy
OD	Optical density
TLC	Thin layer chromatography
SEM	Scanning electron microscopy
ChOx	Cholesterol Oxidase
BiOx	Bilirubin Oxidase
GOx	Glucose oxidase
E. coli	Escherichia coli
S. aureus	Staphylococcus aureus
P. aeruginosa	Pseudomonas aeruginosa
EDAX	Energy dispersive X-ray analysis

AFM	Atomic Force microscopy
CLSM	Confocal laser scanning microscopy
Fl	Fluoride
MUA	Mercaptoundecanoic acid
PA	Propionic acid

Table of Contents

tool for glucose sensing

Chapter 4b) A Development of highly efficient, specific and rapid fluorescence based sensor for Cholesterol sensing

Chapter 4c) Sensitive and selective detection of Bilirubin in blood using water soluble

CdTe-quantum dot based bilirubin biosensor

Chapter 5 A Simple Water Soluble Photoluminescence *On-Off-On* Probe for Speedy and Selective Detection of Fluoride Ions even in HF Vapor

Chapter 6 Mercapto-propionic acid Assisted Supramolecular Assembly of Sophorolipids: A Potential Drug Delivery Vehicle

Chapter 1

Introduction and Motivation

This chapter presents a brief introduction about the research work described in the thesis. An introduction is presented about the semiconductor quantum dots (QDs), basic properties like optical, electrical, and diagnostic properties of QDs-nano-composites systems. A detailed review is given on such properties that are explored for biomedical applications This chapter also discusses brief description about nanobiotechnology, self-assembly, biosensors, therapeutic and diagnostic properties of the composite nanoparticles. The introduction eventually provides a roadmap for the direction of research conferred in the thesis.

1.1 Introduction

Nanotechnology is considered as an emerging technology with existing materials. The nanoscience is defined as the study of phenomena and manipulation of materials at atomic, molecular and macromolecular scales, when at least one of the dimension of materials usually in the range below 100 nm. Nanotechnologies deals with design, characterization, production and application of structures, devices and systems by controlling shape and size at the nanometer scale. Semiconductor quantum dots have been extensively studied due to their extraordinary optical and photo-electrical property which is discussed in the following sections.

1.2 Semiconductor Quantum Dots (QDs)

Semiconductor nanocrystals, or quantum dots (QDs), are nanometer- scale crystals in size range of 1–10 nm which has emerged as an important new class of materials over the past decade. Due to their quantum confinement of charge carriers in tiny spaces, QDs show unique and fascinating optical properties such as high quantum yields, high molar extinction coefficients, size-dependent tunable absorption and emission of light in the UV-Vis-NIR regions, broad absorption and narrow emission bands. The size-dependent tunable optical and electronic properties make semiconductor quantum dots one of the most attractive nanomaterials in the optoelectronic, electro-optical and biomedical fields. Silicon-, gallium-, indium- or germanium-based group IV and VI quantum dots, or alloy quantum dots within the members of these groups or among the members of groups III and V are prevalent in our daily life in the form of semiconductor devices. On the other hand, group II–VI colloidal quantum dots such as ZnX, CdX and HgX (X = S/Se/Te), group IV–VI colloidal quantum dots such as PbX, and group III–V colloidal quantum dots such as InP have become prevalent in light emitting devices and the imaging of biomolecules, cells and tissues. Among these colloidal quantum dots, despite the toxic cadmium content, CdTe-based core and core-shell quantum dots are attractive fluorescent probes, high photoluminescence quantum efficiencies, exceptionally high photostability and chemical stability, large surface to volume ratios and flexible surface chemistry. These attractive fluorescence properties prompt a wide interest in developing QD-based sensors for in vivo cellular imaging and in vitro assay detection [1]. QDs are gradually replacing conventional labels

in many biological applications. Due to their spectral characteristics, QDs are excellent labels for multicolor imaging of multiple targets within a cell using a single excitation wavelength.

Imaging of multiple biomarkers in tumor cells and tissues, multiple cell surface proteins, co localization of cell surface receptors, multicolor coding of beads and cells, and multicolor imaging of tumor cells in vivo was realized. Compared to fluorescent dyes, QDs are much brighter, less prone to photo-degradation, QDs have high resistance to photobleaching and retain their luminescence orders of magnitude longer than most chromophores. This allows performing single cell monitoring over extended periods of time. The low photobleaching thresholds are used in QD based imaging of cell motility and chemical procedures. Advances in QD synthesis resulted in nanoparticles emitting in the near-infrared region, a region of the electromagnetic spectrum with low absorbance by living tissue. Imaging of organs or tumors through thick layers of tissue, metastatic potential . Finally, yet importantly, the synthesis of QDs is relatively simple and one can obtain QDs emitting at different wavelengths using similar at greater depths than with traditional dyes, is therefore possible by using near infrared probes have broad absorption spectra and narrow emission lines. These features are extremely useful in multiplexed imaging and for long-term monitoring and detection of targets at low concentrations. Good photophysical parameters allow one, for instance, to visualize single QDs diffusing in cells or interacting with the biochemical machinery of the cell [2].

When QDs are conjugated with bio-molecules such as proteins, peptides and nucleic acids, they become exceptionally attractive fluorescent probes in biological and medical fields such as clinical diagnosis, bioassay and cell imaging. Chan and Bruchez in 1998, first reported that QDs could be used for bioimaging as well as fluorescent probes. They showed that QDs were exceptionally brighter and more stable than traditional organic fluorescent dye, rhodamine 6G. Eventually, these excellent optical properties of QDs gained interest in biological applications.

Lately, QDs have also been used as immuno-histochemical labels in fixed cell imaging, which majorly included the staining of actin and microtubule fibers in the cytoplasm, detection of nuclear antigens inside the nucleus, labeling of the breast cancer marker Her2 on the cell surface. In live cell imaging, Nie's group first reported that QDs labeled with transferrin could enter the cultured HeLa cells by endocytosis and recognized specific antibodies or antigens. Afterwards, some groups demonstrated that QDs were successfully used for targeting or tracking some membrane or transmembrane proteins, such as human and *Drosophila* serotonin transporters

expressed in HeLa and HEK-293 cells, Glycine receptors in neurons, erbB/HER receptor in Chinese hamster ovary cells[3].

1.3 Quantum Confinement in quantum dot

The band gap generally refers to the energy difference between the top of the valence band and the bottom of the conduction band. The pair of an electron and a hole is called exciton and the distance between them is termed as exciton Bohr radius. Semiconductor nanocrystals whose size range is in sub-10 nm are called quantum dots. In this size range, the energy level of quantum dots should be considered as discrete instead of continuous which is called quantum confinement and the small size will not allow the exciton extend to its natural limit. In this situation, the quantum dots act more like atoms. Therefore, they are called "artificial atoms". Since the band gap energy is determined by the size and the materials of the QDs, the QDs' physical properties can be tuned in a controlled way which gives lots of flexibilities to the researchers. The smaller the size of QD is, the larger the spacing between the energy levels is and thus more energy is needed to bring the electron from the valence band to the conduction band.

1.4 Colloidal Stability of Semiconductor QDs

QD surface ligands prevent aggregation of the nanoparticles and control the growth of the nanocrystals during synthesis. In general, the choice of the stabilizing ligand depends on the solvent, size of the QD and its surface chemistry. Molecules binding strongly to the nanocrystal surface form stable ligand layers, which stabilize the QDs in solution. Chemisorption, electrostatic or hydrophobic interactions provide usually strong binding of the ligand to the nanoparticles surface. The most common examples of binding groups are thiols, phosphines, and amines (Figure 1.1). Polar and charged molecules provide good dispersibility of the QDs in aqueous media while nanocrystals with hydrophobic ligands are only soluble in nonpolar organic solvents. In aqueous media, charged carboxylate, or hydroxylate groups stabilize effectively the QDs at specific pH values and concentrations. However, even in a good solvent the passivating ligand dynamically binds and unbinds to and from the QD surface. [16-18]

Due to this dynamic process the ligand molecules can desorb, e.g., by excessive washing or by competition with another molecule which has affinity for QD surface. This might compromise the stability of the nanoparticles in a given solvent and cause aggregation and precipitation.

Some ligands may also desorb due to chemical reactions. For example, irradiation with light can cause photo-oxidation of thiols, what may result in desorption of the ligands followed by aggregation. [19-21]

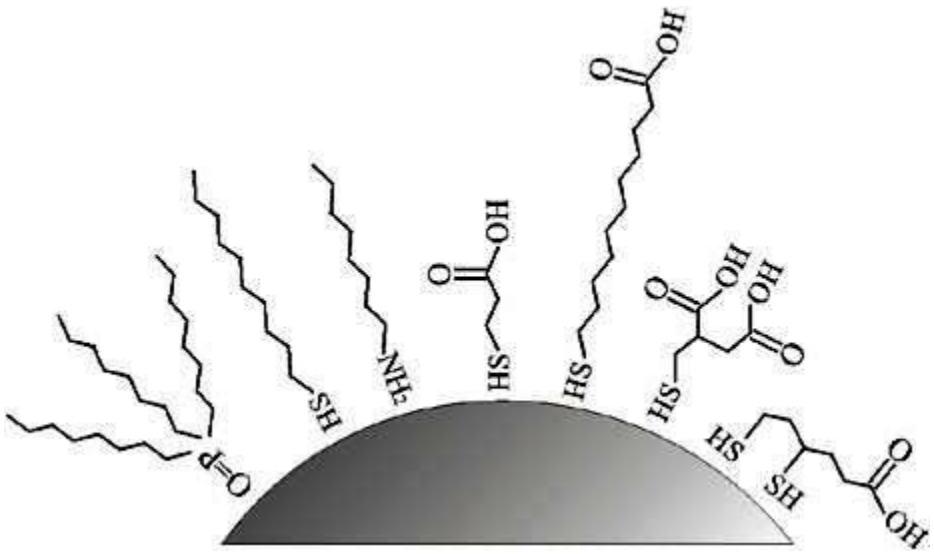

Figure 1.1 *Common hydrophobic and hydrophilic ligands stabilizing QDs. Ligands for nonpolar solvents: trioctylphosphine oxide (TOPO), dodecanethiol (DDT), octylamine (OA); ligands for aqueous solutions: mercaptopropionic acid (MPA), mercaptoundecanoic acid (MUA), mercaptosuccinic acid (MSA), dihydrolipoic acid (DHLA).*

1.5 Optical Properties of QDs

The optical properties of QDs are restricted by the constituent material, particle size and size distribution (dispersity), surface chemistry and specifically the number of dangling bonds favoring nonradiative deactivation. Optical properties of a material are typically determined by electronic transitions within the material and light scattering effects. Owing to Coulomb interaction, the electrons and holes existing in a material are known to form excitons. Therefore, the optical nature of semiconductors can be implicit by determining the properties of the excitons. Some crucial properties of QDs are explained in the subsequent section.

Presence of discrete energy levels in QDs, there is a widening of the energy gap between the highest occupied electronic states and the lowest unoccupied states as compared to the bulk material. As a consequence, the optical properties of the QDs also become size dependent. QDs

have a number of attractive optical properties. For example, monodispersed QDs have narrow size tunable photoluminescence with full width half maximum (FWHM) in the range of 20–40 nm. QDs have broad absorption spectra and narrow and symmetric emission spectra, continuously tuned from 400 nm to 2000 nm by changing both the size and their composition [5].

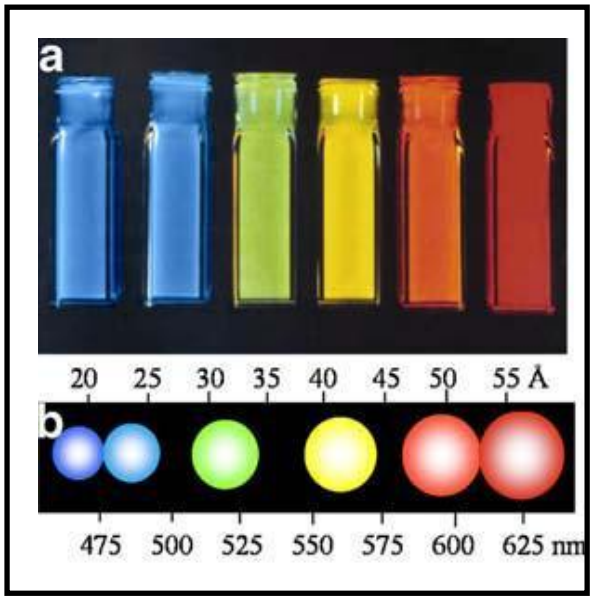

Figure 1.2 *:(a) Size-dependent photoluminescence color and (b) schematic presentation of size, color and photoluminescence wavelength of CdSe-ZnS QDs [5, 6].*

The size dependant photoluminescence colors of quantum dots are distributed throughout the visible region of the electromagnetic spectrum (as shown in above Figure). As the size of the particle decreases the bandgap increases, and the photoluminescence shows a blue shift. It possess high quantum yield (QY) [6]. QD shows higher molar absorption coefficient (10^5-10^6 $M^{-1}cm^{-1}$) compared to organic dyes (10^2-10^3 $M^{-1}cm^{-1}$) [5, 6, 8] hence more useful for fluorescence imaging.

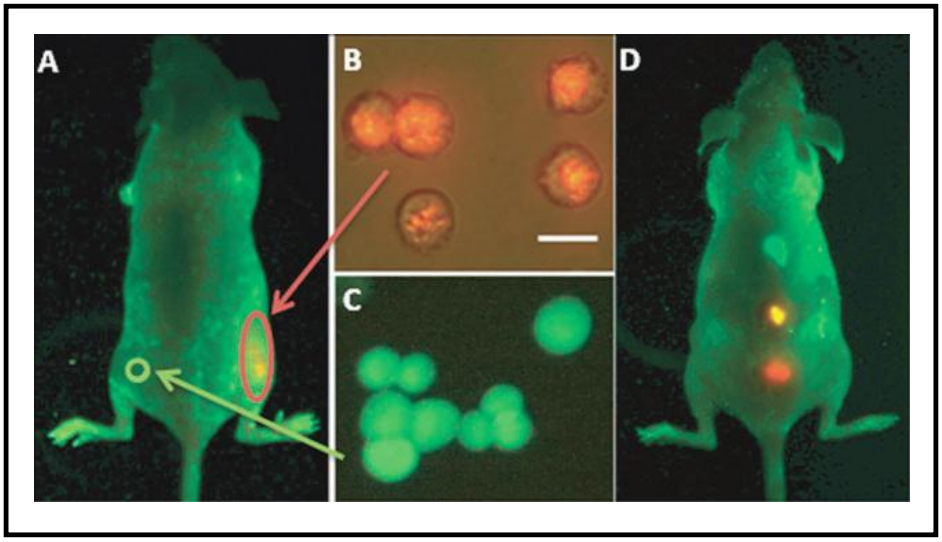

Figure.1.3*: In vivo imaging of implanted QD-tagged tumor cells. (A) Bright QD tags (B) enable visualization of tumor cells through skin with a non-invasive whole-animal fluorescence imaging, whereas organic dye (C) signal is indistinguishable from auto fluorescence. (D) Imaging of subcutaneously implanted QD-loaded micro beads shows the potential for multiplexed in vivo cell detection and tracking [9]*

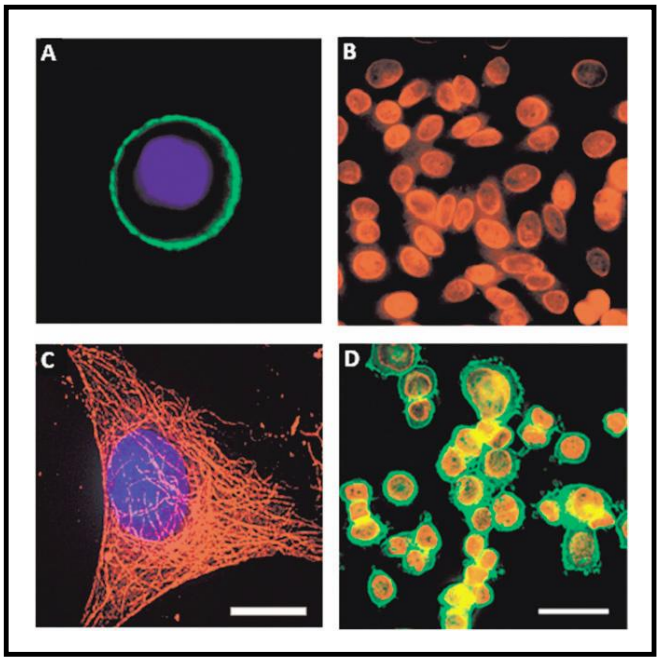

Figure.1.4. *: Fixed cell imaging and simultaneous detection of multiple cellular targets using QD conjugates. In single-color examples membrane-associated Her2 receptors are detected with primary antibodies and QD-labeled secondary IgG (A, green), while intracellular nuclear antigens (B, red) and microtubules (C, red) are visualized with primary IgG/secondary IgG-biotin/ QD-Streptavidin cascade.*

Both labeling routes can be applied simultaneously for a two-color staining (D). The nuclei are counterstained with Hoechst 33 342 (blue) in A and C [7].

In case of immuno labeling vivo fluorescent imaging capability of mice cells has been demonstrated by X. Gao et.al. [4, 6, 9].In vitro vivo fluorescent imaging capability also has been shown in case of fixed cell imaging by Wu et.al. [7]. This functionality has extended for multiplexing capability. Wherein QDs with size distributions are excited with the same wavelength but of light to produce emission of different wavelengths, and thus getting different colors' shown in above figure [7, 10]. Long fluorescence lifetime of the order 10-100 n Sec is achieved in QD systems compared to conventional dyes [11]. Large surface-to-volume ratio allows QDs system superior than organic fluorophores in detection sensitivity as well as in long-term tracking of biological processes [12].

1.6 Quantum yield (QY)

QDs used in biological applications have high photoluminescence emission properties for incident photon intensity. The intensity of the photons that are emitted when QDs are stimulated by external photon field is determined by the percent of absorbed photons that result in emitted photons, is termed as quantum yield (QY). In other words, the QY gives the probability of the excited state being deactivated by fluorescence rather than by another non-radiative transition. QY is generally controlled by the surface properties of the QDs and can often be improved by adding shells to the QD core. For example of coating the CdSe core with a wider band gap semiconductor shell ZnS results in an enhancement of the luminescence by 50-100% [5,13]. The most reliable method for measuring QY is the comparative method developed by Williams et al [15] which involves the use of well characterized standard samples with known QY values. Essentially, solutions of the standard and test samples with identical absorbance at the same excitation wavelength can be assumed to absorb the same number of photons. Hence, a simple ratio of the integrated fluorescence intensities of the two solutions (recorded under identical conditions) will yield the ratio of the QY values. Since QY for the standard sample is known, it is easy to calculate the QY for the test sample. To have the QY measurement more reliable, it is required that the standard and the test samples have similar optimal excitation and emission wavelengths.

Nano-composite, depending upon its enhanced functionality can be used for various biomedical applications however; it should be bio-compatible. Following sections deals with issue related to bio-compatibility.

1.7 Cadmium Telluride Quantum dots Applications in Biomedicines

Biocompatibility is the major concern, when CdTe quantum dot is exploited for biological applications. It is essentially an important aspect to study the cytotoxicity levels of QDs in living systems. For QDs to be useful probes for examination of biological specimens, the surface must be hydrophilic. It also becomes a significant concern to study the size, shape, and surface functional groups on the bioavailability, uptake, sub cellular distribution, metabolism, and degradation of these different QDs based nanocomposites. Since there are various methods for synthesis of QDs and the synthesized QDs are surface functionalized by different ways, each type of QDs must be considered unique and tested for its biocompatibility. A number of strategies have been exploited to stabilize QDs in aqueous medium. Most commonly, thiol(-SH) functionalities used as hydrophilic head are used as capping on the CdTe surface and are reactive to carboxyl (-COOH) functionalities as the hydrophilic ends. Many biological applications of QDs have been achieved by using mercapto-hydro-carbonic acids (SH-,-COOH) to make QDs water soluble [22]

1.8 Motivation of the thesis

It is explained in the previous sections that QDs based nano-composites exhibits excellent optical, electrical, thermal and catalytic properties which are better than that of each individual counterpart to meet different requirements. Quantum dots are an indispensable tool for biological studies. Capped nano-composite system shows excellent bio-compatibility thus useful in biomedical applications. SL properties and

Since detection and analysis of biological agents has become an important frontier in basic life science research, pathology, biosensors technology, clinical diagnosis, drug discovery, and environmental studies - majority of the current techniques in biomolecular detection rely heavily on the phenomenon of fluorescence. Indeed, fluorescence detection is a well established technology which is quite sensitive and is commonly used in biological science research [23]. On

this background we sought to use CdTe quantum dots for therapeutic and diagnostic studies employing various bio-molecules.

1.9 Sophorolipid

Sophorolipid is an amphiphilic biosurfactant which is biologically produced by a number of non-pathogenic yeast species, of which *Candida bombicola* is most intensively studied. They are considered as the most promising bio-surfactant because of their environment friendly nature. In the recent years they have gained attention due to their ability to get utilized in detergent, cosmetics, paint, textile, agriculture, food and pharmaceutical industries. Sophorolipids are preferred over synthetic surfactants because of their stability at wide range of pH, temperatures, less foaming with exemplary detergent properties, excellent surface properties due to their amphiphilic and structural properties. Sophorolipid also exhibit metal reducing and capping potential in one go which brings greater control on the reaction conditions and condenses the steps involved in the synthesis of nanomaterials. Oleic acid, being an interesting choice as a nanoparticles capping agent, is generally used precursor for the synthesis of sophorolipid.

Sophorolipid abbreviated as "SL" is composed of hydrophilic moiety-sophorose, a di-glucose bound to the hydrophobic moiety- a hydroxy fatty acid with a glycosidic bond. The disaccharide moiety may contain acetyl groups at the 6' and/or 6'' positions and the molecule itself may form a lactone through linking the carboxyl group of the hydroxy fatty acid and the 4'' hydroxyl of the sophorose "Fig. 1.5".

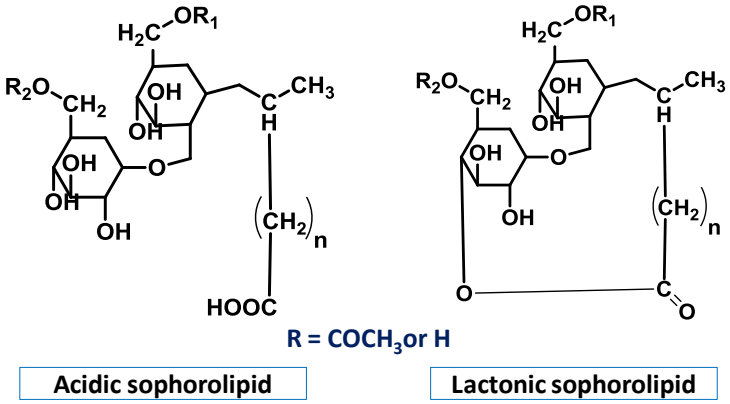

Figure. 1.5 Sophorolipid forms - Lactonic and Acidic produced by Candida bombicola

Crude sophorolipid mixture has both acid and lactonic sophorolipids, the lactonic form is generally considered the major fraction of the product. Lactonic part of the crude sophorolipid is

the critical part for biomedical applications. Lactonic sophorolipids have shown to have excellent antimicrobial activity than the acidic sophorolipid.[25].

We focussed on the conjugation of CdTe to Sophorolipid, a glycolipid molecule obtained from *Candida bombicola* by a cross linking reaction. Sophorolipid has been reported to have various pharmacological properties including antibacterial and anticancerous activity. After being conjugated, CdTe nanoparticle attained enhanced properties of Sophorolipid plus keeping the existing photoluminescence and water solubility property of CdTe intact which is a pre-requisite in order to use it for various biomedical applications. The nano-conjugate was then further exploited for cytotoxic activity and cell imaging studies. **The details are discussed in the Chapter 3.**

1.10 Self-assembly of Sophorolipid biosurfactant

Self assembly is a process where disorganized system of pre-existent components develops into an organized pattern or architecture as a result of the interaction between the components without any external force attributed to the different moieties present in the molecular structure. Self assembly of molecule in water depends on the proportion of hydrophilic and hydrophobic moieties present and the amount of water present in the system.

Sophorolipid being a bio-surfactant has many advantageous properties which makes them qualified for various applications. As an amphiphile, sophorolipid has also been shown to control size and shape of nanomaterial synthesis which is an essential factor of physiochemical properties of metal nanoparticles. They act as both a capping and reducing agent in nanoparticle synthesis. [26].

Sophorolipid belongs to the category of bolaamphiphilic glycolipid biosurfactant. Bolaamphiphiles are the molecules which has polar group at both the ends of a hydrophobe. Bolas has the tendency to form explicit supramolecular structure under mild conditions which has a biological significance due to their strong resemblance to the natural transmembrane lipid. Helical ribbons and fibers, rigid rod, nano-tubes and monolayer vesicles are few of the proclaimed supramolecular structures. [27]

Based on the feature of sophorolipid of forming supramolecular architecture, we studied the molecular assembly of SL in aqueous solution in the presence of one more molecule i.e.

Mercapto-propionic acid. We tried with different ratios of SL and MPA in order to achieve the morphology, best suited for drug delivery application. **Details are discussed in Chapter 6.**

1.11. CdTe quantum dot based Bio-sensors

Fluorescence is a powerful tool for detecting and quantitating biomolecules. Because of their broad absorption spectra, high quantum yield, excellent photostability and resistance to chemical degradation, CdTe QDs are used as an all- round attractive fluorophores for biosensing. [28]. CdTe quantum dots has been extensively used to detect and quantify various organic and inorganic compounds. Generation of H_2O_2 (hydrogen peroxide) by a number of oxidases and sensitivity of CdTe quantum dots to H_2O_2 provide a unique and versatile platform to develop fluorescent QD based sensor. [29]. QDs are explored with different oxidases which biocatalyze the generation of H_2O_2. CdTe QDs bound to any particular oxidase when comes in interaction with their respective substrate generates H_2O_2 thereby reducing or quenching the florescence intensity of QDs. In light of this property, we developed CdTe based **glucose**, **bilirubin** and **cholesterol** sensor for *ex vivo* diagnosis. **The details are discussed in Chapter 4 and Chapter 5.**

Since dental and skeletal fluorosis is a severe health and environmental issue in many countries majorly in two largest countries - India and China which results from the accumulated levels of fluoride in excess of the CDC-recommended safe levels. [30]

Development of an inexpensive, fast and efficient method is an immediate requirement for the detection of fluoride ions due to its harmful side effects. The main challenge involved with the development of fluoride sensor is its high selectivity and sensitivity. There are few existing methods available for fluoride sensing e.g. colorimetric (UV), ion-selective electron method, nuclear magnetic resonance (NMR) spectroscopic analysis, fluorescence sensing. Ion-sensitive electron method is the most extensively used but the major problem associated with this methods is the requirement of trained people, complex instrument and a well-equipped laboratory along with problems such as low specificity and inefficient performance at higher concentrations. In recent years, fluorescence and colorimetric sensing systems are gaining widespread attention over other complex systems due to their high sensitivity, extremely low detection, limit and easy field installation methods. [31].

With this standpoint, we report, the development of an extremely simple, CdTe quantum dot based water soluble photoluminescence probe for speedy and selective detection of fluoride ions not just in water but also detect HF vapors. **The details are discussed in Chapter 6.**

Summary of the thesis and future outlook of the work is present in the **Seventh Chapter**

References:

1. E. Rolf, *'Understanding of Materials Science', 2nd Edition, Springer, June* **2004**.
2. R. Feynman, *Engineering and Science magazine, February* **1960**, XXIII, 5.
3. E. Regis, *Nano: The Emerging Science of Nanotechnology—Remaking the World, Molecule by Molecule, Little Brown and Company, Boston*, **1995**.
4. *http://www.nano.gov*.
5. **(a)** B.Dabbousi, J. RodriguezViejo, F. Mikulec, J.Heine, H. Mattoussi, R.Ober, K. Jensen, M. Bawendi, *J Phys Chem B* **1997**, , 101, 9463, **(b)** S. Rosenthal, *Nat. Biotechnol*, **2001**, 19, 621, **(c)** C. Murphy, *Anal. Chem*. **2002**, 74, 520A, **(d)** W. Parak, *Nanotech*, **2003**, 14, R15, **(e)** C. Niemeyer, Angew. *Chem. Int. Edn Eng*, **2001**, 40, 4128, **(f)** A. Alivisatos, *Nature Biotechnol*, **2004**, 22, 47, **(g)** Miyawaki, *Dev. Cell*, **2003**, 4, 295.
6. **(a)** C. Leatherdale, W.Woo, F. Mikulec, M. Bawendi, *J. Phys. Chem. B*, **2002**, 106, 7619, **(b)** D. Talapin, A. Rogach, A. Kornowski, M. Haase, H. Weller, *Nano Lett*, **2001**, 1, 207.
7. X. Wu, H. Liu, J. Liu, K. Haley, J. Treadway, J. Peter Larson, N. Ge, F. Peale, M.Bruchez, *Nat. Biotechnol*, **2003,** 21, 41
8. D. Norris, *Phys. Rev. B. Condens. Matter*, **1996**, 53, 16338
9. X. Gao, Y. Cui, R. Levenson, L. Chung and S. Nie, *Nat. Biotechnol*, **2004**, 22, 969
10. E.Schrock, *Science*, **1996**, 273, 494.
11. U. Genger, M. Grabolle, S.Jaricot, R. Nitschke, T. Nann, *Nature Methods*, **2008**, 5, 763.
12. Y. Wang, Z. Tang, N. Kotov, *Nanotoday*, **2005**, 8, 20.
13. **(a)** Y. Tian, T. Newton, N. Kotov, D. Guldi, J. Fendler, *J. Phys. Chem*, **1996**, 100, 8927, **(b)** X. Peng, M. Schlamp, A. Kadavanich, A. Alivisatos, *J. Am. Chem. Soc*, **1997**, 119, 7019, **(c)** X.Chen, Y. Lou, A. Samia, C. Burda, Nano Lett, **2003**, 3, 799.
14. D. Battaglia, B. Blackman, X. Peng, *J. Am. Chem. Soc*, **2005**, 127, 10889.
15. A. Williams, S.Winfield, J. Miller, *Analyst*, **1983**, 108, 1067.
16. **(a)** Y. Zheng, S. Gao, J. Ying, *Adv Mater*, **2007**, 19, 376, **(b)** L. Bentolila, Y. Ebenstein, S. Weiss, *J. Nucl. Med*, **2009**, 50, 493, **(c)** I. Medintz, H. Mattoussi, *Phys. Chem. Chem. Phys*, **2009**, 11, 17, **(d)** I. Medintz, H. Mattoussi, A. Clapp, *Int. J. Nanomedicine*, **2008**, 3, 151, **(e)** R. Misra, *Nanomedicine*, **2008**, 3, 271, **(f)** U. Resch-Genger, M. Grabolle, S. Cavaliere-Jaricot, R. Nitschke, T. Nann, *Nat. Methods*, **2008**, 5, 763, **(g)** A. Smith, H. Duan, A.

Mohs, S. Nie, *Adv. Drug Delivery Rev*, **2008**, 60, 1226, **(h)** E. Tholouli, E. Sweeney, E. Barrow, V. Clay, J. Hoyland, R. Byers, *J. Pathol*, **2008**, 216, 275, **(i)** Y. Xing, J. Rao, *Cancer Biomark*, **2008**, 4, 307, **(j)** P. Zrazhevskiy, X. Gao, *Nano Today*, **2009**, 4, 414.

17. **(a)** T. Jamieson, R. Bakhshi, D. Petrova, R. Pocock, M. Imani, A.Seifalian, *Biomaterials* **2007**, 28, 4717, **(b)** F. Patolsky, R. Gill, Y. Weizmann. Mokari, U. Banin U, I. Willner, *J Am Chem Soc* **2003**, 125, 13918, **(c)** C. Zhang, H. Yeh, M. Kuroki, T. Wang, *Nat Mater*, **2005**, 4, 826. **(d)** L. Shi , V. De Paoli, N. Rosenzweig, Z. Rosenzweig, *J Am Chem Soc*, **2006**, 128, 10378.
18. A. Samia, X. Chen, C. Burda, *J. Am. Chem. Soc,* **2003**, 125, 15736.
19. **(a)** U. Boas and P. Heegaard, *Chemical Society Reviews*, **2004**, 33, 43, **(b)** W. Hild, M. Breunig, A. Goepferich A, *Eur J Pharm Biopharm*, **2008**, 68, 153, **(c)** A. Cuenca, H. Jiang, S. Hochwald, M. Delano, W. Cance, S. Grobmyer, *Cancer*, **2006**, 107, 459.
20. **(a)** V. Colvin, M. Schlamp, A. Alivisatos, *Nature*, **1994**, 370, 354, **(b)** R.Somers, M. Bawendi, D. Nocera, *Chem. Soc. Rev,* **2007**, 36, 579, **(c)** A. Nozik, *Phys. E*, **2002**, 14, 115.
21. P. Anikeeva, S. Coe-Sullivan, J. Steckel, M. Bawendi, V. Bulovic, *Nano Lett*. **2008**, 8, 4513.
22. **(a)** B. Sun , W. Xie, G. Yi, D. Chen , Y. Zhou, J. Cheng, *J. Immunol.Method* , **2001**, 249, 85, **(b)** J. Aldana ,Y. Wang, X. Peng, *J. Am. Chem. Soc*, **2001**, 123, 8844.
23. **(a)** H. Ache, *Angew Chem Int Ed Engl*, **1989**, 28, 1, **(b)** R. Haugland, *Molecular Probes*, Eugene, **2002**, **(c)** P. Prasad, *Nanophotonics. Wiley-Interscience, New York*, **2004a, (d)** A. Waggoner, *Curr Opin Chem Biol*, **2006**, 10, 62.
24. Marcos Roberto de Oliveira , Agnes Magri , Cristiani Baldo , Doumit Camilios-Neto , Tamires Minucelli2 , Maria Antonia Pedrine Colabone Celligoi, *International Journal of Advanced Biotechnology and Research*, **2015**, 161-174
25. J. Chen, X. Song, H. Zhang, Y. B. Qu, J.Y. Miao, *Appl Microbiol Biotechnol*. 2006, 72, 52.
26. Sanjay Singh, Pitambar Patel, Swarna Jaiswal, A A Prabhune, BLV Prasad, *New J. Chem* 2009, 33, 646-652
27. Parul Dubey, Kaliaperumal Selvaraj, Asmita Prabhune, *World J of Pharm and Pharm Sci* WJPPS 2013, Vol. 2, Issue 3, 1107-1133.

28. Kim E. Sapsford, Thomas Pons, Igor L. Medintz, Hedi Mattousi, *Sensors* 2006, 6, 925-953.

29. Manuela F. Frasco, Nikos Chaniotakis, *Sensors* 2009, 9, 7266-7286

30. https://en.wikipedia.org/wiki/Skeletal_fluorosis

31. Ravi Chavali, Naga Siva Kumar Gunda, Selvaraj Naicker, Sushant K Mitra, *Analytical chemistry Research*, 2015, 6, 26-31

CHAPTER 2

Synthesis and Characterization Techniques

This chapter gives brief description of the CdTe nanoparticle synthesis by organometallic route and their further conjugation with various biomolecules in order to develop CdTe based biosensors. These nanocomposites are further characterized using different physico-chemical techniques. Optical, thermal, magnetic, and electrical properties of the synthesized nanocomposite carried out using various characterization techniques are briefly described in this chapter. Synthesis of "Sophorolipid" is also described in this chapter.

2. I Synthesis Techniques

During the last few decades, researchers have developed various new methods for synthesizing variety of materials with at least one dimension on the nanoscale, including nanoparticles, nano-wires, nano-tubes, nanocomposites etc [1]. Still, the synthesis of nanoscale materials with controlled properties is a crucial and ongoing challenge in nanoscience and technology. New materials are being synthesized on small scales (few hundreds of milligrams or less) but they may not be attractive for commercially purposes. The synthesis of various semiconductor quantum dots and their nanocomposites under desirable low temperature conditions with controlled size, shape and pure phase remains a major task. Soft chemical routes represent the most attractive alternatives, because they allow good control from the molecular precursors to the final product at low processing temperatures, result in the formation of nanomaterials with high purity and compositional homogeneity with advantages such as (a) wet chemical control on oxidation states, (b) ability to template various nanostructures, and (c) relatively cheap. Present research work is mainly based on organometallic route for synthesis of semiconductor quantum dots and their nanocomposites.

2. I.1 Organometallic Method

Organometallic method is currently considered as the most important technique for synthesis of semiconductor quantum dots (QDs). In present study we synthesized various QDs and their nano-composites by using this method. In order to produce QDs of desired shape, size and crystallinity, it is important to understand nucleation and growth at various conditions. Organometallic method also provides a convenient pathway to produce monodisperse QDs and their nanocomposites in organic and aqueous solvents. Herein, typical example of synthesis of CdTe QDs which is mostly employed for present study shown in schematics **Fig. 2.1**

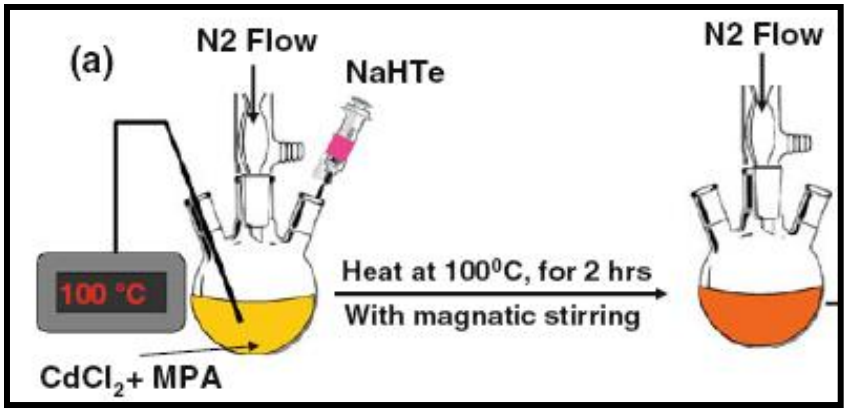

***Figure 2.1**: Schematics of synthesis of CdTe-MPA nanoparticles*

2.II Characterization Techniques

To understand the morphology, composition and crystal structure of the synthesized material, it is very important to characterize the as synthesized material using various characterization techniques. Desired resolution, higher sensitivity and greater precision of characterization tools can give better insights of the materials; hence will be much helpful to exploit for suitable applications.

2.II.1 Optical characterizations

2.II.1. (a) UV-VIS Spectroscopy (UV-Vis)

Absorption spectroscopy in the UV and visible region has long been an essential tool to the analyst [19]. It measures the intensity of absorption of near-ultraviolet and visible light (wavelength region from 200-800 nm) by a sample. The transitions arise due to molecular and structural changes in the substances being examined, leading to corresponding changes in the ability to absorb light in the UV and visible region of the electromagnetic spectrum. UV and visible light are energetic enough to promote the outer electrons in an atomic, molecular or material system to higher energy levels depending on the specific nature of the electronic states of a given material. Absorption of energy leads to a transition of electron from ground state to excited state. In semiconductors, when the incident photon energy more than or equal to the band gap energy of the material then absorption takes place and signal is recorded by the spectrometer.

This spectrometer can operate in two modes (i) transmission and (ii) reflection mode. In transmission mode usually thin films and colloidal nanoparticles well-dispersed in solvent are used. The optical measurements for those nanoparticles which are not dispersible in solvents are done in diffuse reflectance spectra (DRS) mode. Reflectance spectra provide information about the scattering and absorption coefficient of the samples and hence their optical properties. Schematic of UV-Vis spectrometer is shown in **Fig 2.2.** The light from the deuterium source is alternatively split into one of two beams by a chopper; one beam is passed through the sample and the other through the reference. The detector, which is often a photodiode, alternates between measuring the sample beam and the reference beam (see schematic **Fig. 2.2)**. Some double beam instruments have two detectors, and the sample and reference beam are measured at the same time. In other instruments, the two beams pass through a beam chopper which blocks one beam at a time. The source used for the UV and visible light are deuterium and tungsten lamps respectively and the detector used is PMT.

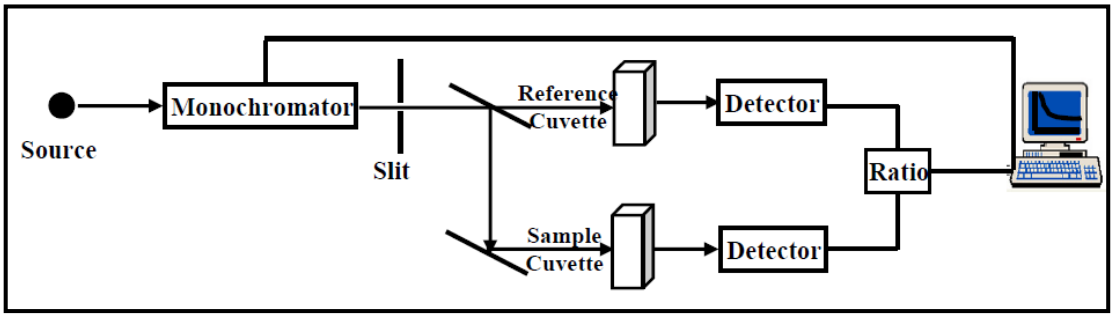

***Figure 2.2**: Schematics of UV-VIS Spectrophotometer*

Diffuse Reflectance Measurement using Uv-Vis spectroscopy: Since light cannot penetrate opaque (solid) samples, it is reflected on the surface of the samples. As shown in the below **Fig.2.3**, incident light reflected symmetrically with respect to the normal line is called "specular reflection," while incident light scattered in different directions is called "diffuse reflection."

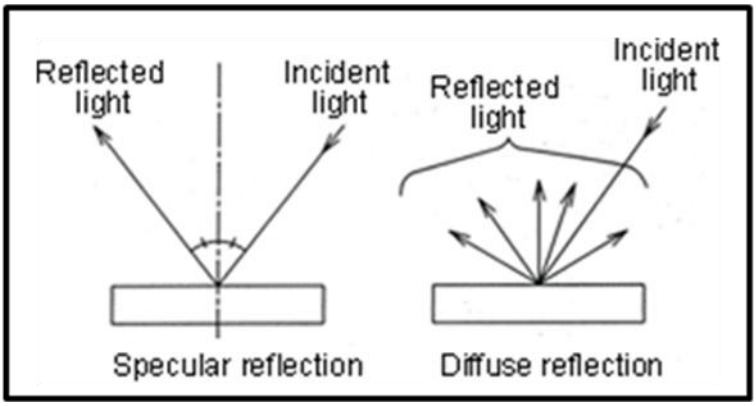

***Figure 2.3.**: Schematic of Specular and diffuse reflection [20]*

With integrating spheres, measurement is performed by placing the sample in front of the incident light window, and concentrating the light reflected from the sample on the detector using a sphere with a barium sulfate-coated inside. The obtained value becomes the reflectance (relative reflectance) with respect to the reflectance of the reference standard white board, which is taken to be 100%.

When light is directed at the sample at an angle of 0°, specular reflected light exits the integrating sphere and is not detected. As a result, only diffuse reflected light is measured. Models of integrating spheres with different angles of incidence are available, enabling measurement of both specular and diffuse reflected light in instances such as these as shown in **Fig 2.4**.

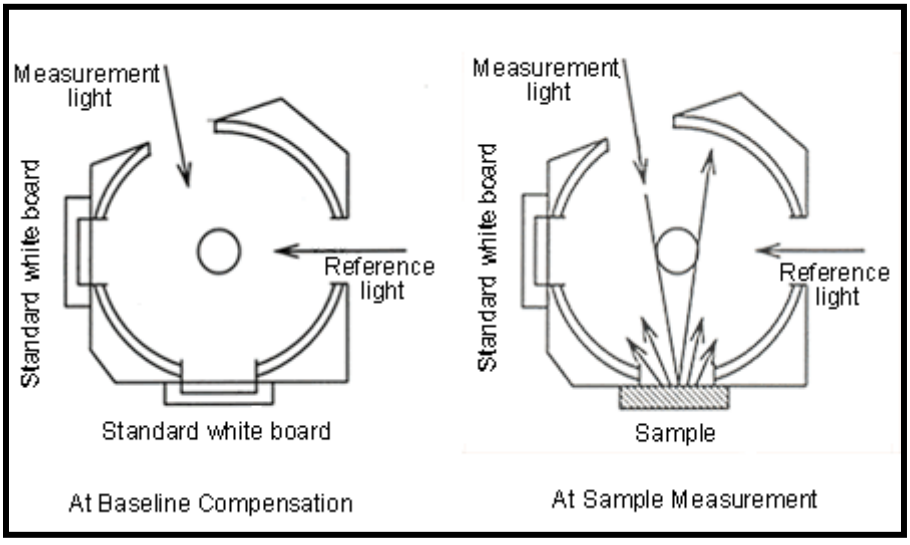

***Figure 2.4**: Measurement of diffuse and specular reflection using an integrating Sphere [20]*

Generally it is plotted as percent reflectance as a function of wavelength of light in Uv-vis range. In Present study we used UV–visible spectrophotometry in absorbance and diffuse reflectance mode used over the spectral range of 200 – 800 nm. The measurements were carried out on a Jasco V-570.

2.II.1. (b) Photoluminescence Spectroscopy:

Photoluminescence (PL) is the spontaneous emission of light from a material under excitation of incident light. The appropriate excitation wavelength is required to determine the sample's discrete electronic states. When light of enough energy (greater than HOMO-LUMO gap) is incident on a material, photons are absorbed and e-h pairs are generated and electrons are excited to higher energy levels. Eventually, these excitations relax and the electrons return to the ground state. If radiative relaxation occurs, the emitted light is called PL. This light can be collected and analyzed to obtain information about the photo-excited material. The PL spectrum provides the transition energies, which can be exploiting to determine electronic energy levels, defects impurity states and the relative rates of radiative and non-radiative recombination mechanism [13, 21].

PL is divided into two categories, fluorescence and phosphorescence, depending upon the electronic configuration of the excited state and the emission pathway. Fluorescence is the property of material to absorb light at a particular wavelength then consequently emit light of longer wavelength after an interval of time, termed the fluorescence lifetime. The process of phosphorescence occurs in a similar manner to fluorescence, but with a much longer excited state lifetime. PL is simple, versatile, and nondestructive measurement technique. The PL signal often depends on the density of photo-excited electrons and the intensity of the incident beam. The intensity of the PL signal depends on the rate of radiative and nonradiative events, which depends in turn on the density of nonradiative interface states.

In a typical PL setup for liquid samples (**Fig.2.5**), the sample is placed in a quartz cuvette with a known path length. Double beam optics is generally employed. The first beam passes through an excitation filter or monochromator, then through the sample and onto a detector. This incident light causes photoluminescence, which is emitted in all directions. A small portion of the emitted light arrives at the detector after passing through an optional emission filter or monochromator [22]. A second reference beam is attenuated and compared with the beam from the sample. Solid

samples can also be analyzed, with the incident beam made incident on the material (thin film, powder etc). Generally an emission spectrum is recorded, where the sample is irradiated with a single wavelength and the intensity of the luminescence emission is recorded as a function of wavelength. Usually, defects and impurities break the periodicity of the lattice and perturb the band structure locally. This perturbation is attributed to the discrete energy levels lying within the band gap. Depending on the defect or impurity, the state acts as a donor or acceptor of electrons in the lattice. Surfaces and interfaces contain a high concentration of impurity or defect states. Dangling bonds at a semiconductor surface or defects give rise to electronic states within the bandgap. These mid-gap states fill up to the Fermi level with electrons that originate in the bulk of the material.

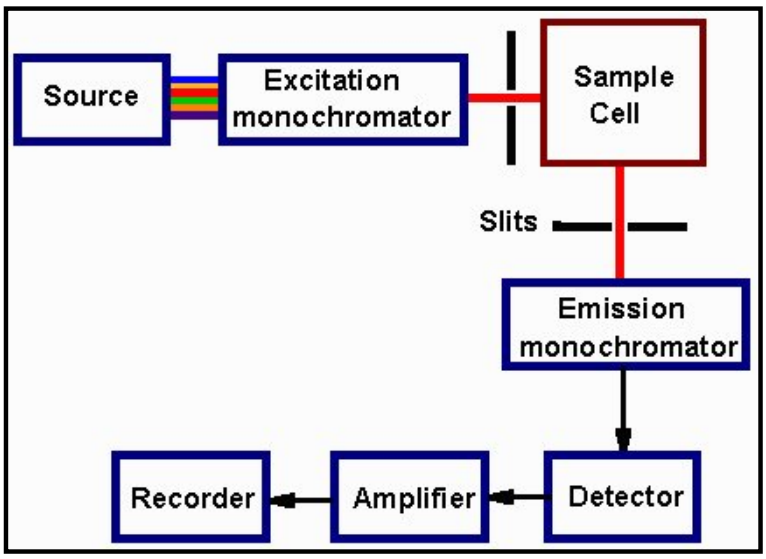

***Figure 2.5**: Schematic of PL Spectrophotometer [23]*

The fundamental limitation of PL analysis is its dependence on radiative events. Materials with poor radiative efficiency, such as low-quality indirect bandgap semiconductors, are difficult to study via ordinary PL. In present study PL measurements were performed on a Perkin-Elmer LS 55 spectrophotometer

2.II.1. (c) Zeta potential

Zeta potential is a powerful tool in understanding the stability of a particulate suspension. Zeta potential usually denoted using the Greek letter ζ, hence ζ-potential. It is electric potential in the interfacial double layer at the location of the slipping plane versus a point in the bulk fluid away

from the interface. It is measured by applying an electric field across the dispersion. Particles within the dispersion with a zeta potential will migrate toward the electrode of opposite charge with a velocity proportional to the magnitude of the zeta potential**.** The electrostatic potential near the particle surface is shown in **Fig. 2.6**. It changes very quickly from its value at the surface through the first layer of counter ions and then changes more or less exponentially through the diffuse layer. The junction between the bound charges and the diffuse layer is again marked by the line. That surface, which separates the bound charge from the diffuse charge around the particle, marks where the solution and the particle move in opposite directions when an external field is applied. It is called the surface of shear or slipping plane. The electrostatic potential on that surface is called the zeta potential. Zeta potential is an important and useful indicator of the charge which can be used to predict and control the stability of colloidal suspensions or emulsions. The greater the zeta potential the more likely the suspension is to be stable because the charged particles repel one another and thus overcome the natural tendency to aggregate. The measurement of zeta potential is often the key to understanding dispersion and aggregation processes.

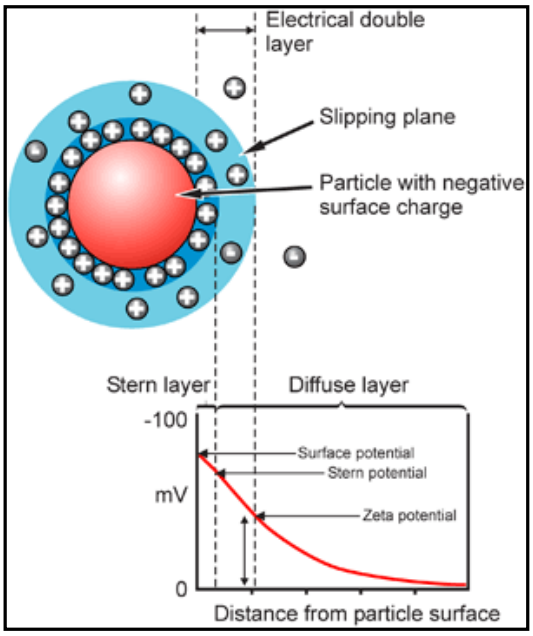

***Figure 2.6**: Schematic representation of zeta potential [24]*

For molecules and particles that are small enough, a high zeta potential will give stability, i.e., the solution or dispersion will defy aggregation. When the potential is low, attraction exceeds repulsion and the dispersion will break and flocculate. Particles with a high zeta potential of the

same charge sign, either positive or negative, will repel each other. Conventionally a zeta potential can be in a positive or negative sense, i.e. < -30mV and > +30mV would both be considered as minimum range of zeta potentials. So, colloids with high zeta potential (negative or positive) are electrically stabilized while colloids with low zeta potentials tend to coagulate or flocculate as shown in below table [25]

Sr. No.	Zeta Potential (mV)	Stability behavior of colloid
1	0 to ± 5	Rapid coagulation or flocculation
2	± 10 to ± 30	Incipient instability
3	± 31 to ± 40	Moderate stability
4	± 41 to ± 60	Good stability
5	More than ± 61	Excellent stability

The magnitude of the zeta potential gives an indication of the potential stability of the colloidal particle. Also zeta potential measurement brings detailed insight into the causes of dispersion, aggregation or flocculation, and can be applied to improve the formulation of dispersions, emulsions and suspensions. In the present study measurements were carried out using a Zetasizer, model 3000HS, Malvern, UK.

2.II.1. (d) Dynamic Light Scattering (DLS)

Dynamic Light Scattering (DLS), also known as quasi-elastic light scattering and photon correlation spectroscopy, is commonly exploit for studying colloidal systems in which a light beam is directed onto a sample that scatters the light elastically. DLS measures variation in scattered intensity with time at a fixed scattering angle (typically 90^{o}), while static light scattering measures scattered intensity as a function of angle. This light is scattered over a period of time and then analyzed statistically [26].DLS also used to study the system dynamics in real time; and the absolute determination of particle sizes [27].In fact, it is well suited for examining the monodispersity of synthesized nanoparticles and also time-dependent DLS is suitable for studying the growth of nanocrystals in solution, unlike other techniques that require the samples to be dried [28]. A typical setup is shown in **Fig. 2.7.** a beam of monochromatic light passes

through a solution containing the nanoparticles, which are generally colloids or micelles and scattering occurs. The intensity of the scattered light is identical in all directions with the amount of Rayleigh scattering depending on the size of the particles and the wavelength of the incident light. Whilst in solution, the particles move about in small random patterns (Brownian motion). At constant temperature, larger particles move slowly than the smaller ones, and hence the distance between the particles is constantly varying.

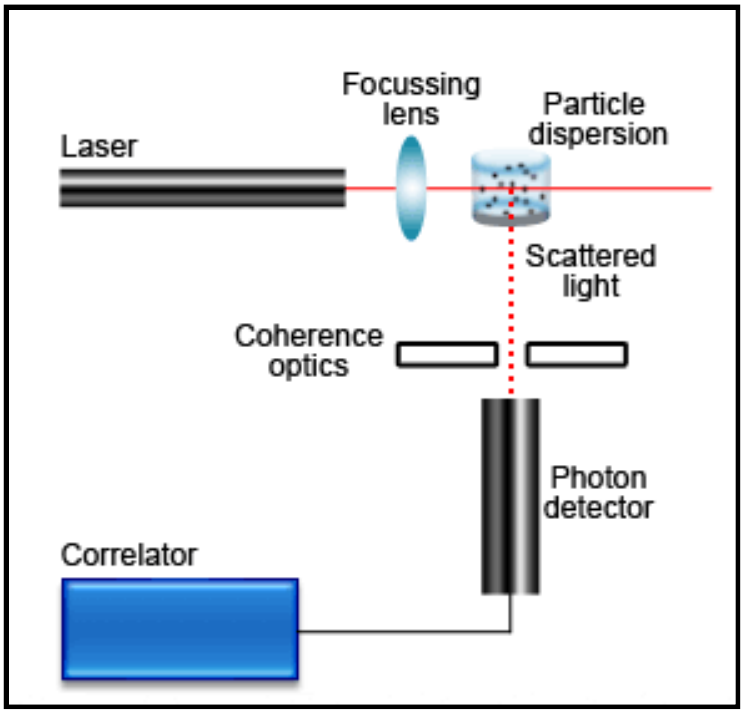

***Figure 2.7.**: Schematics of DLS techniques [29]*

Analysis of the time dependent fluctuation gives the diffusion coefficient D of the particles, if the viscosity η, of the solution is known, then the hydrodynamic radius or a spherical particle, R can be obtained from the Stokes-Einstein relation [30]

$$R = \frac{kT}{6\pi\eta D}$$

Where k_B is Boltzmann's constant and T is the absolute temperature.

However, DLS does have some limitations; it is only suitable for particles that exhibit Rayleigh scattering where particle size is larger than about $1/10^{th}$ of the illuminating wavelength [31]. DLS is utilized only to measure particle sizes in the range from nanometers to micro-meter. In most

cases dilute suspensions to minimize multiple scattering is require. Tiny fluctuation and noise could not differentiable. In present study we done DLS measurement on a Brookhaven Instrument (BIC-Brookhaven Instruments Corporation) 90 Plus particle size analyzer at a 90^{o} angle.

2.II.2 Structural Characterizations

2.II.2 (a) Fourier Transform Infrared Spectroscopy (FTIR)

FTIR is a technique that provides information about the chemical bonding or molecular structure of materials, whether organic or inorganic and identifies chemical bonds or functional groups by the absorption of infrared radiation which excites vibrational modes in the bond. The atoms in a molecule do not remain in a fixed relative position and vibrate about their mean position. Owing to this vibrational motion, if there is a periodic change in the dipole moment then such mode of vibration is infrared active. The IR region of the electromagnetic spectrum is 100 μm –1 μm wavelength [12,17].The advantage of using FTIR is that the whole spectrum is obtained across the entire frequency range at once with constant resolving power over entire range. A molecule that is exposed to infrared rays absorbs infrared energy at frequencies which are characteristic to that molecule. Each functional group have particular range of vibrational frequencies and are extremely sensitive to the chemical environment and the neighboring, therefore they provide important information about the presence of certain functional groups in the particular sample. The frequency of vibration is given by the relation

$$\nu = \frac{1}{2\pi}\sqrt{\frac{k}{\mu}}$$

Where, *k* is force constant and μ is a reduced mass [18] Schematic of FTIR spectrophotometer is shown in **Fig 2.8**. The apparatus derives from the classical attempt by Michelson to measure the 'ether wind' by determining the velocity of light in two perpendicular directions. A parallel beam of radiation is directed from the source to the interferometer, consisting of the beam splitter B and two mirrors, M1 and M2. The beam splitter is a plate of suitably transparent material (e.g. KBr) so as to reflect just 50% of the radiation falling on it. Thus half the radiation goes to M1, and half to M2, returns from both these mirrors along the same path, and is then recombined to a single beam at the beam splitter. It is well identified that if monochromatic radiation emitted by

the source, the recombined beam leaving B shows constructive or destructive interference, depending on the relative path lengths B to M1 and B to M2. Thus if the path lengths are the same or differ by integral multiple of wavelengths, constructive interference gives bright beam leaving B, whereas if the difference is a half integral number of wavelengths, the beam cancels at B. As the mirror M2 is moved smoothly away or towards from B, therefore, a detector sees radiation alternating in intensity It is rather easy to visualize that if the source emits two separate monochromatic frequencies, υ1 and υ2 then interference pattern of υ1 and υ2 would overlay the interference caused by M1 and M2; the detector would see a more complicated intensity fluctuation as M2 is moved, but computing the Fourier transform of the resultant signal is very rapid way of obtaining the original frequencies and intensities emitted by the source.

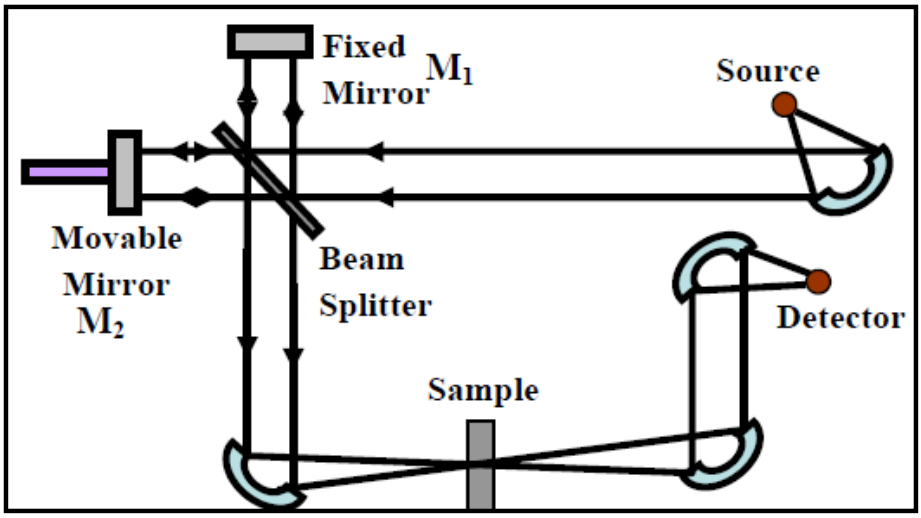

***Figure 2.8.**: Schematic of FTIR Spectrophotometer*

Taking the process further, even white radiations emitted by the source produces an interference pattern which can be transformed back to the original frequency distribution. The production of a spectrum is a two-stage process: (a) Without a sample in a beam, mirror M2 is moved smoothly over period of time through a distance of about 1 cm, while the detector signal the interferogram is collected into multi-channel computer; the computer carries out the Fourier transformation of the stored data to produce background spectrum. (b) A sample interferogram is recorded in exactly the same way, Fourier transformed, and then rationed against the background spectrum for plotting as transmittance spectrum. Alternatively, the sample and background spectra may each be calculated in absorbance forms and the latter simply subtracted from the former to give an absorbance spectrum of the sample alone. The advantage of using FTIR is that the whole

spectrum is obtained across the entire frequency range at once with constant resolving power over entire range. In present study FTIR measurements were performed on a Perkin-Elmer Spectrum One B spectrophotometer over the spectral range of 400– 4000 cm^{-1}

2.II.3 Imaging of surface morphology

Electron Microscopy: Electron microscopes have a much better resolution than the optical microscopes because of the interaction of an electron's matter wave with the sample. From Bragg's law, the minimum separation, d_{min}, which can be resolved by any microscope, is given

$$d_{\min} = \frac{\lambda}{2\sin\theta}$$

The resolution can be improved by using shorter wavelengths. The wavelength associated with an electron is given by the de Broglie relation [32]

$$\lambda = \frac{h}{p} = \frac{h}{\sqrt{2m_e E_k}}$$

Where, m_e the electron mass, E_k is its kinetic energy, and *h* is Planck's constant. The electrons in the microscope have kinetic energy in the kilo volt (kV) to even (MV) Depending on the kinetic energy, a typical range of wavelengths can be between 1– 0.005 Å, which is much smaller than that of visible light (400-700 nm) used in optical microscopes, resulting in far better resolution. As a consequence, nanoscale features, not observable with optical microscopes, can be observed by electron microscope.

During present study, we mainly used two electron microscopes such as Transmission Electron Microscopy (TEM) and Scanning Electron Microscope (SEM) for characterization of materials.

2.II.3 (a) Transmission Electron Microscopy (TEM):

Transmission electron microscopy (TEM) is one of the most powerful and versatile techniques for the characterization of nanomaterials. Its unique characteristics allocate one to achieve atomic resolution of crystal lattices as well as to obtain (with the help of energy-dispersive X-ray spectroscopy (EDS)) chemical and electronic information at the sub-nanometer scale. TEM mechanism based on the principle alike to that of an optical microscope with the main distinction that it uses electrons instead of photons as the source. The uncertainty principle sets a basic limit on the spatial resolution while using a beam of particles with de Broglie wavelength.

Consequently, smaller the wavelength of the source, higher will be the resolution of the system. The wavelength of the electrons is much shorter than that of light; much higher spatial resolution is attainable for TEM images than for a light microscope. It is also used to study the internal structure of nanomaterial. It works by passing electrons through the sample and using magnetic lenses to focus the image of the structure, much like light is transmitted through materials in usual light microscopes. TEM can reveal the finest details of internal structure, in some cases individual atoms. The most important advantage of a TEM is that it can concurrently give the information in real space (in the imaging mode) and reciprocal space (in the diffraction mode).The line diagram of a typical TEM column is shown in **Fig. 2.9.** In TEM, a thin sample is illuminated with collimated beam of accelerating electrons in which the electron intensity is identical over the illuminated area. The interaction of an electron beam with a solid sample results in a number of elastic or inelastic scattering phenomena such as backscattering or reflection, emission of secondary electrons, X-rays or optical photons etc.

In low resolution TEM, the objective aperture will be adjusted for selection of the central beam (containing the less-scattered electrons) or of a particular diffracted (or scattered in any form) beam to form the bright-field or dark-field image, respectively. In high resolution TEM (HRTEM), which is usually performed in bright-field mode, the image is formed by collecting a few diffracted beams in addition to the central one. HRTEM is an imaging mode of the TEM that allows the imaging of the crystallographic structure of a sample at an atomic scale. Because of its high resolution, it is essential tool to study nanoscale properties of crystalline material such as semiconductor QDs, nanocomposites and metal nanoparticles.

Angular distribution of scattering can be viewed in the form of scattering patterns, usually called diffraction patterns referred as selected area electron diffraction (SAED). The spherical aberrations of the objective lens limit the area of the selected object to few hundred nanometers. However, it is feasible to get diffraction patterns of a smaller object by focusing the electron beam with the projector lenses to obtain a small spot size on the object surface (2-10 nm). The spots of SAED become disks whose radii depend on the condenser diaphragm. This is called microdiffraction. SAED and microdiffraction pattern of a crystal is used to obtain symmetry of lattice and further to calculate inter-planar distances. Spatial distribution of scattering can be observed as contrast in images of the sample. The benefit of this arrangement is the possibility of directly viewing the area from which the diffraction pattern arises. Further, Kikuchi patterns

obtained by inelastic scattering of electrons is also very useful for understanding the crystallographic orientation as these are rigidly attached to a crystal plane and therefore move in the diffraction pattern when the crystal is tilted.

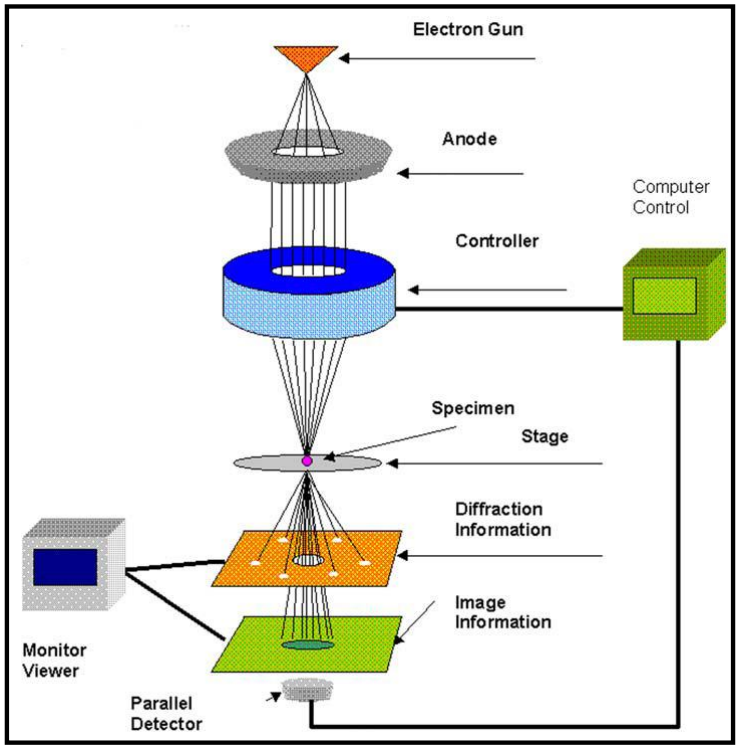

***Figure 2.9.**: Schematic diagram of the Transmission Electron Microscope [33]*

Many materials require extensive sample preparation and thinning steps to produce a sample thin sufficient to be electron transparent and changes in the structure may be caused during this process. Also there is prospective that the sample may be damaged by the electron beam, particularly in the case of biological materials. Despite these limitations, TEM has been the technique of choice due to atomic-level resolution leading direct visual information of size, shape, dispersion and structure. Further, when coupled with SAED, the technique can provide significant information on the crystallographic directions in the structures, helpful to understand the growth kinetics [34-35]. In present study we used transmission electron microscope (TEM) by model JEOL 1200 EX, on a carbon coated TEM copper grid and HRTEM analyses were done on an FEI Tecnai 30 system operated at 300 kV.

2.II.3 (b) Scanning Electron Microscope (SEM):

Scanning Electron Microscopy (SEM) is very useful tool for the direct observations of surfaces since they offer enhanced resolution and depth of field than optical microscope. A typical schematic of a SEM is shown in **Fig. 2.10**. The two major components of an SEM are the electron source and control comfort [36]. The electron source consists of an electron gun and two or more electron lenses, which influence the path of electrons travelling down an evacuated tube. The control comfort consists of a cathode ray tube viewing screen and computer to control the electron beam. The function of electron gun is to give a stable beam of electrons. Generally, tungsten or Lanthanum hexaboride (LaB6) thermionic emitters are used as electron gun. The electrons from thermionic emitters is exploiting for the visualization of surface of the sample. The filament is heated resistively by a current to get a temperature among 2000-2700 K. The electron gun generates electrons and accelerates them to energy in the range 0.1 – 30 keV towards the sample [36]. The spot size from a tungsten gun is too large to produce a sharp image unless electron lenses are used to demagnify it and place a much smaller focused electron spot on the sample.

When the electron beam impinges on the sample, different types of electronic signals are generated due electron scattering. The two signals most frequently exploiting to produce SEM images are secondary electrons (SE) and backscattered electrons (BSE). Most of the electrons are scattered at large angles (from 0^o to 180^o) when they interact with the positively charged nucleus. These elastically scattered electrons usually called 'backscattered electrons' (BSE) are exploiting for SEM imaging. A few electrons scatter inelastically due to the loss in kinetic energy upon their interaction with orbital shell electrons.

Incident electrons may knock off loosely bound conduction electrons out of the sample. These are secondary electrons (SE) and along with backscattered electrons are widely used for SEM topographical imaging. Both SE and BSE signals are collected when a positive voltage is applied to the collector screen in front of detector. When a negative voltage is applied on the collector screen only BSE signal is captured. Electron beam knocks off the inner shell electron, electron from higher energy levels drop to lower energy levels ensuing into emission of Auger electrons. Auger electron spectroscopy (AES) is useful to provide compositional information. Instead of excited atom releasing Auger electron, it can release a photon of electromagnetic radiation.

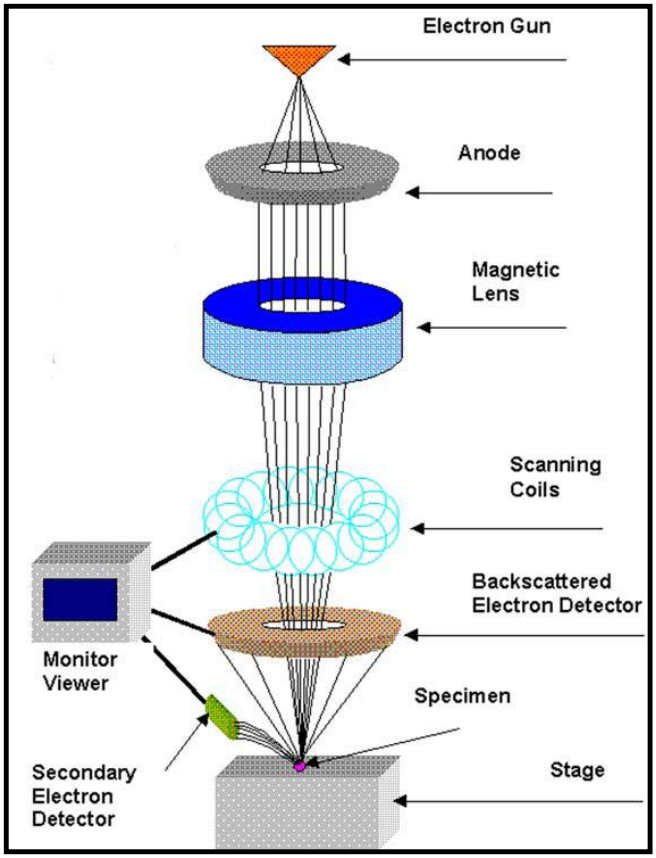

***Figure 2.10**: Schematic diagram of the Scanning Electron Microscope [33]*

If the more amount of energy released, the photon will be an X-ray photon. These electrons are attribute of the sample and can be used for analysis. This type of analysis is known as Energy Dispersive analysis of X-rays (EDAX). Electrons captured by the scintillator/ photomultiplier are then amplified and exploit to form an image in the SEM. In the present study samples were observed under the SEM (Joel, Japan)

Energy dispersive analysis of X-rays (EDAX)

Energy Dispersive analysis of X-rays (EDAX) is a chemical microanalysis technique. It utilizes X-rays that are emitted from the sample during bombardment by the high energy electron beam to characterize the elemental composition of the analyzed sample. Features or phases as small as about 1 μm can be analyzed using EDAX [36]. When the sample is bombarded by the electron beam, electrons are ejected from the atoms comprising the sample's surface. A resulting electron vacancy is filled by an electron from a higher shell, and X-ray photon is emitted to balance the energy difference. The detector measures the number of emitted X-rays versus their energy. The

energy of the X-ray is characteristic of the element from which the X-ray was emitted. A spectrum of the energy versus relative counts of the detected X-rays is obtained and evaluated for qualitative and quantitative determinations of the elements present in the sample.

2.II.3 (c) Atomic Force Microscopy (AFM)

Atomic Force Microscopy (AFM) is a probe microscopy and operates on different principle than optical microscopy. It consists of a microscale cantilever with a sharp tip at its end used to scan the specimen surface. The cantilever is typically silicon or silicon nitride with a tip radius of curvature on the order of nanometers. When the tip is brought near sample surface with few nanometers, the forces between the tip and the sample lead to the deflection of cantilever according to Hooke's law. The force between the cantiliver tip and the sample surface is usually within nN (10^{-9} N) regime. Depending on the situation, forces that are measured in AFM include mechanical contact force, vander Waals forces, capillary forces, chemical bonding, electrostatic forces, magnetic forces, Casimir forces, solvation forces etc. Typically, the deflection is measured using a laser spot reflected from the top of the cantilever into an array of photodiodes. Other methods that are used includes optical interferometry, capacitive sensing or piezoresistive AFM probes. These probes are fabricated with piezoresistive elements that act as a strain gage. Using a Wheatstone bridge, strain in the AFM probe due to deflection can be measured, but this method is not as sensitive as laser deflection or interferometry. If the tip were scanned at a constant height, there would be a risk that the tip would collide with the surface, causing damage. Hence, in most cases a feedback mechanism is employed to adjust the tip-to-sample distance to maintain a constant force between the tip and the sample. Usually, the sample is mounted on a piezoelectric tube that can move the sample in the z direction for maintaining a constant force, and in *xy* plane for scanning the sample. Alternately a 'tripod' configuration of three piezo crystals may be employed, with each responsible for scanning in the *x*, *y* and *z* directions. This eliminates some of the distortion effects seen with a tube scanner. The resulting map of the area $s = f(x, y)$ represents the topography of the sample. The block diagram of AFM shown in **Fig.2.11**

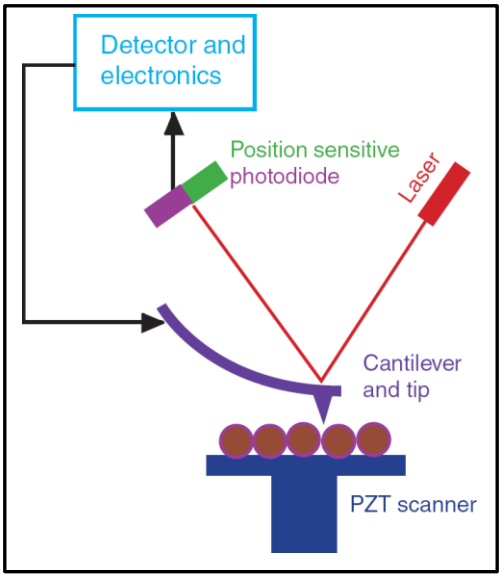

***Figure 2.11**: Block diagram of atomic force microscope [37]*

AFM measurements can be performed in two modes such as contact and tapping or non-contact, the difference between the two modes is only the tip-sample interaction during the measurement. In contact mode AFM is the most commonly used method where the tip is constantly adjusted to maintain a constant deflection, and therefore constant height above the surface. The force of interaction between the tip and the sample lies in the repulsive regime in the intermolecular force curve shown in **Fig. 2.12**.

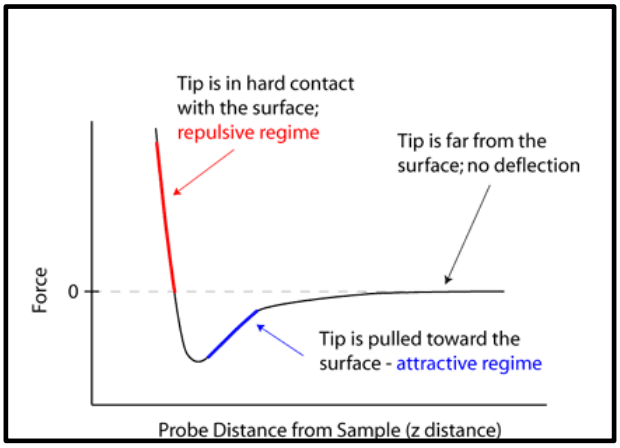

***Figure 2.12**: Force measurement curve of AFM [38]*

Contact mode AFM provides 3D information of the sample non-destructively with 1.5 nm lateral and 0.05 nm vertical resolutions. Tapping mode or non-contact is generally used for imaging soft and poorly immobilized samples. The tip is oscillated at its resonating frequency and positioned

over the sample so that it contacts the sample for a short time interval during oscillation. The forces between the tip and sample are quite low, on the order of pN (10^{-12} N). In present study we used variable temperature and high vacuum commercial system by RHK technologies, USA (SPM 100).

2.II.3 (d) Confocal Laser Scanning Microscopy (CLSM)

CSLM has become very important tool in biology and the biomedical sciences, as well as in materials science [39-40]. The purpose of a broad range of novel synthetic and naturally occurring fluorophores has made it possible to recognize cells and sub-microscopic cellular components with a high degree of specificity among non- fluorescing material [41]. CSLM exploit for obtaining high-resolution optical images with depth selectivity [42]. The non-invasive confocal optical sectioning technique enables the examination of both living and fixed specimens under a variety of conditions with enhanced clarity. The ability to acquire in-focus images from selected depths, a process known as optical sectioning is main characteristic of CSLM. Images are acquired point-by-point and reconstructed with a computer, allowing three-dimensional reconstructions of topologically complex objects.

The CSLM is diagrammatically presented in **Fig.2.13** coherent light emitted by the laser system passes through a pinhole opening that is located in a conjugate plane with a scanning point on the specimen and a second pinhole aperture positioned in front of the detector. The laser is reflected by a dichromatic mirror and scanned across the sample in a defined focal plane; secondary fluorescence emitted from points on the sample pass back through the dichromatic mirror and is focused as a confocal point at the detector pinhole aperture. The considerable amount of fluorescence emission that occurs at points above and below the objective focal plane is not confocal with the pinhole and forms extended Airy disks in the aperture plane [43]. Because only a little fraction of the out-of-focus fluorescence emission is passed through the pinhole aperture, the majority of this inappropriate light is not detected by the photomultiplier and does not give to the resulting image. The primary advantage of CSLM is the capability in order to produce thin (0.5 to 1.5 micrometer) optical sections through fluorescent specimens that have a thickness ranging up to 50 micrometers or more [44].

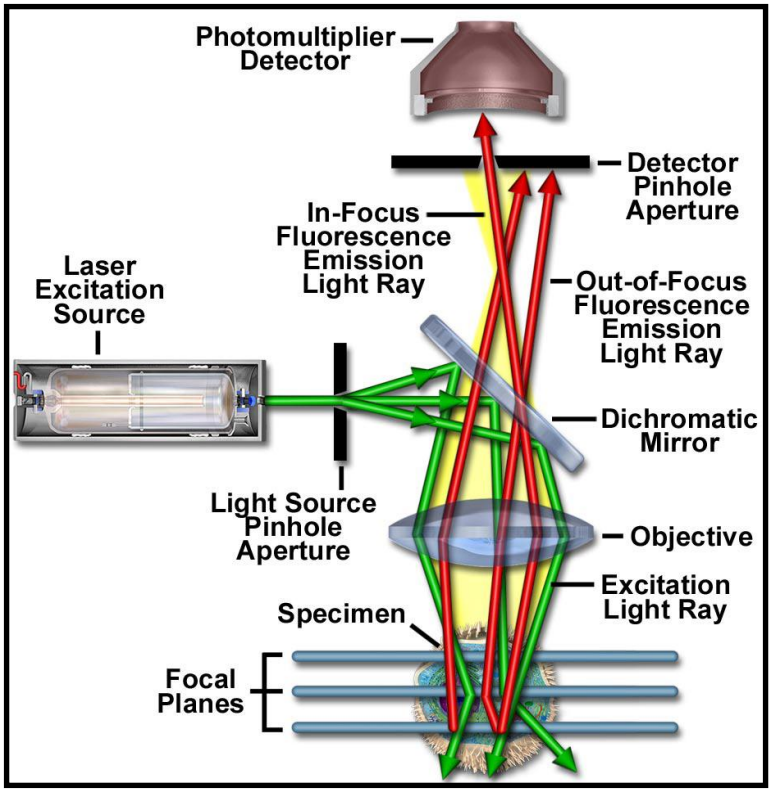

***Figure 2.13**: Schematic of the optical pathway and principal components in a laser scanning confocal microscope [45]*

The series of images is collected by coordinating incremental changes in the microscope fine focus mechanism with sequential image gaining at each step. Furthermore, optical sectioning eliminates artifacts that occur during physical sectioning and fluorescent staining of tissue specimens for traditional forms of microscopy. In present study the cells were viewed under CLSM (Zeiss LSM 510, Germany) equipped with argon and helium lasers.

2.II.4 Biological Characterizations

2.II.4 (a) MTT assay

The MTT assay is a colorimetric assay to determine cell metabolic activity. The assay measures the reduction of yellow 3-(4,5-dimethythiazol- 2-yl)-2,5-diphenyl tetrazolium bromide (MTT) by mitochondrial succinate dehydrogenase as shown in (Fig.2.14) This NAD(P)H-dependent cellular oxido-reductase enzymes under specified conditions, reflect the number of viable cells

present. The MTT enters the cells and passes into the mitochondria where it is reduced to an insoluble formazan product which has a dark purple color as shown in Fig. 20. The cells are then solubilised with an organic solvent (eg. isopropanol) and the released, solubilised formazan reagent is measured spectrophotometrically. Since reduction of MTT can only occur in metabolically active cells the level of activity is a measure of the viability of the cells. MTT assays are mainly done in the dark since the MTT reagent is sensitive to light.

Tetrazolium dye assays can also be used to measure cytotoxicity (loss of viable cells) or cytostatic activity (shift from proliferation to quiescence) of potential medicinal agents and toxic materials. Tetrazolium dye reduction is dependent on NAD(P)H-dependent oxidoreductase enzymes largely in the cytosolic compartment of the cell. Therefore, reduction of MTT and other tetrazolium dyes depends on the cellular metabolic activity due to NAD(P)H flux. Cells with a low metabolism such as splenocytes and thymocytes reduce very little MTT in contrast to the rapidly dividing cells which exhibit high rates of MTT reduction. It is important to keep in mind that assay conditions can alter metabolic activity and thus tetrazolium dye reduction without affecting cell viability. In addition, the mechanism of reduction of tetrazolium dyes, *i.e.* intracellular (MTT, MTS) *vs.* extracellular (WST-1), will also determine the amount of product.

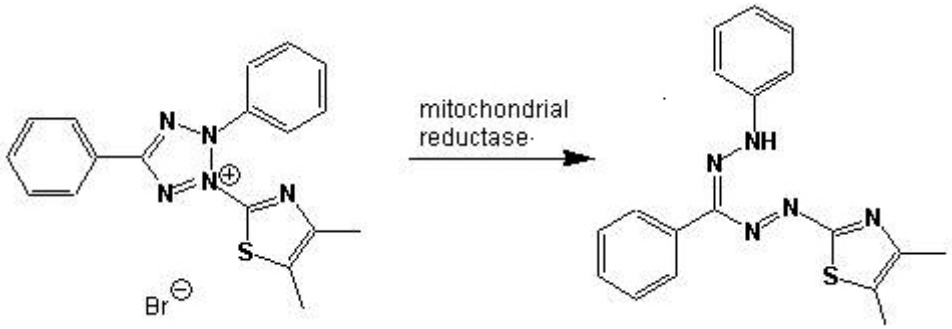

MTT (Yellow) **Formazan (Blue/purple)**

Figure 2.14: Cell viability with MTT reaction

2.II.4 (b) Antibacterial assay

In the last few decades, there has been a growing interest in the research and development of a new antimicrobial agents from various origin to encounter microbial resistance. Antimicrobial susceptibility testing is employed for epidemiology, drug discovery and therapeutic approaches. Antimicrobial test is the most preliminary in vitro investigation of any promising compound, particle or molecule which seem to be a potential antimicrobial agent. A variety of laboratory method are used to screen or investigate the antimicrobial activity of a compound. To Further investigate the antimicrobial effect in detail, cytofluorometric, time kill methods are used in order to get information about the nature of inhibitory effect (whether its bacteriostatic or bactericidal) and time dependent or concentration dependent damage on the test organism. We used spread plate method to quantify results. [46].

In **spread plate method**, sample or compound/ composite is serially diluted till a considerable concentration. A small aliquot of each dilution is transferred onto agar plate, and bacteria with a known concentration is then evenly distributed over the surface with a sterile spreader. is Bacteria are commonly grown up to density of 10^9 CFU/mL, although the vary tremendously depending on the species of bacteria and the media they are growing in One plate is kept as a control without any compound. Every single dilution and control will be done in triplicates which is then kept in incubator for 8-12 hrs. After colonies are grown, they are counted and are compared with the control plate in order to evaluate the inhibitory concentration of the compound added.

Diluting the bacteria

In order to get countable numbers of bacteria, we have to make a wide range of dilutions and assay with an objective to achieve one or two dilutions with countable numbers. We do this by making serial 10-fold dilutions of the bacteria that cover the whole probable range of concentrations. We then transfer 0.1 mL of each dilution to an agar plate, which in effect makes another 10-fold dilution since the final units are CFU/mL and we are only streaking 0.1 mL

Inoculating and incubating the plate

In this technique, streaking is done using a bent glass rod. 0.1 mL of bacterial suspension is dropped at the center of the plate using a sterile pipette. The glass rod is sterilized by first dipping it into a 70% alcohol solution and then passing it quickly through the Bunsen burner flame. The burning alcohol sterilizes the rod at a lower temperature than holding the rod in the burner flame and also reduces the chances of burning fingers. When all the alcohol is burned off and the rod is air-cooled, the rod is streaked back and forth across the plate working up and down several times in order to distribute the bacteria as evenly as possible. Plate is turned 90 degrees and repeated the side to side, up and down streaking. The plate is then turned 45 degrees and streaked a third time. Plate is then covered with lid and is allowed to wait for few minutes before turning it upside down for incubation. This practice allows the broth to soak into the plate so that bacteria doesn't weep onto the plate lid.

Counting bacteria

Colonies are most readily counted using a plate counter. The plate counter has a magnifying glass and a light source which makes the colonies easier to see. After counting the colonies, its is multiplied by an appropriate dilution factor in order to determine the number of CFU/mL in the original sample. [47]

2.II.5 Synthesis of Sophorolipid

The process of biosynthesis starts with a hydroxylation of the fatty acid present in the medium. This fatty acid can be of any source : supplemented in the form of fatty acid; in the form of n-alkanes, alcohol, aldehyde, triglycerides or esters of fatty acids, which is metabolized until its corresponding fatty acid. Sophorolipid is synthesised by inoculating the culture of *Candida bombicola* ATCC 22214 in 10mL of freshly prepared MGYP nutrient medium (1 g % glucose, 0.3 g % malt extract, 0.5 g % mycological peptone, 0.3 g % yeast extract) and incubated for 24 h at 30°C under shaking condition (200 rpm). The cells are separated from the broth by centrifugation at 5000 rpm, 10 °C for 20 min. The SL produced is extracted with ethyl acetate from the supernatant. Anhydrous sodium sulfate is added to the ethyl acetate phase in order to remove residual water which is filtered and ethyl acetate is further removed under vacuum. The unconverted fatty acid is removed by washing with n-hexane. This crude SL is a mixture of both lactonic and acidic form and is refluxed in 5 M NaOH at 100 °C for 10 min. The solution is then

quenched with 2 N HCl (up to pH 6) to convert all SL into an acidic form. It is further extracted with n-pentanol to obtain the desalted product, which is dried through evaporation and lastly washed with diethyl ether to remove the impurities such as hydroxyl ions, and dried under vacuum. The product recovered is the acidic form of deacetylated SL, which is confirmed by nuclear magnetic resonance spectroscopy (NMR).

In case, if fatty acid is not present, synthesis will be formed from the acetyl-CoA through de novo synthesis and if there is low concentration of glucose, these hydrophobic carbon sources are metabolized via β-oxidation and is use for the cellular maintenance instead of the sophorolipid synthesis.

The production, type and ratio of the lactonic/acidic forms of Sophorolipid, produced depend on various factors like - producer strain, the composition of the environment (hydrophilic and hydrophobic carbon sources, nitrogen and salt source), environmental conditions (temperature, pH, agitation, aeration and time) and the kind of cultivation process employed (batch, feed batch and continuous). Though SL can be produced with a single source of hydrophilic carbon which is mainly glucose but when two sources of carbon (hydrophilic and lipophilic) are present in the medium, the production of SL is vigorously accelerated.[48]

References:

1. C. Koch, *Nanostructured Materials, Processing, Properties and Applications* Ed.; *Noyes Publications: Norwich, New York*, **2002**.
2. M. Yoshimura, W. Suchanek, K. Byrappa, *Mater. Res. Soc. Bull., USA*, **2000**, 25, 17.
3. K. Byrappa, T. Adschiri, *Progress in Crystal Growth and Characterization of Materials*, **2007**, 53, 117.
4. N. Gaponik, D. Talapin, A. Rogach, K. Hoppe, E. Shevchenko, A. Kornowski, A. Evchmüller, H. Weller, *J. Phys. Chem. B*, **2002**, 106, 7177.
5. I. Martinez-Mera, M. Espinosa, R. Perez-Hernandez, J. Arenas-Alatorre, *Mater. Lett*, **2007**, 61, 4447.
6. A. Gupta, A. Curtis, *Biomaterials*, **2004**, 25, 3029.
7. C. Zhang, B. Wangler, B. Morgenstern, H. Zentgraf, M. Eisenhut H. Untenecker, R.Kruger, R. Huss, C. Seliger, W. Semmler, F. Kiessling, *Langmuir*, **2007**, 23, 1427.
8. F. Xu, L. Sun, *Energy Environ. Sci*, **2011**, 4 23, 453.
9. B. Cullity, *Elements of X-ray Diffraction, 2 ed., Addison-Wesley Publishing Company, Inc., Massachusetts*, **1978**.
10. G. Cao, *Nanostructures and Nanomaterials: Synthesis, Properties and Applications, Imperial College Press*, **2004.**
11. L. Azaroff, *X-Ray diffraction, McGraw Hill company*, **1974**.
12. C. Banwell, E. McCash, *A Book: Fundamentals of Molecular Spectroscopy, 4th Ed., Tata McGraw Hill Publishing Co. Ltd*, **2002**.
13. S. Kulkarni, *Book-Nanotechnology: Principles and Practices by, Capital publishing Company, New Delhi*, **2007**.
14. www.bartal.com/~zra/work1_files/Ramancompilation.ppt (Accessed on...14 Jan., 2013)
15. M. Fernandez-Garcia, A. Martinez-Arias, J. Hanson, J. Rodriguez, *Chem. Rev*.**2004**,104, 4063.
16. R. Atalla, U. Agarwal, and J. Bond, *Springer-Verlag Berlin Heidelberg*, **1992**.
17. J. Coates, *Interpretation of Infrared Spectra: A Practical Approach, Encyclopedia of Analytical Chemistry, R.A. Meyers (Ed.), 10815, John Wiley & Sons Ltd*, **2000**.

18. W. George, P. Mcintyre, *Infrared Spectroscopy: Analytical Chemistry by open learning, John Wiley, USA*, **1987**.

19. M. Li, H. Schnablegger, S. Mann, *Nature*, **1999**, 402, 393.

20. *http://www.ssi.shimadzu.com(Accessed on 14 Jan., 2013)*

21. T. Gfroerer, *Photoluminescence in Analysis of Surfaces and Interfaces, Encyclopedia of Analytical Chemistry, R.A. Meyers (Ed.), 9209, John Wiley & Sons Ltd, Chichester*, **2000**.

22. C. Mann, T. Vickers, W. Gulick, *Instrumental analysis (Harper & Row, New York, USA*, **1974**.

23. *www.chemistry.adelaide.edu.(Accessed on 14 Jan., 2013)*

24. *http://www.malvern.com/labeng/technology/zeta_potential (Accessed on 14 Jan., 2013)*

25. R. Greenwood, K. Kendall, *Journal of the European Ceramic Society*, **1999**, 19, 479.

26. A. Milling, *Surface characterization methods: principles, techniques, and applications (Marcel Dekker, New York, USA*, **1999**.

27. G. Bryant, C. Abeynayake, J. Thomas, *Langmuir*, **1996**, 12, 6224.

28. H. Cölfen, L. Qi, *Chemistry-A European Journal*, **2001**, 7, 106.

29. *http://www.malverninstruments.fr/LabEng/technology (Accessed on 14 Jan, 2013)*

30. P. Hiemenz, R. Rajagopalan, *Principles of colloid and surface chemistry (Marcel Dekker, New York, USA*, **1997**).

31. C. Bohren, D. Huffman, *Absorption and scattering of light by small particles Wiley, New York, USA*, **1983**.

32. L. Feldman, J. Mayer, *Fundamentals of surface and thin film analysis (North-Holland Publishing, New York, USA*, **1986**.

33. *http://www.rpi.edu/dept/materials/COURSES/NANO/shaw/Page5.html.(Accessed on 14 Jan., 2013)*

34. J. Duan, S. Yang, H. Liu, J. Gong, H. Huang, X. Zhao, R. Zhang, Y. Du, *J. Am. Chem. Soc*, **2005**, 127, 6180,

35. Y. Ding, Z. Wang, *J. Phys. Chem. B*, **2004**, 108, 12280.

36. G. Lawes, *Scanning electron microscopy and X-ray microanalysis: Analytical chemistry by open learning, John Wiley & sons*, **1987**.

37. J. Zhng Zhang, Optical *properties and spectroscopy of nanomaterials by, World Scientific Publishing Co. Pte. Ltd*, **2008**.

38. *http://www.nanoscience.com/education/afm.html.(Accessed on Jan., 14, 2013)*

39. J. Pawley (ed.), *Handbook of Biological Confocal Microscopy, New York: Plenum Press*, **1995**.

40. S. Paddock (ed.), *Confocal Microscopy: Methods and Protocols, Totowa, New Jersey: Humana Press*, **1999**.

41. W. Mason, *Fluorescent and Luminescent Probes for Biological Activity, New York: Academic Press*, **1999**.

42. J. Pawley editor *Handbook of Biological Confocal Microscopy (3rd ed.) Berlin: Springer. ISBN 0-387-25921-X.*, **2006**.

43. E. Stelzer, *Practical Limits to Resolution in Fluorescence Light Microscopy, in R. Yuste, F. Lanni, A. Konnerth (eds.), Imaging Neurons: A Laboratory Manual, New York: Cold Spring Harbor Press*, **2000**, 12.1-12.9.

44. D. Sandison, W. Webb, *Background Rejection and Signal-to- Noise Optimization in the Confocal and Alternative Fluorescence Microscopes, Applied Optics*, **1994**, 33, 603.

45. *http://www.olympusfluoview.com/theory/LSCMIntro.pdf (Accessed on Jan. 14, 2013)*

46. Mounyr Balouiri, Moulay Sadiki, Saad Koraichi Ibnsouda, Journal of Pharmaceutical Analysis, 2016, 6, 71-79.

47. http://www2.hendrix.edu/biology/CellWeb/Techniques/microspread.html

48. Marcos Roberto de Oilviera, Doumit Camilios-Neto, Cristiani Baldo, Agnes Magri, Maria Antonia Pedrine Colabone Celligol, *International Journal of Scientific and Technology Research*, 2014, 3, 133-146

CHAPTER 3

Chemically conjugated sophorolipids on CdTe QDs: a biocompatible photoluminescence nanocomposite for theranostic applications

Functional nontoxic cadmium telluride (CdTe) quantum dots (QDs) have been synthesized using a natural functional glycolipid belonging to the family of sophorolipids (SL) as a surface-modifying agent. These SLs with open acidic form are highly suitable for QDs stabilization, are readily obtained by a fermentation process of the yeast Candida bombicola (polymorph Starmerella bombicola) in large amounts. In this work chemically stable, water soluble, and photoluminescent CdTe QDs were successfully conjugated to sophorolipids via a cross-linking reaction. The formation of SLs conjugated CdTe QDs was confirmed using different analytical techniques X-ray Diffraction (XRD), Fourier Transform Infrared Spectroscopy (FTIR), Transmission Electron Microscopy (TEM), Electron Diffraction (ED), Atomic Force Microscopy (AFM), Dynamic Light Scattering (DLS), and Photoluminescence (PL). It was shown that after being conjugated with SL the SL-CdTe QDs becomes biocompatible, still maintaining its water solubility and photoluminescence properties. The final SL coated photoluminescent CdTe QDs represent interesting biocompatible materials

The content of this chapter is published in Journal "RSC Advances 2013, 3, 22319*".*

3.1 Introduction

Semiconductor nanocrystals1 (often known as quantum dots) have been attracting wide interest due to their various potential applications such as in optoelectronic devices [2,3], photovoltaic devices, [4–7] and sensors for chemical and biological detection [8–13]. In particular, semiconductor quantum dots (QDs) having unique size dependent fluorescent properties [14] are used for fluorescence-based bio-labeling and imaging applications [15,16] at the sub-cellular length scales. However in spite of having unique optical and electronic properties, biomedical applications of QDs show some restrictions due to their toxicity or biocompatibility, especially for in vivo conditions [17]. Cytotoxicity of quantum dots (QDs) has been reported in a large number of in vitro studies, affecting cell growth and viability [11,15]. The extent of cytotoxicity has been found to be dependent upon a number of factors including size, capping materials, color, dose of QDs, surface chemistry, coating bioactivity and processing parameters [17]. Even though they do not induce significant alterations in cell physiology, QDs can produce subtle alterations of function, which may affect the quality of outcomes derived from their use. To introduce biocompatibility in QDs, which is major concern in current research, surface modification of QDs with suitable biomolecules is one of the finest approaches [18–20]. Zhan et al. have reported design and synthesis of compact multi-coordinating (lipoic acid-appended) zwitterion ligands for the capping of luminescent quantum dots to increase colloidal stability of QDs [21]. Wegner et al. have studied the influence of surface coating and functionalization of QDs on luminescence quantum yield, and on the sensitivity of time resolved FRET bioassays [22]. Recently Zhang and his group have encapsulated QDs into enveloped virus in living cells for tracking virus–cell interaction.23 A number of biomolecules, mainly lipids such as rhamnolipids (*Pseudomonas aeruginosa*), sophorolipids (*Candida bombicola*), trehalose lipids, cellobiose lipids, mannosylerythritol lipids, surfactin (*Bacillus subtilis*) and emulsan (*Acinetobacter calcoaceticus*) have been explored by different scientific studies to introduce biocompatibility in QDs [24,25]. Among them SLs are biosurfactants produced by yeast C. bombicola. SLs, which are biologically, derived glycol-conjugates with a well-defined molecular structure given in Scheme 1. They are generally present in the form of disaccharide sophorose linked β-glycosidically to the hydroxyl group at the penultimate carbon of fatty acids. They are amphiphilic molecules, which contain both hydrophobic (non-polar) and hydrophilic (polar) groups. The foremost reasons for a high and increasing level of interest in sophorolipids are their

biodegradability and low toxicity as well as their unique structures that can facilitate their engineering to suit a specific application domain. SLs have been used so far for detergents and skin care applications [26]. More recently their anticancer, antibacterial, self-assembly, templating and metal-complexing properties have been also put in evidence [25]. SLs, in their open acidic form, are composed of a sophorose unit (i.e. 2-*O*-*b*-Dglucopyranosyl- D-glucopyranose; a-Glc-(1–2)-Glc), attached to oleic acid through an ether bond on the C-17 carbon atom of the fatty acid chain, thus leaving the COOH group accessible. Hence, acidic SL is water-soluble, non-toxic, and biocompatible and the COOH becomes an interesting functional, surface binding group. SLs are produced in large quantities from crops-based resources using a white biotechnology route, constituting a large advantage from an environmental point of view with respect to a chemical engineering approach. There are a few reports on metal and metal oxide nanoparticles capped with SL; Prasad and his group successfully synthesized SL capped silver nanoparticles and *Baccile et al*. synthesized ultra small 2 nm Fe_3O4 nanoparticles using SLs as capping agents and those exhibit excellent antibacterial [27,28] and superparamagnetic behavior [29] respectively. In this work, we show that SL can be successfully used as CdTe QDs stabilizer. Foremost, carboxylic acid terminated water-soluble mono-dispersed CdTe QDs have been synthesized using 3-mercaptopropionic acids (MPA) as capping agent. Then amine terminated CdTe QDs were prepared applying simple amine coupling reaction between MPA capped CdTe QDs with ethylene-diamine (EDA). Same amide coupling methodology was applied to get final SL functionalized CdTe QDs. EDA was used as an anchoring molecule between MPA capped CdTe QDs with SLs. The overall reaction scheme is schematically given in Scheme 2. To the best of our knowledge there is no such report yet in the literature where SL is used as surface modifying agent to encapsulate CdTe QDs with fluorescence property intact.

3.2 Materials and methods

High purity cadmium chloride (CdCl2) and tellurium powder (Te) (SD Fine Chemicals), 3-mercaptopropionoic acid (MPA) and ethylene-diamine (EDA), 1-ethyl-3-(3-dimethylaminopropyl) carbodiimide (EDC) were used as obtained (SRL Chemicals) and ammonium hydroxide (NH_4OH) (Merck Laboratories), sodium borohydride (NaBH4) (30% w/v), Agarose (Merck Laboratories). Isopropanol and Acetone (Merck Laboratories) was used as received. Deionized water was acquired from a Millipore milli-Q system.

3.2.1 Synthesis of water soluble MPA capped CdTe QDs (MPA-CdTe)

Mercaptopropionic acid stabilized CdTe nanoparticles were synthesised using an organometallic route.30 In brief, NaHTe was prepared just before starting the CdTe QDs synthesis by reacting NaBH4 and Te powder in molar ratio of 3 : 1. Round bottom flask was flushed with N_2 and then 0.5 mL N2 purged water was added into it through a syringe. Te powder (3.0 mmol) was mixed with NaBH4 in water under nitrogen-saturated condition. The reaction was carried out at room temperature under nitrogen flow with the magnetic stirring of 150 rpm for 25–30 min. The reaction was stopped when the black Te powder was completely reduced and the solution turned to be absolutely transparent pink in color. This freshly prepared NaHTe solution was hot injected (100°C) to the N2 saturated solution of $CdCl_2$ (15 mM) and MPA (36 mM) at pH 10. This solution was then refluxed under nitrogen flow for 2 h at 100°C. The CdTe solution was cooled to room temperature and precipitated with acetone and washed with water to get rid of Na^+ ions and unbound MPA. The solution was centrifuged at 10 000 rpm for 10 min at room temperature. The pellet was collected which comprised of CdTe nanocrystals and was dried with a rotary evaporator. The resulting solid CdTe QDs readily re-dispersed in water resulting in a clear solution. Then amine terminated CdTe QDs were prepared applying simple amine coupling reaction between MPA capped CdTe QDs with Ethylenediamine (EDA).

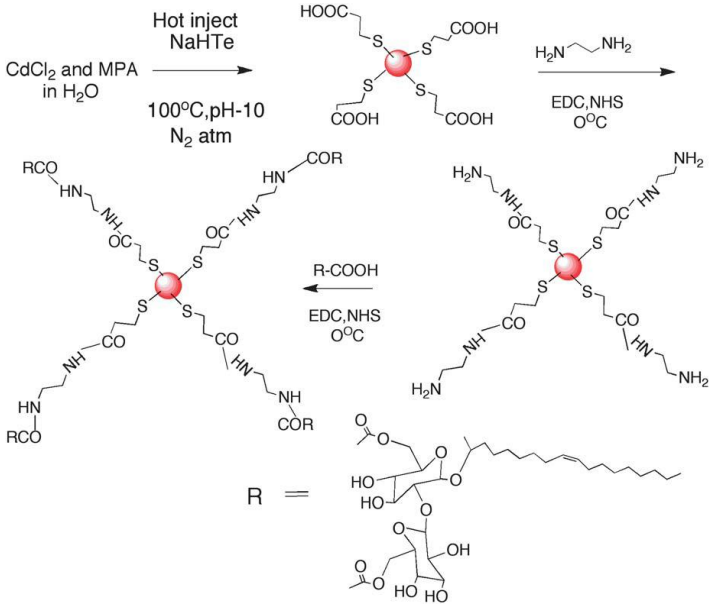

Figure.3.1. Schematic diagram of overall reactions to get SL functionalized CdTe QDs.

3.2.2 Synthesis of sophorolipids (SLs)

Sophorolipid was synthesised in our lab as reported in our early reports.[31]. For this the seed culture of *Candida bombicola* ATCC 22214 was inoculated in 10mL of freshly prepared MGYP nutrient medium (1 g% glucose, 0.3 g% malt extract, 0.5 g% mycological peptone, 0.3 g% yeast extract) and incubated for 24 h at 30°C under shaking condition (200 rpm). This pre-inoculum was added to 90 mL MGYP nutrient medium in a 500 mL Erlenmeyer flask and incubated for 48 h at 30°C on a shaker (200 rpm). Cells were washed twice with Millipore water under sterile conditions. The cell pellets (biomass 5–6 g wet weight in 100 mL medium) were re-dispersed in 100 mL 10% glucose with 1 mL of fatty acid (dispersed in 1 mL ethanol) and the flask was kept on a shaker (200 rpm) at 30°C for 96 h. As a result of the reaction between the yeast biomass with glucose and fatty acid, a brown and viscous liquid (crude SL) settled at the bottom of the flask, (method modified by S. Shah, A. Prabhune, unpublished data). The cells were separated from the broth by centrifugation at 5000 rpm, 10°C for 20 min. The SL formed was extracted from the supernatant with ethyl acetate. Anhydrous sodium sulfate was added to the ethyl acetate phase to remove residual water, filtered and then ethyl acetate was removed under vacuum. The unconverted fatty acid was removed by washing with n-hexane. This crude SL (a mixture of lactonic and acidic form) was refluxed in 5 M NaOH at 100°C for 10 min. The solution was quenched with 2 N HCl (up to pH 6) to convert all SL into an acidic form. It was further extracted with n-pentanol to obtain the desalted product, which was dried through evaporation and finally washed with diethyl ether to remove the impurities such as hydroxyl ions, and dried under vacuum. The product contained the acidic form of de-acetylated SL, which was confirmed by NMR.

3.2.3 Synthesis of amine terminated CdTe QDs

Conjugation of amine terminated CdTe QDs with SLs was achieved by sulfo-NHS (N- hydroxy sulfo-succinimide) and EDC (1-ethyl-3(3- dimethylaminopropyl) carbodiimide hydrochloride) amide coupling reaction. 100 mg of amine terminated CdTe was mixed in 20 mL Millipore water and was allowed to stir for 30 min at room temperature in order to achieve a proper dispersed solution.160 µL EDA (0.0023 mmol ethylene diamine) was added in the solution and was allowed to stir for 30 min at room temperature. 8 mg (0.069 mmol NHS) was added in the solution and was allowed to stir for 20 min. After this 40 mg (0.25 mmol EDC) and 40 mL

(0.0002 mmol DIPEA (N,N-di isopropyl ethylamine)) were added in the mixture and it was kept for stirring for the next 20 h. The reaction mixture obtained was precipitated with acetone and washed several times with Millipore water to get rid of all the unbound EDC. Encapsulation of CdTe particles with EDA was further validated by various physical characterizations. EDA linked CdTe nanocrystals were concentrated and dried using rotary evaporator.

3.2.4 Synthesis of sophorolipid encapsulated CdTe QDs (SL-CdTe QDs)

In order to further encapsulate amine terminated CdTe QDs with acidic form of sophorolipids, 100 mg amine terminated CdTe QDs were mixed with 100 mg acidic form of sophorolipids and the mixture was kept on stirring for 30 min in order to achieve dispersed solution. The same EDC–NHS coupling procedure was carried out as before and the final product was washed with Millipore water and dried in vaccum for further characterizations.

3.3 Cell culture studies

MCF-7 (human breast adeno carcinoma cell line) cells were grown in Eagle's Minimum essential Medium (MEM Gibco, Carlsbad, CA, USA) supplemented with 10% Fetal Bovine serum and penicillin/streptomycin, under 5% CO2 atmosphere at 37° C. NIH3T3 (Mouse Embryonic fibroblast cell line) cells were grown in Dulbecco's Modified Eagle's medium (DMEM, Gibco, Carlsbad, CA, USA) medium supplemented with bovine calf serum to a final concentration of 10% and penicillin/streptomycin under 5% CO2 atmosphere at 37 °C. Thp-1 (Human acute monocytic leukemia cell line) cells were grown in RPMI 1640 at pH 7.4 at 37 ° C for 4 days in the presence of 5% CO_2 as well as 95% humidity to reach the density upto 6 $\times 10^6$ cells per mL followed by treatment with 100 nM of phorbol myristate acetate. The culture was then incubated for 24 h to allow them converted into macrophages.

3.4 Results and discussions

The samples were characterized by powder X-ray diffraction measurements (Panalytical Xpert Pro) with Cu KR radiation using a Ni filter. Optical properties of the nanoparticles were studied by UV-visible-NIR spectrophotometry in diffuse reflectance mode over the spectral range of 190–1400 nm. The measurements were done on a Jasco V-570 spectrophotometer. Photoluminescence measurements were performed on a Perkin- Elmer LS 55 spectrophotometer.

FTIR measurements were performed on a Perkin-Elmer Spectrum One B spectrophotometer over the spectral range of 450–4000 cm^{-1}. The particle size characteristics were investigated by Transmission Electron Microscopy (TEM), model JEOL 1200 EX, on a carbon coated TEM copper grid. HRTEM analysis was done on an FEI Tecnai300 system operated at 300 kV. The zeta potential as a function of the magnitude of the electric potential and the stability of the nanoparticles dispersed in water were measured using a Zetasizer model 3000HS, Malvern, UK. Hydrodynamic radii were measured on a Brookhaven Instrument (BIC-Brookhaven Instrument Corporation) 90 Plus particle size analyzer at a 90 ° angle using 100 mg mL^{-1} water based particle suspensions. Atomic force microscopy AFM with [RHK technologies, USA (SPM 100)] was employed for surface characterization.

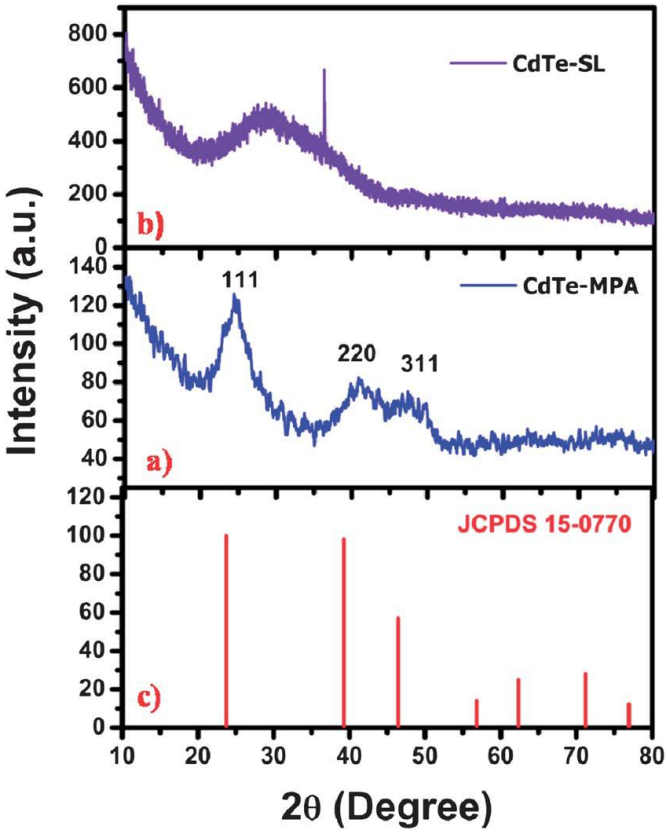

Figure. 3.2. XRD patterns of MPA-CdTe and SL-CdTe QDs with standard JCPDS data.

Fig. 3.2 shows X-ray diffraction pattern of as synthesized MPA capped CdTe QDs. The line broadening at the full width at half maximum (FWHM) allows approximate estimation of the mean size of the crystallites from the Scherrer's formula. Here in MPA capped CdTe, the

diffraction peaks are broad and the three main peaks centred at about 2 θ ~25° (111), 40° (220) and 47° (311) correspond well to the three most intense peaks for CdTe, matching well with JCPDS file no. 15-0770. The mean estimated size of CdTe is found to be ~3 nm by the Scherrer formula. After encapsulation with SLs, no characteristic peak of CdTe QDs was observed. The broad peak of SL molecule masks the characteristic peak of MPA-CdTe. The presence CdTe QDs in SL shielded QDs was further validated by HRTEM and SAED analysis.

The morphology of MPA capped CdTe QDs and SL capped CdTe QDs was analyzed using TEM micrographs. Figure.3.11a and (d) shows low magnification TEM image of MPA-CdTe and SL-CdTe QDs, respectively. The sizes of MPA-CdTe QDs reflect their nearly mono-dispersed spherical character, with mean particle diameter 5±1 nm which remain unchanged after SL modification. area diffraction patterns (SAED) of MPA-CdTe QDs and SL-CdTe QDs are shown in Figure.3.3 (c) and (f).

In Figure. 3.3(a) self-assembled superlattices are also seen indicating high uniformity of the particles. After being capped with SLs, the SL molecules totally screened the surface of CdTe QDs, (Figure.3.1(d)). This effect is observed in Figure.3.3(b) and (e) which show HRTEM images of MPA-CdTe QDs and SL-CdTe QDs, respectively. In both the cases the lattice fringes with line spacing of 0.37 nm, which correspond to (111) plane of face centred cubic phase of CdTe QDs, are seen. The selected The selected area diffraction patterns (SAED) of MPA-CdTe QDs and SL-CdTe QDs are shown in Fig. 3.3 (c) and (f).

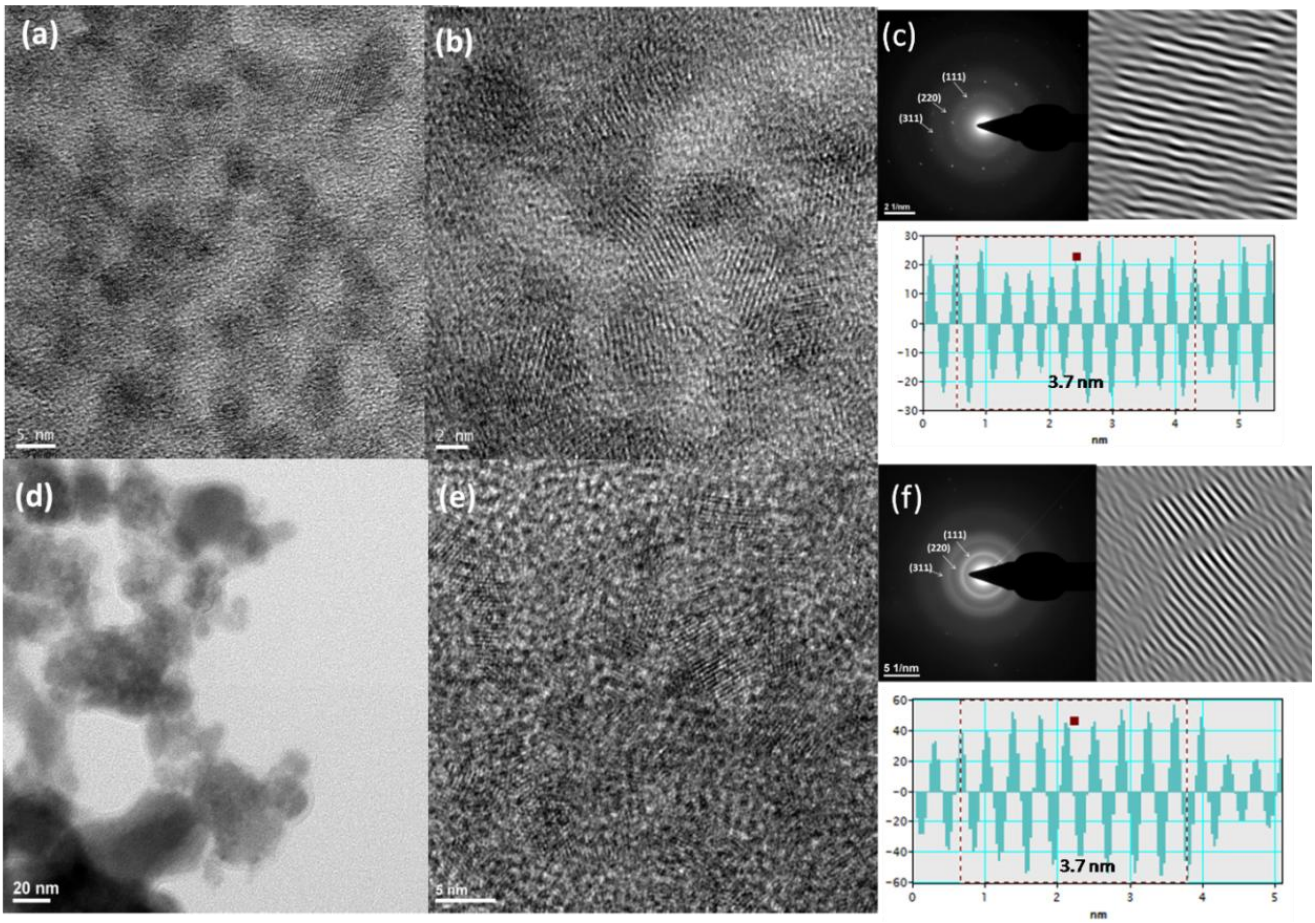

Figure.3.3 TEM, HRTEM, and SAED of MPA-CdTe QDs (a), (b), and (c) SL-CdTe QDs (d), (e) and (f).

The dynamic light scattering (DLS) spectra of MPA-CdTe QDs and SL-CdTe QDs was also performed in order to further validate the size of . The hydrodynamic size of MPA-CdTe is 8nm, which perfectly matches with the actual particles size obtained from TEM images. The mean hydrodynamic size of SL-CdTe QDs is 118 nm, which implies that CdTe QDs are fully encapsulated with SL molecules, which is clearly observed in TEM image.

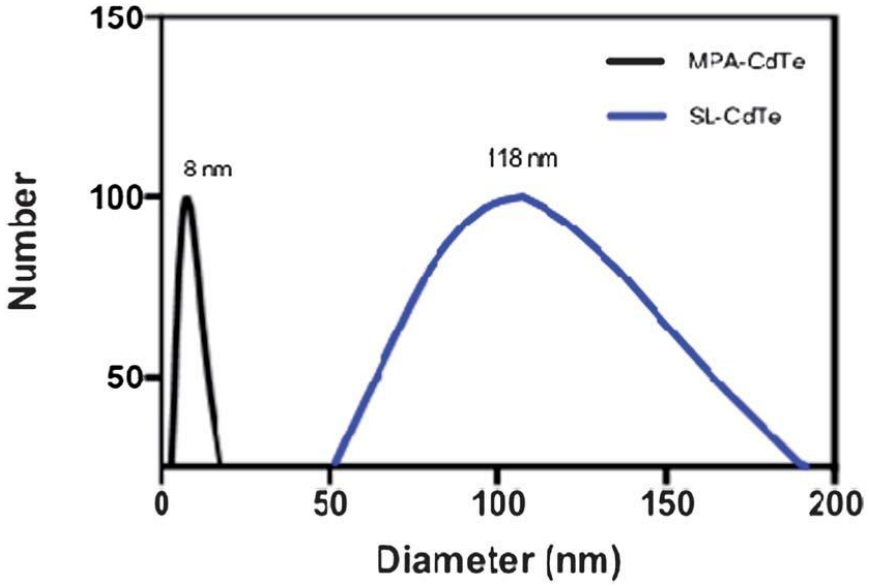

Figure. 3.4 DLS spectra of MPA-CdTe QDs and SL-CdTe QDs.

3.5 Gel electrophoresis of MPA-CdTe and SL-CdTe nanocomposites

Gel electrophoresis was also performed to check the mono-dispersibility of MPA-CdTe QDs and SL-CdTe QDs. Agarose gel (0.8%) was used for the electrophoresis study. After running 30 min in gel under 70 V potential, the movements of MPA-CdTe QDs and SL-QDs materials are shown in Figure.3.5. The movement of SL-CdTe QDs was found to be almost similar to MPA-CdTe QDs with or without tracking dye (bromophenol blue) indicating its monodispersed nature.

Fig 3.5 Gel electrophoresis of MPA-CdTe and SL-CdTe nanocomposites. Lane 1 - MPA-CdTe, Lane 2- SL-CdTe, Lane 3- MPA-CdTe with tracking dye (Bromophenol blue), Lane 4- SL-CdTe with tracking dye (Bromophenol blue)

3.6 Optical studies

3.6.1 UV-Vis spectra

Typical UV-visible absorption spectra of MPA-capped CdTe and SL capped CdTe QDs are shown in Figure.3.6. The peak in the absorption spectrum of MPA-CdTe QDs is at 517 nm and that is seen to have shifted to 527 nm after SL capping. The 10 nm red shift can be attributed to encapsulation of QDs inside the SL molecules.

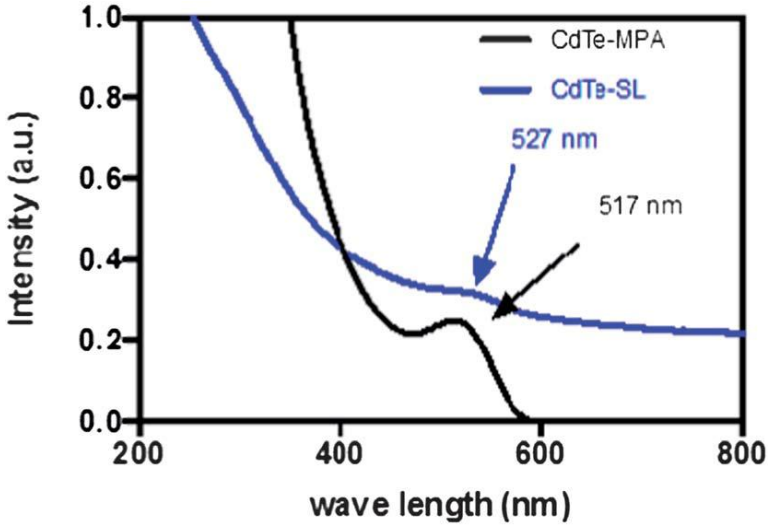

Figure.3.6.UV-visible spectra of MPA-CdTe QDs and SL-CdTe QDs.

3.6.2 Photoluminescence studies

The photoluminescence (PL) emission spectra of MPA and SL capped CdTe QDs are shown in Fig 3.7. The fluorescence emission maximum for MPA capped CdTe QDs is observed at 579 nm when excited by the radiation at 380 nm. According to previous work, CdTe QDs capped with MPA have a typical emission band located at 500-600 nm. The presence of the sophorolipid bound to the surface of CdTe QDs is seen to induce a pronounced (~ 16 nm) red shift in the PL. It has been established that quantum yield (QY) and peak position are dependent on size as well as surface modifying agent[32]. MPA, a small carboxylic acid terminated ligand, first reacts with EDA and then with SL, which results in a new bulky surface functional agent and that affects the QY as well as peak position directly. The red shift is reflected in the PL (image taken under UV as shown in the insets of Fig 3.7. The quantum yield of SL-CdTe QDs was calculated with reference with rhodamine B in water, which was found to be 20 % as against 31% of rhodamine B. The PL stability remained unaffected for 3 days under laser irradiation.

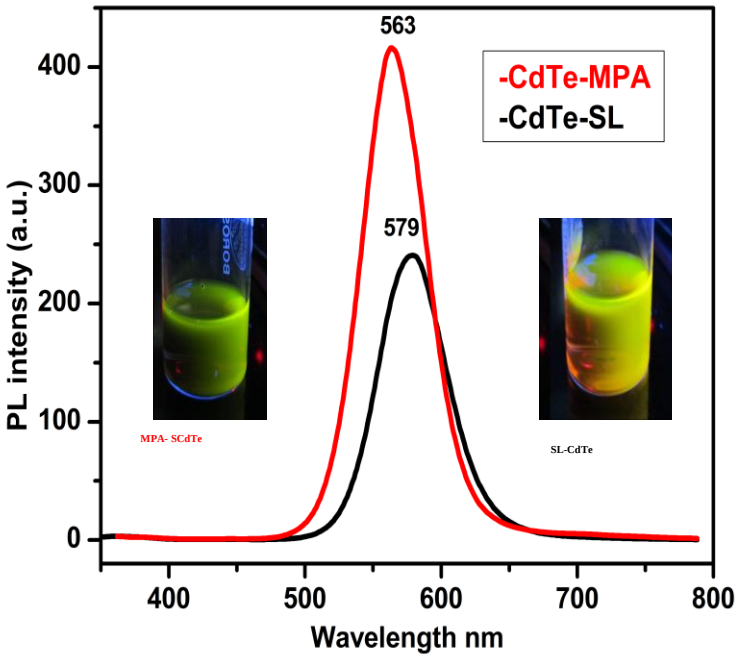

Fig.3.7 Photoluminescence spectra and visual pictures of MPA-CdTe QDs and SL-CdTe QDs

Figure.3.8 shows the FTIR spectra of MPA-CdTe QDs and SL-CdTe QDs. The following

important resonances =CH stretch (U= 2915 cm^{-1}), C=O group in -CONH (U=1713 cm^{-1}) in SL-CdTe QDs confirms the presence of SL on the surface of MPA-CdTe QDs. The sharp peak is generally attributed to the =CH vibration of oleic acid moeity. The peak at 1395 cm^{-1}corresponds to -CH bending. The -COH groups of sophorose head i.e. glucose moeity whose resonances are detected in the region between 1200 cm^{-1} and 750 cm^{-1}. The peaks at 1032 cm^{-1} and 1230 cm-1 attributed to a C-O stretching coupled with C-C stretching and -OH deformation.

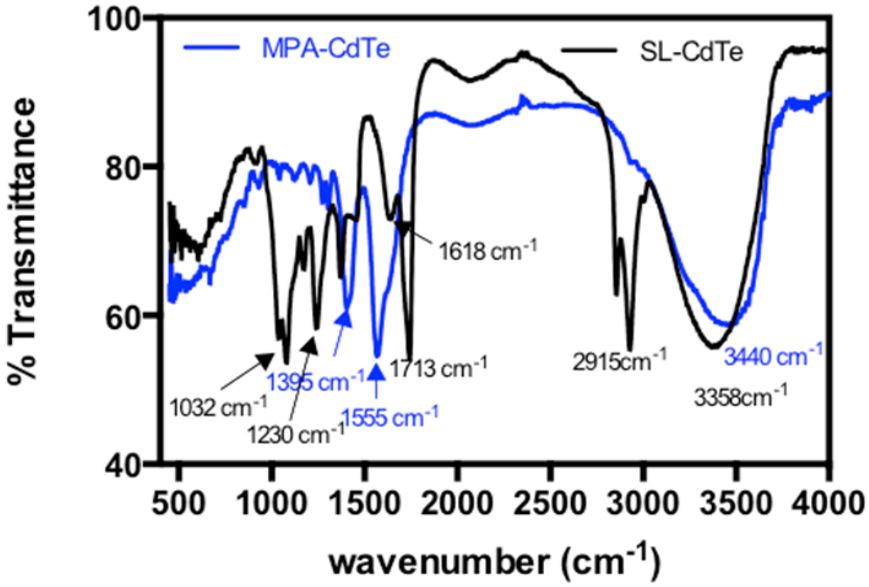

Figure.3.8. shows the FTIR spectra of pure Sophorolipids, MPA functionalized CdTe QDs, SL functionalized CdTe QDs

To determine whether SLs are capable of capping MPA-CdTe QDs, colloidal samples of MPA-CdTe and SL-CdTe QDs were assembled on sillicon substrate at 25 C. AFM was employed to further establish and elucidate the encapsulation of SL molecules on MPA-CdTe QDs. Consequently, when SL was wrapped around QDs, large aggregates were observed with an average diameter larger than 100 nm that also matched with the value obtained from TEM images (Fig. 3.3(d)).

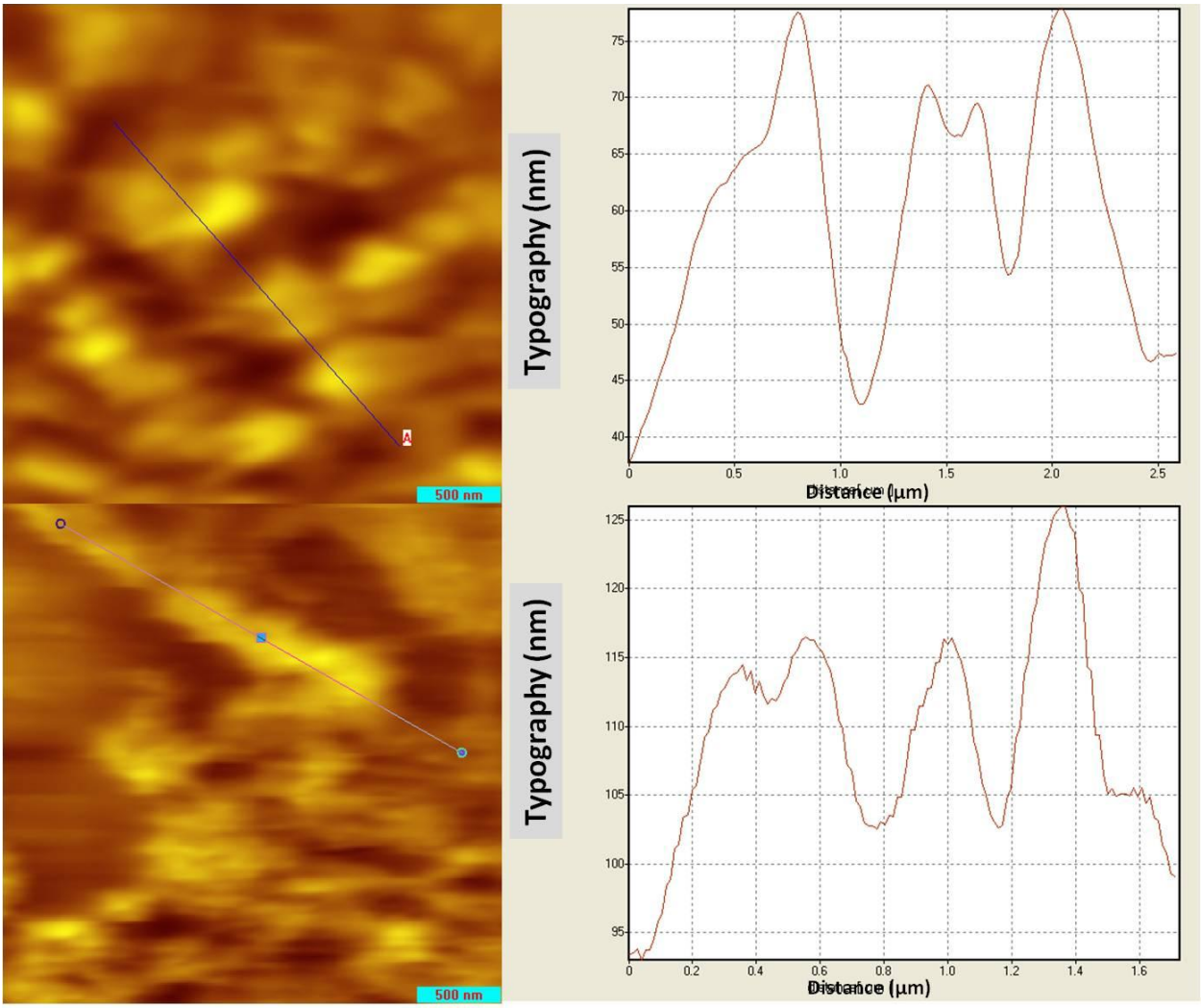

Fig. 3.9. AFM images of CdTe-MPA (a) and CdTe-SL(b) QDs respectively

3.7 Cytotoxicity assay

The cytotoxicity of sophorolipid capped CdTe particles on MCF-7 and NIH3T3 was assessed by MTT (3-(4,5-dimethylthiazol-2-yl)-2,5-diphenyltetrazolium bromide) assay. For MTT assay, cells were seeded at the density of 10^4 cells/ well in 96 well plates and incubated for 12-16 hs at 37º C before starting the treatment. Cells were treated with increasing concentration of sophorolipid capped CdTe QDs (in the range of 0.01µg/ ml to 10µg/ ml) and incubated for 48 hs. At the end of incubation period, MTT solution was added to a final concentration of 0.05mg/$_{mL}^{-1}$ to each well and incubated in dark at 37°C for 4 h. Formazan crystals were dissolved by adding 100 mL DMSO to each well and the optical absorbance was measured at 540 nm on a plate reader. The readings in untreated cells were considered to be 100% viable as shown in

Figure.3.10.. The cells were also exposed to physically mixed CdTe and SL with increasing concentration of SL keeping the MPA-CdTe concentration constant for comparison with chemically linked SL-CdTe QDs.

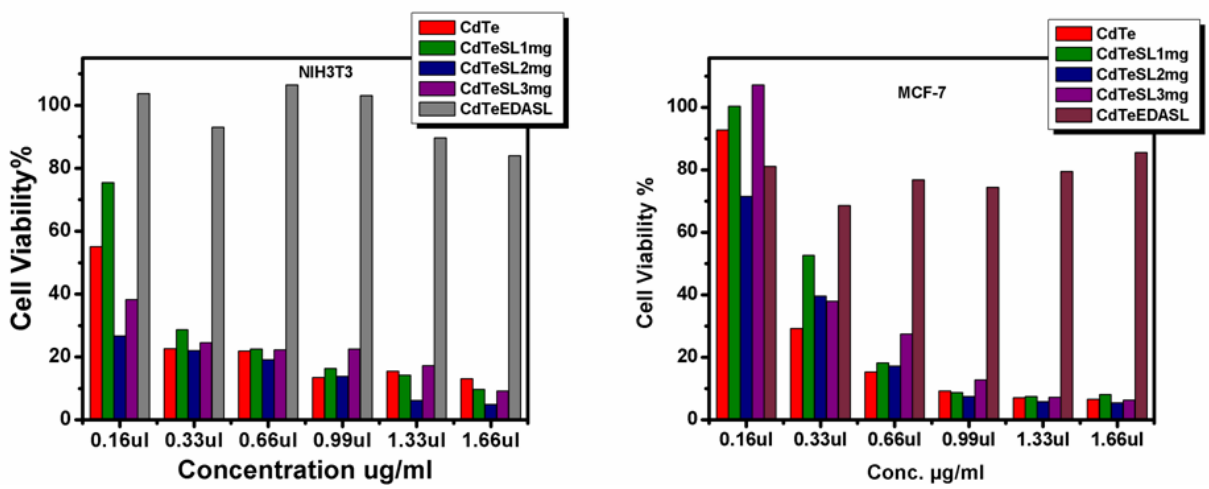

Figure. 3.10. MTT assay of CdTe-MPA and CdTe-SL on NIH3T3 and MCF-7 cell lines respectively

3.8 Bioimaging studies

To study the general use of SL capped CdTe QDs as diagnostic probes, we used them to detect MCF-7 cell line. The cells were cultured in their respective appropriate medium and were incubated with the fluorescent SL-CdTe QDs for 30 min. Figure. 3.11. shows the confocal microscopy images, obtained at an excitation wavelength of 405 nm. It was clearly observed that the SL-CdTe QDs are specifically present inside the cytosol around the nucleus as shown in Fig 8c. The cells incubated with SL-CdTe QDs were compared with cells incubated with MPA-CdTe (positive control, see Fig. 3.11 b) and only cells (negative control) without any probe (Fig 3.11a). In case of MPA-CdTe incubated cells, fluorescence was observed all over on the cell surface whereas in case of SL-CdTe QDs incubated cells, particles are entering inside the cells specifically in the cytosol, and no particle fluorescence was observed on the cell surface. SL on the QD surface is actually aiding in the entry of particle inside the cells.

3.9 Cellular internalisation studies

We studied the uptake and cellular localization of SL-CdTe QDs in live ThP-1 cells. 50µg of SL-

CdTe was added into the media along with ThP-1 cells, which was then allowed to incubate for different time periods till 1 h in order to assess their potentiality as a diagnostic tool for biological imaging as well as their ability to penetrate cell membrane. Figure 3.9a shows that SL-CdTe are present inside the cells after co-incubation time of only 5 min. Z-stack was done to ensure that particles are present in the cells as shown in Fig 3.12b. Distribution of SL QDs is more visible inside the cytoplasm after extended co-incubation of 15 min and 60 min (Fig 3.12c and 3.12d, respectively).

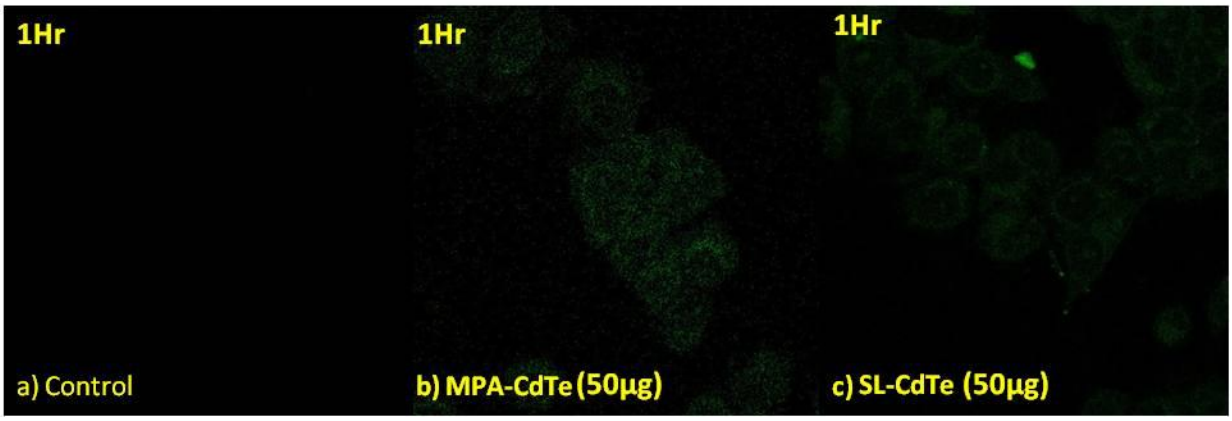

Figure.3.11. MCF-7 cells a) control b) with MPA-CdTe (50µg) SL-CdTe (50µg)

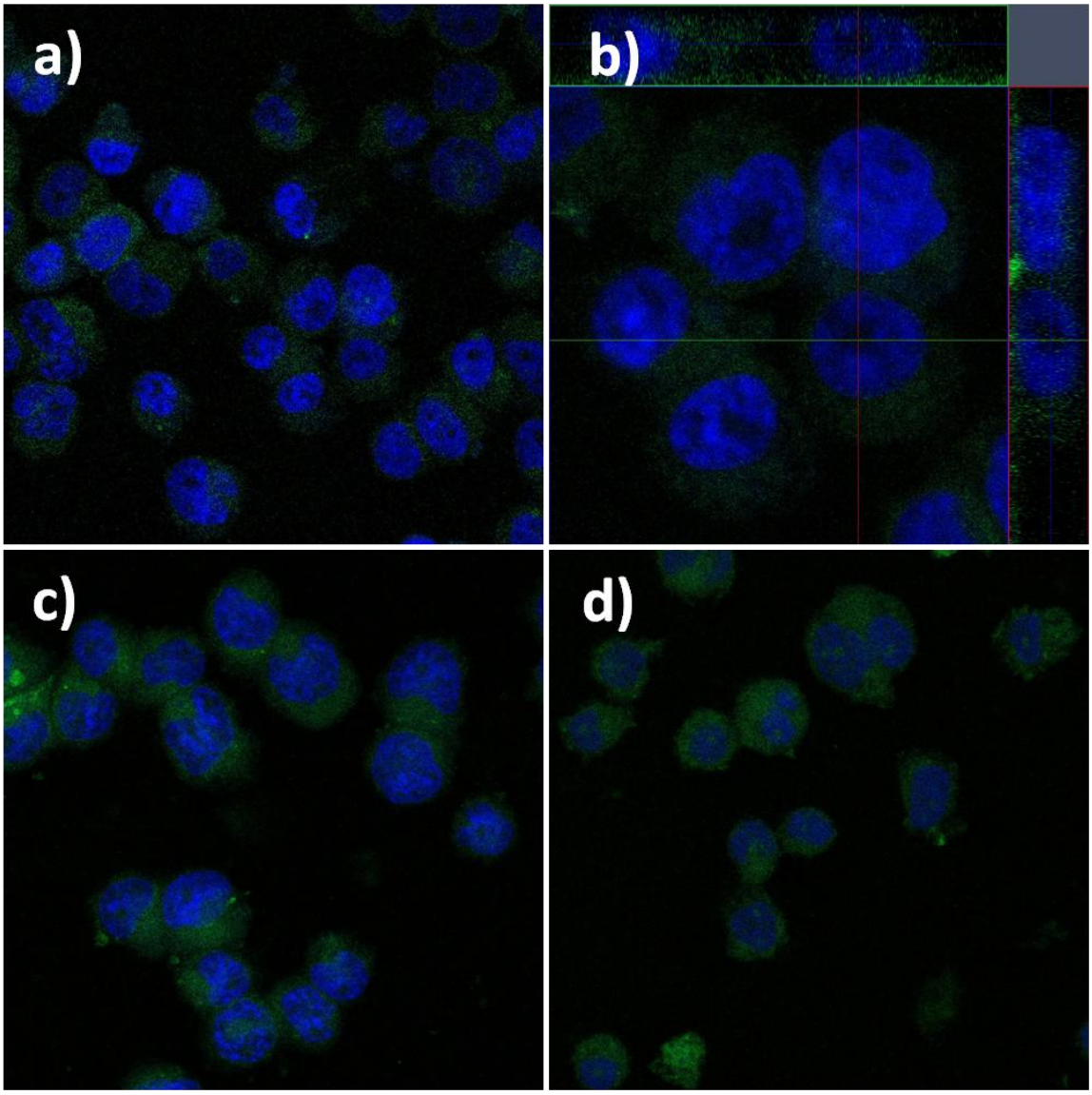

Figure.3.12. Confocal microscopy images of ThP-1 cells after co-incubation of SL-CdTe in media for different time period a) 5 min, b) Z- stacking of the latter, c) 15 min, and d) 60 min incubation

Conclusion

The CdTe QDs and SL functionalised CdTe QDs were successfully synthesized by using organo-metallic technique. The water solubility, and fluroscence properties remain unchanged after surface functionalization with SLs. Confocal studies showed their enhanced cellular association and their uptake. The synthesized SL capped CdTe QDs tested for their biocompatibility in both normal and cancer cell line. It is shown that the SL capped CdTe QDs become biocompatible in both the cell lines we have tested on. Thus we have made fluorescent quantum dots capped with sophorolipid which enhanced the cellular association and their uptake. which is also showing almost 100% viability in case of NIH3T3 cell lines and in case of MCF-7 it is showing only 65% viability, clearly indicating that composites are not just providing a mode to diagnose but at the same time killing cancer cell lines but absolutely safe for other control cell line i.e. NIH3T3, thus we can conclude that we have made a composite particle which has a high potential as a theranostic weapon.

References;

1. A. P. Alivisatos, *Science*, 1996, **271**, 933-937.
2. A. L. Rogach, N. Gaponik, J. M. Lupton, C. Bertoni, D. E. Gallardo, S. Dunn, N. Li Pira, M. Paderi, P. Repetto, S. G. Romanov, C. O'Dwyer, C. M. Sotomayor Torres and A. Eychmüller, *Angewandte Chemie International Edition*, 2008, **47**, 6538-6549.
3. S. Coe, W.-K. Woo, M. Bawendi and V. Bulovic, *Nature*, 2002, **420**, 800-803.
4. H. Lili, Q. Donghuan, J. Xi, L. Yanshan, W. Li, C. Junwu and C. Yong, *Nanotechnology*, 2006, **17**, 4736.
5. S. A. McDonald, G. Konstantatos, S. Zhang, P. W. Cyr, E. J. D. Klem, L. Levina and E. H. Sargent, *Nat Mater*, 2005, **4**, 138-142.
6. T. Xu and Q. Qiao, *Energy & Environmental Science*, 2011, **4**, 2700-2720.
7. Y. Zhou, M. Eck and M. Kruger, *Energy & Environmental Science*, 2010, **3**, 1851-1864.
8. M. Bruchez, M. Moronne, P. Gin, S. Weiss and A. P. Alivisatos, *Science*, 1998, **281**, 2013-2016.
9. M. E. Davis, Z. Chen and D. M. Shin, *Nat Rev Drug Discov*, 2008, **7**, 771-782.
10. O. C. Farokhzad and R. Langer, *ACS Nano*, 2009, **3**, 16-20.
11. X. Gao, Y. Cui, R. M. Levenson, L. W. K. Chung and S. Nie, *Nat Biotech*, 2004, **22**, 969-976.
12. I. L. Medintz, H. T. Uyeda, E. R. Goldman and H. Mattoussi, *Nat Mater*, 2005, **4**, 435-446.
13. Z. Yue, F. Lisdat, W. J. Parak, S. G. Hickey, L. Tu, N. Sabir, D. Dorfs and N. C. Bigall, *ACS Applied Materials & Interfaces*, 2013, **5**, 2800-2814.
14. W. W. Yu, L. Qu, W. Guo and X. Peng, *Chemistry of Materials*, 2004, **16**, 560-560.
15. X. Gao, L. Yang, J. A. Petros, F. F. Marshall, J. W. Simons and S. Nie, *Current Opinion in Biotechnology*, 2005, **16**, 63-72.
16. M. Green, H. Harwood, C. Barrowman, P. Rahman, A. Eggeman, F. Festry, P. Dobson and T. Ng, *Journal of Materials Chemistry*, 2007, **17**, 1989-1994.
17. N. Lewinski, V. Colvin and R. Drezek, *Small*, 2008, **4**, 26-49.
18. C. Zhang, R. J. Macfarlane, K. L. Young, C. H. J. Choi, L. Hao, E. Auyeung, G. Liu, X. Zhou and C. A. Mirkin, *Nat Mater*, 2013, **12**, 741-746.

19. R. Di Corato, A. Quarta, P. Piacenza, A. Ragusa, A. Figuerola, R. Buonsanti, R. Cingolani, L. Manna and T. Pellegrino, *Journal of Materials Chemistry*, 2008, **18**, 1991-1996.
20. T. Pellegrino, L. Manna, S. Kudera, T. Liedl, D. Koktysh, A. L. Rogach, S. Keller, J. R√§dler, G. Natile and W. J. Parak, *Nano Letters*, 2004, **4**, 703-707.
21. N. Zhan, G. Palui, H. Grise, H. Tang, I. Alabugin and H. Mattoussi, *ACS Applied Materials & Interfaces*, 2013, **5**, 2861-2869.
22. K. D. Wegner, P. T. Lanh, T. Jennings, E. Oh, V. Jain, S. M. Fairclough, J. M. Smith, E. Giovanelli, N. Lequeux, T. Pons and N. Hildebrandt, *ACS Applied Materials & Interfaces*, 2013, **5**, 2881-2892.
23. Y. Zhang, X. Ke, Z. Zheng, C. Zhang, Z. Zhang, F. Zhang, Q. Hu, Z. He and H. Wang, *ACS Nano*, 2013, **7**, 3896-3904.
24. R. Glenns and D. Cooper, *J Amer Oil Chem Soc*, 2006, **83**, 137-145.
25. I. A. Van Bogaert, K. Saerens, C. De Muynck, D. Develter, W. Soetaert and E. Vandamme, *Appl Microbiol Biotechnol*, 2007, **76**, 23-34.
26. I. K. A P F Turner, G S Wilson, *Theory and application of calorimetric sensors in biosensors*, New York: Oxford University Press, 1987.
27. V. D'Britto, H. Kapse, H. Babrekar, A. A. Prabhune, S. V. Bhoraskar, V. Premnath and B. L. V. Prasad, *Nanoscale*, 2011, **3**, 2957-2963.
28. S. Singh, P. Patel, S. Jaiswal, A. A. Prabhune, C. V. Ramana and B. L. V. Prasad, *New Journal of Chemistry*, 2009, **33**, 646-652.
29. N. Baccile, R. Noiville, L. Stievano and I. V. Bogaert, *Physical Chemistry Chemical Physics*, 2013, **15**, 1606-1620.
30. T. Fang, K. Ma, L. Ma, J. Bai, X. Li, H. Song and H. Guo, *The Journal of Physical Chemistry C*, 2012, **116**, 12346-12352.
31. P. K. Singh, R. Mukherji, K. Joshi-Navare, A. Banerjee, R. Gokhale, S. Nagane, A. Prabhune and S. Ogale, *Green Chemistry*, 2013, **15**, 943-953.
32. L. Qu and X. Peng, *Journal of the American Chemical Society*, 2002, **124**, 2049-2055.

CHAPTER 4 (a)

Glucose oxidase conjugated H_2O_2 sensitive CdTe QDs: an effective fluorescence tool for glucose sensing

Water-soluble quantum dots (QDs) are extensively used for molecular sensing because of the flexibility they offer in terms of modification of the QDs surface with a variety of functional groups using thiol chemistry and monitoring by fluorescence intensity. We describe a simple assay that allows the photoluminescence (PL) detection of H_2O_2 and glucose in aqueous samples and demonstrate its applicability by estimating glucose in blood. To enable the glucose detection, we functionalized the 3-mercaptopropanoic acid (MPA) capped CdTe QDs with glucose oxidase (GOx), the enzyme specific to b-D-glucose, using carbodiimide chemistry. The fluorescence of the GOx-functionalized CdTe QDs was quenched on the interaction with glucose. The same photoluminescence quenching was also observed in gel form, when a GOx modified CdTe QDs loaded agarose gel was dipped in H_2O_2 and glucose solutions, respectively.

4.1 Introduction

H_2O_2 detection is of critical importance in the fields of food, chemistry, biology, clinical control, and environmental protection. [1] H_2O_2 is one of the most important and widely used analytes in electrochemical analysis, since it is an intermediate of biological reactions and an oxidant in industry and municipal wastewater treatment. [2] Over the last few decades, many techniques have been employed to determine H_2O_2, such as titrimetry, [3] spectrometry, [4] electrochemistry, [5,6] and luminescence. [7–9]] Although these methods have the practical advantages of sensitivity and specificity, they also have several disadvantages, such as difficult or time-consuming operating procedures. Thus, rapid, sensitive, and cost-effective approaches for the detection of H_2O_2 are of significant importance. More recently, optical sensing approaches have attracted the immense attention of many researchers owing to their intrinsic sensitivity, high selectivity and simplicity. Based on the photoluminescence quenching of QDs by H_2O_2, there are plenty of strategies that have been applied for using QDs to detect H_2O_2. [10–13] These reports have indicated that monitoring the optical changes of the QDs photoluminescence by H_2O_2 may provide a simple method to develop a QD-based photoluminescence probe, an extremely sensitive H_2O_2 optical detector. On the other hand the glucose level in blood is used as a clinical indicator of diabetes. According to the World Health Organization, over 150 million people in the world were affected with diabetes in the year 2004 and it is expected to climb further to 366 million by 2030. The affected population has to be tested for blood glucose levels daily for an effective treatment. Glucose oxidase generates H_2O_2 as a product in its reaction with glucose. In fact, the biocatalyzed generation of H_2O_2 by oxidases was used for the development of different electrochemical biosensors, and recently for the development of optical biosensors using Au nanoparticles. [14] Until now, many glucose-assay methods, such as surface plasmon resonance (SPR) spectroscopy, [15] fluorescence signal transmission, [16, 17] and electrochemical signal transduction, [18, 19] have been reported for the determination of blood glucose. Among these, the widely used commercial glucose test employs electrochemical sensors, and is based on an amperometric electrode at which the glucose concentration is monitored by a change in the current flow caused by the enzyme converting glucose into gluconic acid and hydrogen peroxide. However, these sensors are prone to interference by other electro active species such as ascorbate and ureate in biological systems. In contrast to the electrochemical sensing method, the fluorescence-assay method is highly

selective and non-destructive, and has been extensively as well as exclusively used for glucose detection. Recently Zhai et al. reported a highly sensitive glucose sensor based on Pt nanoparticle/polyaniline hydrogel heterostructures. [20] Cao et al. showed a considerable enhancement of glucose oxidase (GOx) activity and thermal stability when conjugated with CdTe QDs. [21] Recently, Radhakumary and group presented a naked eye detection of glucose in a urine sample, using glucose oxidase immobilized gold nanoparticles. [14]

There has been an ever-increasing demand for the development of simple, cost-effective methodologies in an easy to read out format, for the detection of clinically relevant molecules to aid in diagnosis. Such approaches are extremely important, particularly in third world countries, where high technology diagnostics aids are inaccessible to the bulk of the population, mainly amongst the low socio-economic classes. As quantum dots (QDs) are bright fluorescence emitters, having high quantum yields, high molar extinction coefficients, size dependent tunable emission and a high photostability, [22–25] these attractive fluorescent properties prompt a wide interest in developing QD-based sensors for biological detection and imaging. Again, as numerous oxidases generate hydrogen peroxide (H_2O_2) as a product, [26] controlling the photophysical properties of QDs by H_2O_2 may provide a new and versatile method to develop QD-based sensors. To introduce simple, cost effective methodologies for the detection of clinically relevant molecules to aid diagnosis, here we demonstrate a simple CdTe QDs based fluorescent tool for sensitive and selective H_2O_2 and glucose sensing. This sensitivity enables the synthesis of glucose oxidase immobilized on CdTe QDs for the detection of glucose. Herein, we report the conjugation of GOx, the enzyme specific to b-D-glucose, onto 3-mercaptopropionic acid (MPA) capped water soluble CdTe QDs, using carbodiimide chemistry and their use in the photoluminescence detection of H_2O_2, as well as glucose. The synthesized glucose oxidase conjugated CdTe QDs were incorporated into agarose powder to form a highly stable fluorescent hydrogel, and it was observed that the photoluminescence property was quenched instantly when immersed into a glucose solution. The photoluminescence quenching was also observed significantly with a human blood sample. The overall synthetic protocol and reaction mechanism is schematically given below (Scheme 1).

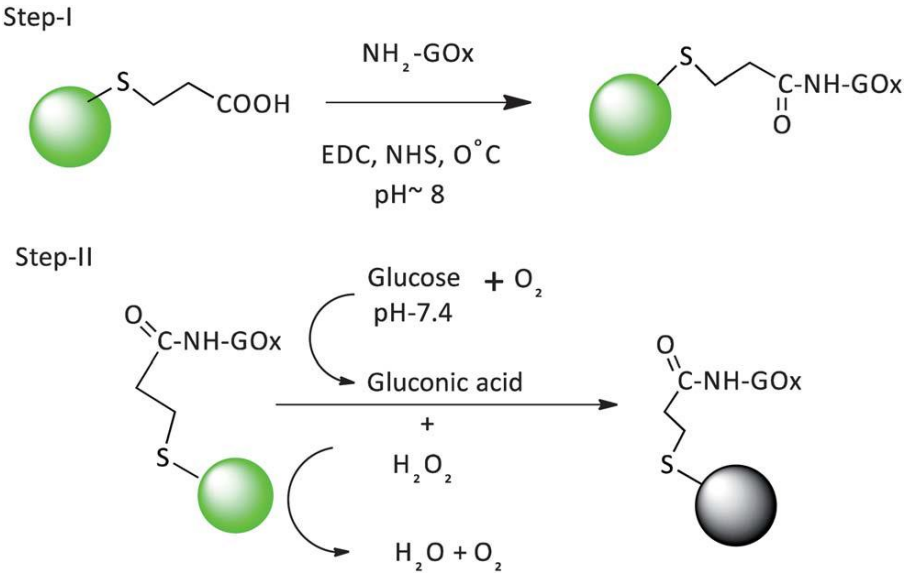

Scheme 1. Synthetic route for the conjugation of GOx on MPA–CdTe QDs (Step I) and reaction mechanism of CdTe–GOx QDs on interaction with glucose (Step II)

4.2 Materials and methods

Cadmium chloride ($CdCl_2$), tellurium powder (Te) and sodium borohydride ($NaBH_4$) (SD Fine Chemicals Limited, India), 3-mercaptopropanoic acid (MPA) (Sigma Aldrich, India), ammonium hydroxide (NH_4OH) (Merck Laboratories, India), hydrogen peroxide (50% w/v) (Merck Laboratories, India) and glucose oxidase (GOx) (Sigma Aldrich, India), 1-ethyl-3-(3-dimethylaminopropyl)carbodiimide (EDC) (Spectrochem Private Limited India), N-hydroxysuccinimide (NHS) (Sisco Research Laboratories India), agarose powder (Merck Laboratories, India) were used as obtained. Isopropanol and acetone (Merck Laboratories, India) were used as received. Deionized water was acquired from a Millipore Milli-Q system.

4.2.1 Preparation of water soluble MPA capped CdTe QDs (CdTe–MPA)

3-Mercaptopropanoic acid stabilized CdTe QDs were synthesised using an organometallic route.[27] In brief, NaHTe was prepared just before starting the CdTe QDs synthesis by reacting $NaBH_4$ and Te powder in a molar ratio of 3 : 1. A round bottom flask was flushed with N_2 and then 0.5 mL N_2 purged water was added to it, through a syringe. Te powder (3.0 mmol) was mixed with $NaBH_4$ in water under nitrogen saturated conditions. The reaction was carried out at

room temperature under a nitrogen flow with the magnetic stirring of 150 rpm for 25–30 min. The reaction was stopped when the black Te powder was completely reduced and the solution turned transparent pink in color. This freshly prepared NaHTe solution was hot injected (100 $^{\circ}$C) to a N_2 saturated solution of $CdCl_2$ (15 mM) and MPA (36 mM) at pH 9. This solution was then refluxed under a nitrogen flow for 2 h at 100 $^{\circ}$C. The CdTe QDs solution was cooled to room temperature and precipitated with acetone and washed with water to remove Na^+ ions and unbound MPA. The solution was centrifuged at 10, 000 rpm for 10 min at room temperature. The pellet was collected, which was comprised of CdTe QDs and was dried with a rotary evaporator. The resulting solid CdTe QDs were readily redispersed in water, resulting in a clear solution.

4.2.2 Conjugation of GOx on MPA capped CdTe QDs (CdTe–GOx QDs)

The conjugation of CdTe QDs with GOx was done on the basis of EDC/NHS chemistry via the formation of an amide linkage between the carboxyl groups of the MPA and the primary amine groups of the GOx. The thiolated CdTe QDs (100 mg in 20 mL of distilled water) were activated with 5 mL of a mixture of 0.26 mmol (40 mg) EDC and 0.05 mmol (8 mg) NHS in distilled water at pH 7.0 by incubating the mixture at room temperature for 30 min. Then, 4 mg of a GOx solution (4 mg mL^{-1} of water) was added to the above mixture and then kept overnight at 4 $^{\circ}$C. Acetone was used to precipitate the CdTe–GOx QDs. The precipitate was washed with water and reprecipitated with acetone. After centrifugation at 10,000 rpm, the GOx immobilized CdTe QDs (CdTe–GOx) were suspended in 10 mL of distilled water and kept at 4 $^{\circ}$C until use.

4.2.3 Immobilization of CdTe–GOx QDs into agarose

2 mg CdTe–GOx QDs was mixed with 8 mg agarose powder in 2 mL of doubly distilled water and was heated to obtain a clear homogeneous solution. The solution was then drop cast into a small circular glass mold which was then allowed to cool to room temperature to obtain the CdTe–GOx QDs immobilized agarose hydrogel.

4.2.4 Photoluminescence spectroscopy study (PL)

The photoluminescence measurements were performed on a Perkin-Elmer LS 55 spectrophotometer. All the samples were prepared in distilled water, as well as PBS (pH 7.4). The initial concentration of the CdTe–GOx for all the experiments was kept constant i.e. 1 mgL^{-1}

4.2.5 Transmission electron microscopy (TEM)

The transmission electron microscopy (TEM) images were obtained on a model JEOL 1200 EX. The CdTe–MPA QDs colloid and CdTe–GOx QDs colloid were diluted 1000-fold with distilled H_2O, deposited onto a 200 mesh copper grid coated with a Formvar film and were dried overnight.

4.2.6 Fourier transform infrared spectroscopy (FTIR)

The FT-IR spectra of the CdTe–MPA QDs and CdTe–GOx QDs were recorded in the range 600–4000 cm_1 on Perkin-Elmer Spectrum One B spectrophotometer. 2 mg of the QDs was mulled with 5 mg KBr and dried under an IR lamp.

4.2.7 Hydrodynamic size and zeta potential determination

The technique of dynamic light scattering was used to determine the hydrodynamic radii of the conjugate nanoparticles ,as well as in the presence of different concentrations of glucose. The hydrodynamic radii were measured on a Brookhaven Instrument (BIC – Brookhaven Instrument Corporation) 90 Plus size analyzer at a 90 ◦C angle using 100 mg $mL^{-}1$ water based particle suspensions. All the measurements were performed at a fixed angle of 90° at 25 °C. The zeta potential as a function of the magnitude of the electric potential and the stability of the nanoparticles dispersed in water, were measured using a Zetasizer model 3000HS, Malvern, UK. The zeta potential of a particle is the overall surface charge that the particle acquires in a particular medium and was also measured using the same instrument at 25 °C.

4.2.8 Atomic force microscopy (AFM)

For a further validation of the morphology of the CdTe–GOx QDs, with and without glucose, the CdTe–GOx QDs were dissolved in distilled water and were drop cast onto a clean silica substrate for atomic force microscopy (AFM) analysis. The samples were air-dried overnight and were imaged in the contact mode with a PPP-NCH probe atomic force microscope. AFM with a RHK

Technology, USA (SPM 100) was employed for the surface characterization. The AFM images were quantified the Picoview software (version 1.2.4) provided with the microscope.

4.2.9 Selectivity of the method

The selectivity of the method was investigated by checking the PL absorption maxima of the CdTe–GOx QDs on their interaction with ascorbic acid and uric acid in the range 20–100 mg mL-1. To confirm the precision and recovery of the probe, each set of experiments were carried out in triplicate, and similar results within a maximum error of 2–3% were obtained.

Fig. 3 Visual and under UV light pictures (a) CdTe–GOx QDs, (b) CdTe–GOx QDs on reacting with 100 mgmL^{-1} glucose and (c) CdTe–GOx QDs loaded agarose gel (LHS); with glucose (RHS).

4.3 Results and Discussion

The basic mechanism of a QDs based glucose sensor is schematically shown in Scheme 1. Glucose oxidase (GOx) oxidizes glucose to gluconic acid and produces H_2O_2 in the presence of oxygen. The product of the reaction; H_2O_2, directly affect the photoluminescence of the CdTe QDs. In order to verify the quenching activity of H_2O_2 on the fluorescence intensity of the CdTe–GOx, we examined the effect of H_2O_2 directly on the CdTe–GOx by the addition of H_2O_2, shown in Fig.4.1. It was show that the photoluminescence of the CdTe–GOx QDs quenched periodically with an increasing concentration of H_2O_2, in both water and PBS buffer (pH-7.4). 100 mL of 50% H_2O_2 was dissolved in 9900 mL of a H_2O–buffer and used as a stock H_2O_2 solution for the PL study.

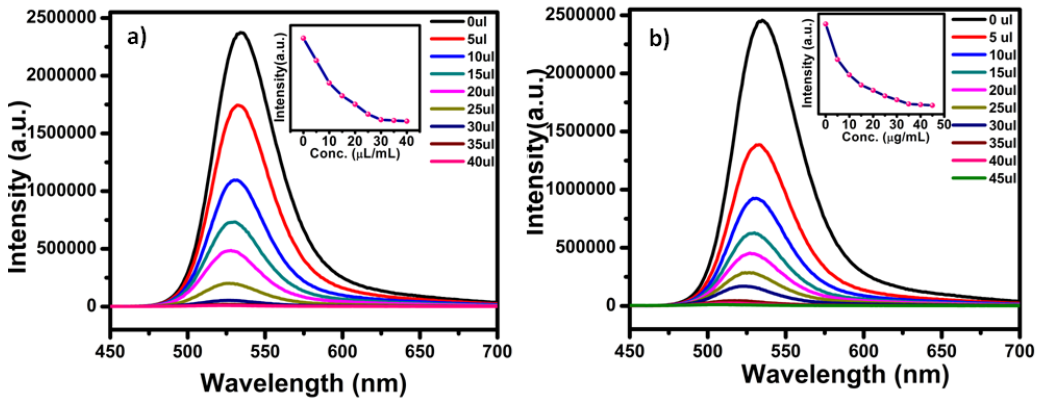

Fig.4.1 Photoluminescence spectra of GOx conjugated CdTe QDs with increasing concentration of H_2O_2 carried out in (a) water and (b) PBS buffer (inset is the respective graphical relationship of the PL intensity against an increasing concentration of H_2O_2).

A similar result is observed with the addition of glucose to the CdTe–GOx QDs (1 mg mL^{-1}) to both water and a PBS buffer solution. On adding a varied amount of glucose (from 20 to 260 mg mL^{-1}), the photoluminescence of the CdTe–GOx QDs was found to be quenched with an increasing concentration of glucose, thus reflecting the formation of H_2O_2 generated due to the reaction between glucose with the glucose oxidase of the CdTe–GOx QDs. The reaction was instant, and no incubation time was required between the glucose and the CdTe–GOx QDs. The corresponding spectra are shown in Fig.4. 2. The dependence of the intensity at 560 nm as a function of the glucose concentration is shown as an inset in each case. The limit of detection of glucose in water and the PBS buffer was measured to be 20 mg mL^{-1} and 40 mg mL^{-1}, respectively and the range for glucose detection was from 20 mg mL^{-1} to 260 mg mL^{-1} in distilled water and from 40 mg mL^{-1} to 140 mg mL^{-1} in the PBS buffer solution. In the most common practical application of glucose detection for the diagnosis of a diabetic condition, a linearity of such dependence is required up to about 400 mg dL^{-1}, which corresponds to 4000 mg mL^{-1}.28 Since the CdTe–GOx concentration used for recording the data of Fig.4. 2 was only 1 mg mL^{-1}, it seems to become almost saturated, for a glucose concentration of about 300 mg mL^{-1} or more. Hence, to explore the detectivity and linearity up to a much higher glucose concentration of 4000 mg mL^{-1} as desired in practical applications, we examined the PL data for a CdTe–GOx concentration of 10 mg mL^{-1}. The corresponding PL variation as a function of the glucose concentration up to 700 mg dL^{-1} (or 7000 mg mL^{-1}) is shown in Fig. 4.2(c). A good linear dependence is observed, as desired. 1 mg mL^{-1} of a CdTe–GOx QD solution was prepared in water and 100 mg mL^{-1} of a glucose solution was then added to it, to observe the visual and photoluminescence changes in solution. Similarly, the CdTe–GOx QDs immobilized into an agarose gel were dipped into the same concentration of glucose solution. The fluorescence of both the solution and agarose gel before and after the glucose addition are shown in Fig.4.3. It was observed that the photoluminescence of the CdTe–GOx QDs was quenched in the presence of glucose (100 mg mL^{-1}) in both the solution and gel form. A visual change was also observed with the naked eye.

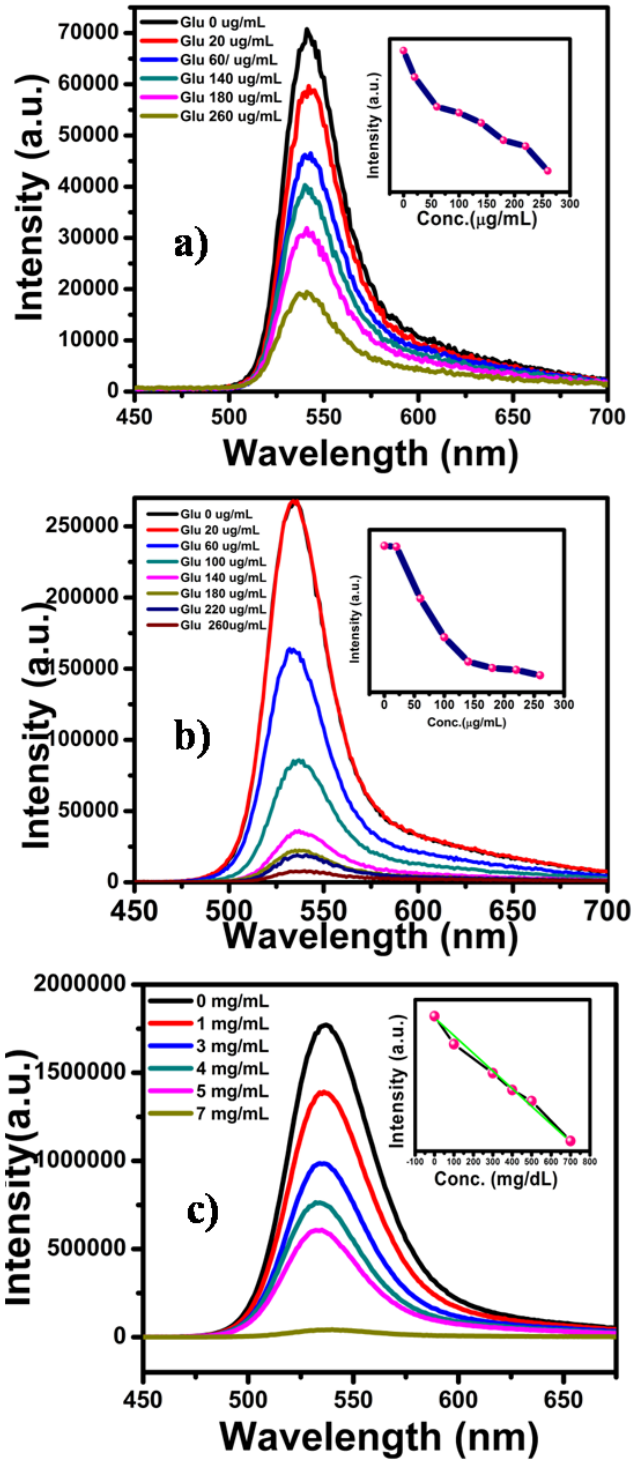

Fig. 4.2 Photoluminescence spectra of GOx conjugated CdTe with increasing concentration of glucose in (a) water as well as (b) PBS buffer (inset is the respective graphical relationship of PL intensity against increasing concentration of glucose) (c) PL spectra of CdTe–GOx (10 mg mL^{-1})

with various concentrations of glucose from 1 mg to 7 mg and inset is the corresponding calibration curve (intensity vs. concentration of glucose).

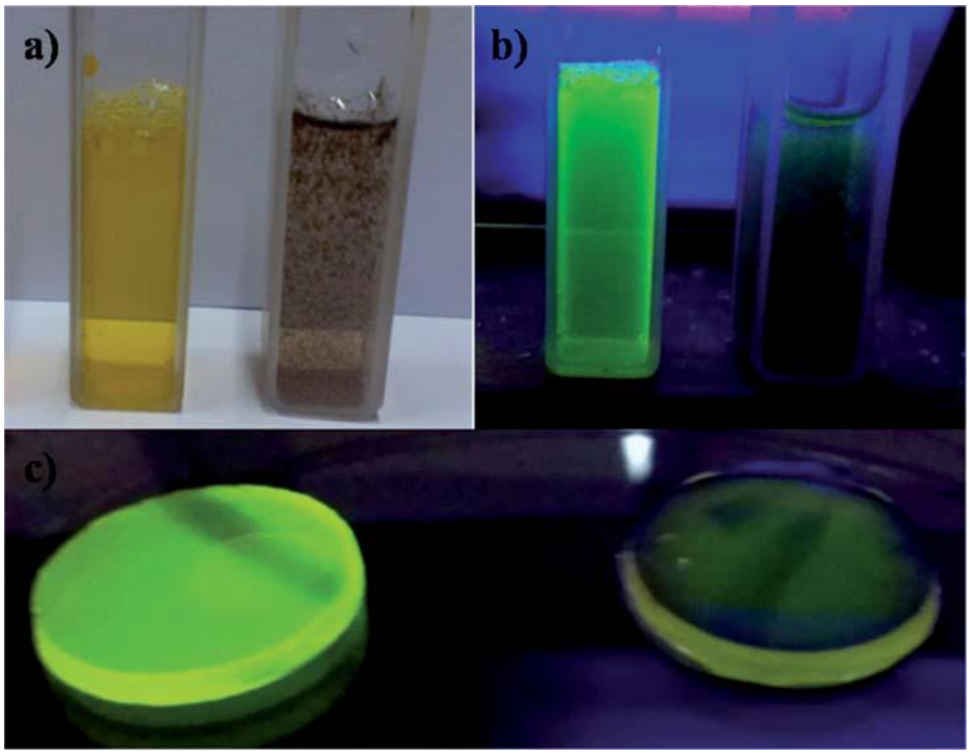

Fig.4.3 Visual and under UV light pictures (a) CdTe–GOx QDs, (b) CdTe–GOx QDs on reacting with 100 $mgmL^{-1}$ glucose and (c) CdTe–GOx QDs loaded agarose gel (LHS); with glucose (RHS).

4.4 TEM and high resolution transmission electron microscopy (HRTEM) analysis

We measured the size of the particles using TEM analysis. Fig.4.4(a) shows the size of the MPA capped CdTe QDs is 4 nm. The size remains unchanged after the GOx conjugation with MPA capped CdTe QDs (Fig. 4.4(b)). Fig. 4.4(c) and (d) display the sizes of the GOx functionalized CdTe QDs on interaction with 50 and 100 mg of glucose, respectively and aggregates of QDs were observed in both cases. The HRTEM images of the MPA–CdTe QDs, CdTe–GOx QDs and CdTe–GOx QDs on interaction with 50 and 100 mg of glucose are shown in the inset in their respective images. In all the cases the lattice fringes with a d-line spacing of 0.37 nm, which correspond to the (111) plane of a face centered cubic phase of the CdTe QDs, are seen.

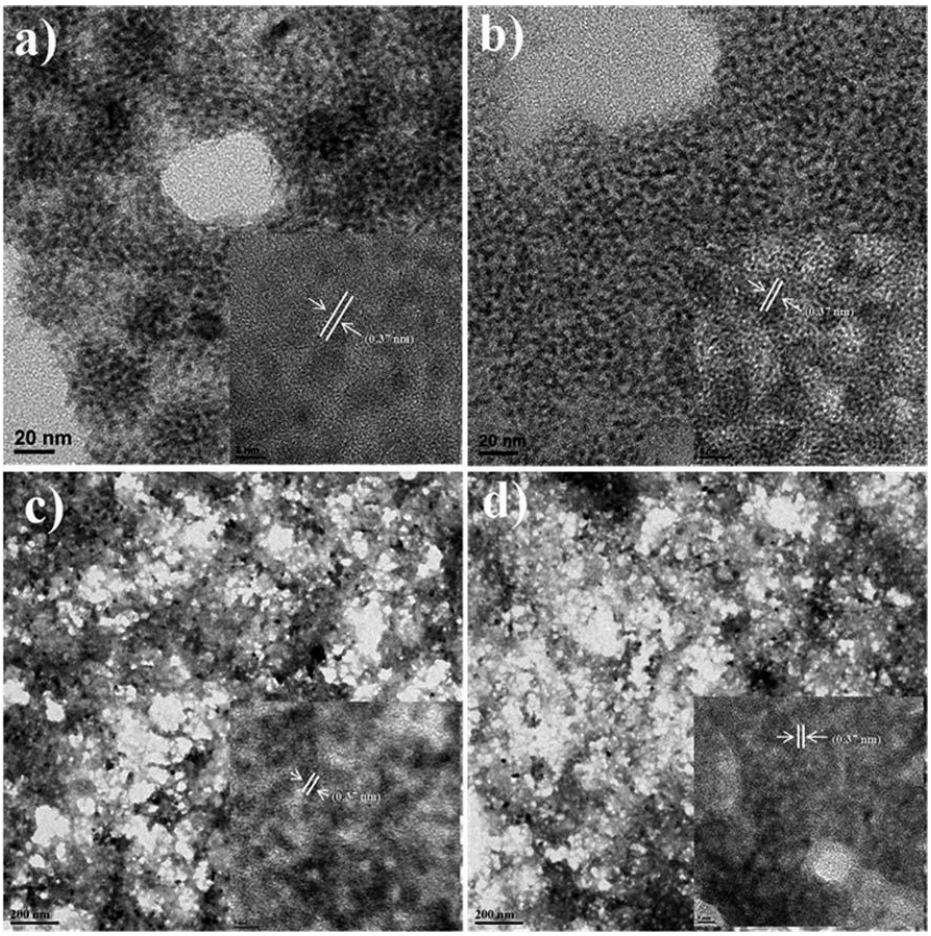

Fig. 4.4 TEM and HRTEM (inset) of (a) CdTe–MPA (b) CdTe–GOx (c) CdTe–GOx with 50 mg mL^{-1} of glucose (d) CdTe–GOx with 100 mg mL^{-1} of glucose.

4.5 Dynamic light scattering studies

Information on hydrodynamic size of CdTe–MPA, CdTe– GOx and CdTe–GOx with 50 and 100 mg mL^{-1} of glucose is given in Table 1. The average hydrodynamic size of the MPA capped CdTe QDs was 8 nm, which increased to 51 nm, on conjugation with GOx. On adding 50 mg mL^{-1} glucose, the hydrodynamic size was increased to 94 nm and the size was further increased to 114 nm on the addition of 100 mg mL^{-1} glucose, showing the tendency toward the formation of aggregates. The surface charge also became reduced with the addition of glucose from -48 mV to -14 mV because of the glucose interference on the surface of the CdTe–GOx QDs (shown in Table 1)

Sample	Hydrodynamic size (nm)	Zeta Potential (mV)
CdTe-MPA	08	-67
CdTe-GOx	51	-48
CdTe-GOx-Glu (50µg/mL)	95	-26
CdTe-GOx-Glu (100µg/mL)	114	-14

Table 4.1. Hydrodynamic size and Zeta potential of - CdTe-MPA, CdTe-GOx, CdTe-GOx-Glu (50µg/mL) and CdTe-GOx-Glu (100µg/mL)

4.6 Fourier transformed infrared spectroscopy (FTIR)

We recorded FT-IR spectra of the nanoparticles to get a further insight on the surface modification. The MPA capped CdTe QDs showed peaks at 1560 and 1367 cm^{-1} corresponding to the C=O and CH_2 bending frequencies, respectively, of the MPA molecule. The GOx conjugated CdTe–MPA showed intense peaks at 1650 and 1565 cm^{-1} typical of the amide I (–C=O) and amide II (N–H bending) bands of GOx. A broad peak at 3278 cm^{-1} was assigned to the N–H/O–H stretching frequency of the GOx and a peak at 2971 cm^{-1} corresponds to the CH_2 stretching of the GOx moiety. MPA capped CdTe QDs showed peaks at 1560 and 1367 cm^{-1} corresponds to C=O and CH_2 bending frequencies respectively of MPA molecule. GOx conjugated GNPs showed intense peaks at 1650 and 1565 cm^{-1} typical of amide I (-C=O) and amide II (N-H bending) bands of the GOx and a The broad peak at 3278 cm^{-1} was assigned the N-H/O-H stretching frequency of GOx and peak at 2971cm^{-1} corresponds to CH_2 stretching of GOx moiety.

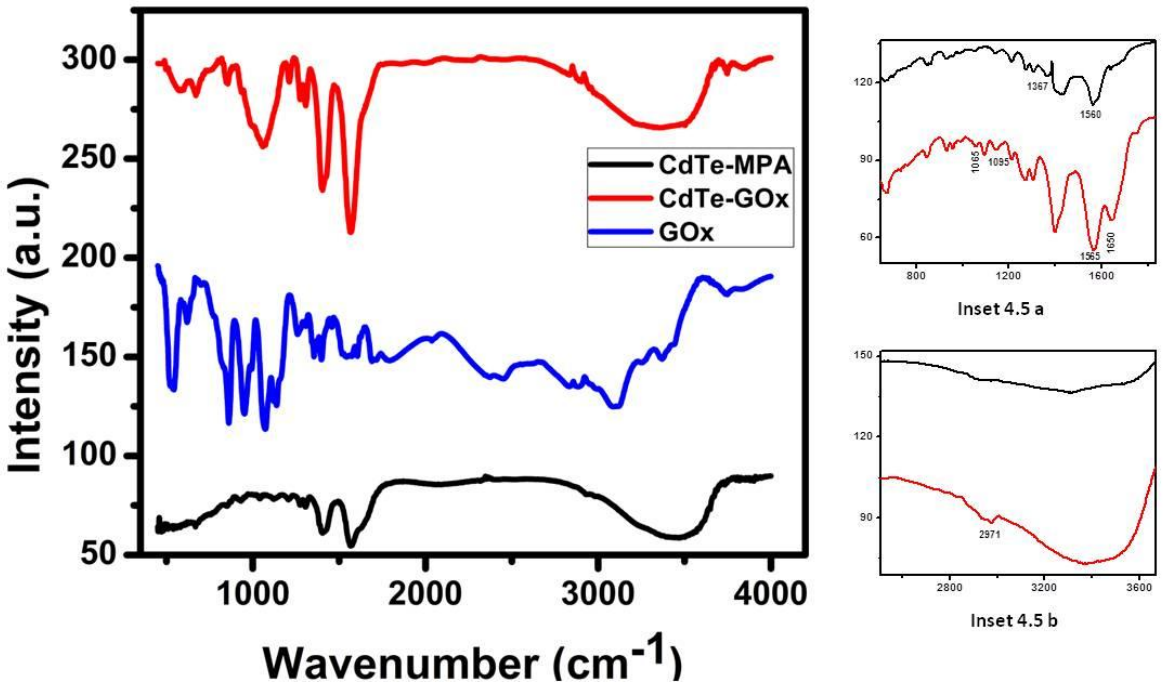

Figure. 4.5 shows the FTIR spectra of CdTe-MPA QDs (black), CdTe-GOx QDs (red) and Gox (blue) Inset 4.5 a shows the enlarged version of graph of Fig 4.5 X axis (Wavenumber-800-1600 cm^{-1}), Y-axis (Intensity- 60 -120 a.u.) and Inset 4.5 b (Wavenumber- 2000-3400 cm^{-1}), Y-axis (Intensity- 90 -150 a.u)

4.6 Atomic Force Microscopy (AFM) imaging and Force measurements

To observe the surface morphology of the CdTe–GOx QDs and to identify the aggregation with the addition of glucose into the CdTe–GOx QDs, atomic force microscopy (AFM) was used. The AFM images of the CdTe–GOx QDs before the addition of glucose (Fig. 4.6(a)) shows that their diameters are mainly distributed around 100 nm. The topographic heights are between 3.5 and 5.0 nm. Consequently, it can be concluded that most of the CdTe–GOx QDs are single layered, monodispersed particles. When glucose was introduced, large aggregates formed, with almost unchanged heights and an average diameter larger than 30 nm (Fig. 4.6(b)).

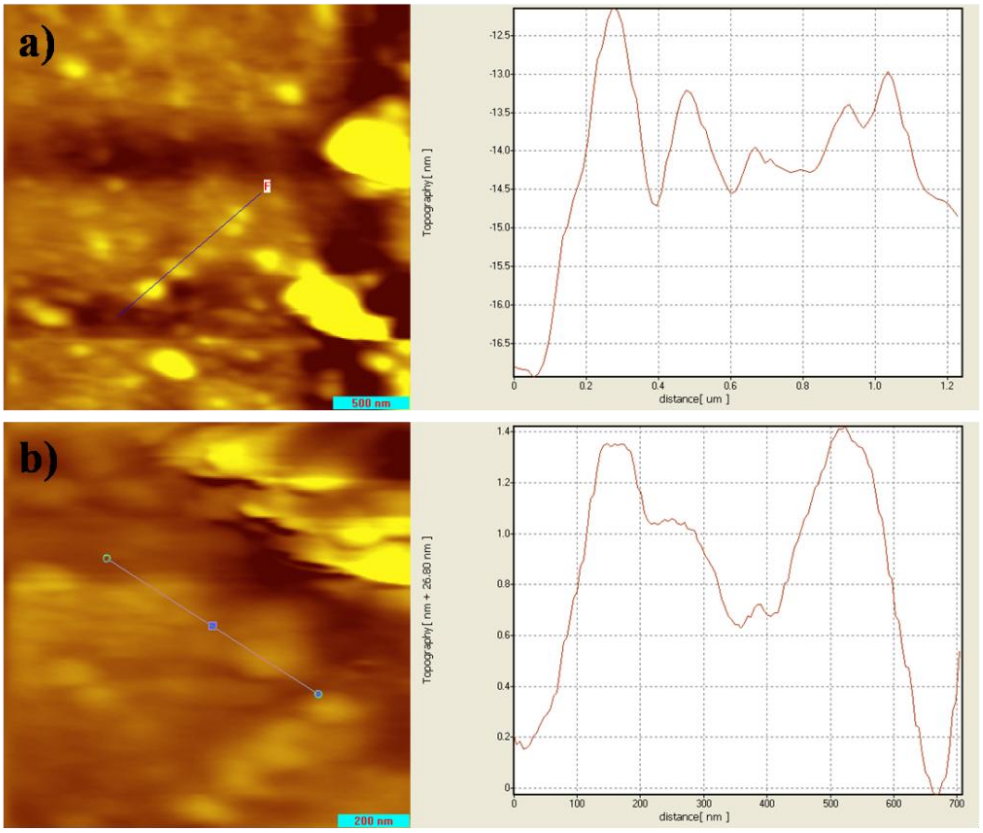

Figure.4.6. AFM images of CdTe-GOx QDs before (a) and after glucose addition respectively

4.7 Selectivity and cross reactivity test

To check the cross reactivity and selectivity of the CdTe–GOx QDs, we conducted the following studies. As ascorbic acid and uric acid are major components of human blood, we performed a photoluminescence study of the CdTe–GOx QDs with increasing concentrations of ascorbic acid and uric acid. The results showed that the fluorescence intensity remains unchanged with the addition of these compounds (shown in Fig. 4.7(a) and (b) respectively). In the case of uric acid addition, PL intensity quenching (25%) observed with the addition of 100 mg mL^{-1} of uric acid, whereas no significant photoluminescence quenching was observed with the addition of 100 mg mL^{-1} of ascorbic acid. These results confirmed that the GOx functionalized CdTe QDs were highly specific to glucose and had no interference with any other molecules present in the blood.

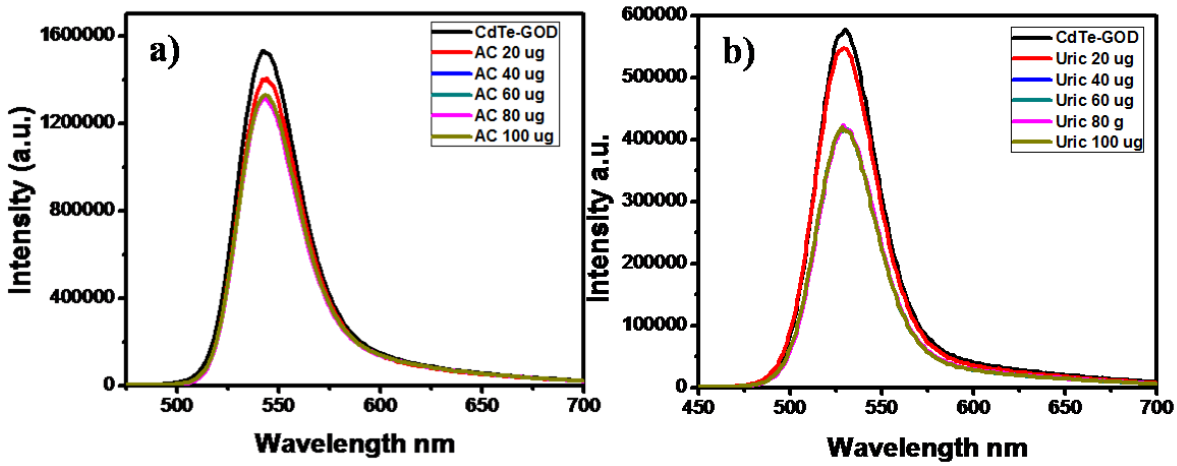

Figure.4.7. Photoluminescence spectra of GOx conjugated CdTe with increasing concentration of a) Ascorbic acid and b) Uric acid in water.

4.8 Photoluminescence studies with blood samples

We also carried out the glucose sensing with blood collected from four different individuals and from there we optimized that our CdTe-GOx sensor can sense glucose even in 10uL of blood as shown in Figure S2 and S3. We also optimized the amount of serum required to observe a significant change in the PL intensity, as shown in Fig. 7.

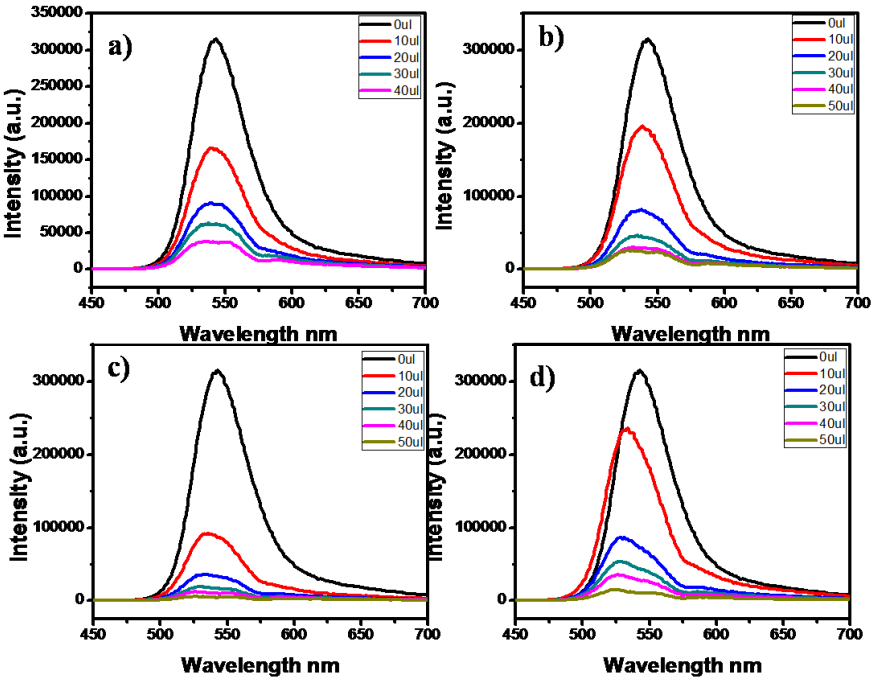

Figure 4.8. Photoluminescence spectra of GOx conjugated CdTe with human blood samples.

(a-Sample1, b-Sample-2, c-Sample-3, d-Sample4)

The calibration curve of the PL intensity against the blood serum amount is plotted in Fig. 7, which shows, with the addition of 10 mL of blood, the intensity of the CdTe–GOx was significantly quenched.

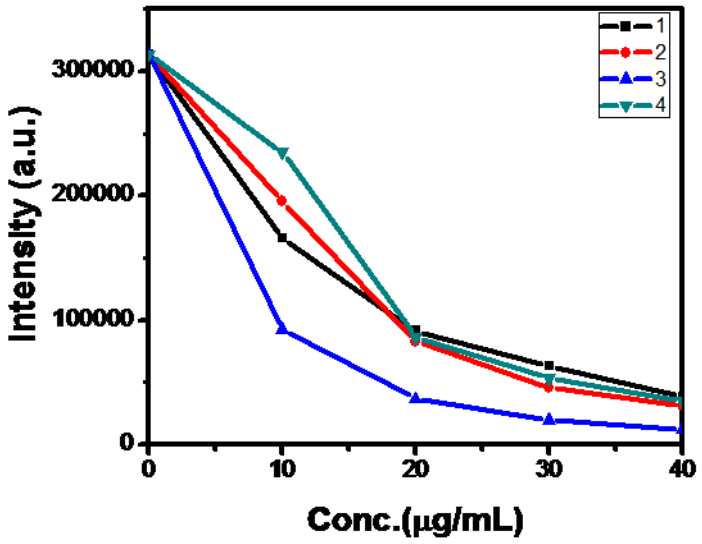

Fig. 4.9. Calibration curve for all the blood samples tested for glucose sensing (a-d)

Conclusion

We have devised a simple method for the detection of glucose in blood samples using GOx functionalized CdTe QDs. The color of the solution was found to change from red to brown in the presence of 20 mg mL^{-1} of glucose in water. The fluorescence intensity was quenched with the addition of glucose and the same result was observed when the CdTe–GOx QDs were incorporated in an agarose gel and then exposed to a glucose solution. This showed the feasibility of the method for the quantitative measurement of glucose in blood. The color change observable with the naked eye can advantageously be used for a preliminary screening in the home, ahead of referral for more focused investigations. The method seems to have potential, particularly for the rural population in third world countries.

References :

1. W. Chen, S. Cai, Q.-Q. Ren, W. Wen and Y.-D. Zhao, *Analyst*, 2012, 137, 49–58.

2. X. Cao, Z. Zeng, W. Shi, P. Yep, Q. Yan and H. Zhang, *Small*, 2013, 9, 1703–1707.

3. E. C. Hurdis and H. Romeyn, *Anal. Chem*., 1954, 26, 320–325.

4. C. Matsubara, N. Kawamoto and K. Takamura, *Analyst*, 1992, 117, 1781–1784.

5. R. P. Singh and A. C. Pandey, *Anal. Methods*, 2011, 3, 586–592.

6. Y.-C. Gao, K. Xi, W.-N. Wang, X.-D. Jia and J.-J. Zhu, *Anal. Methods*, 2011, 3, 2387–2391.

7. B. C. Dickinson and C. J. Chang, *J. Am. Chem. Soc*., 2008, 130, 9638–9639.

8. M. Zayats, R. Baron, I. Popov and I. Willner, *Nano Lett.*, 2005, 5, 21–25.

9. L. Lin, Y. Wen, Y. Liang, N. Zhang and D. Xiao, *Anal. Methods*, 2013, 5, 457–464.

10. Z. Yue, W. Zhang, C. Wang, G. Liu and W. Niu, *Mater. Lett*., 2012, 74, 180–182.

11. R. Gill, L. Bahshi, R. Freeman and I. Willner, *Angew. Chem*., 2008, 120, 1700–1703.

12. B. Tang, L. Cao, K. Xu, L. Zhuo, J. Ge, Q. Li and L. Yu, *Chem.– Eur. J*., 2008, 14, 3637–3644.

13. S.-N. Ding, J.-J. Xu and H.-Y. Chen, *Chem. Commun*., 2006, 3631–3633.

14. C. Radhakumary and K. Sreenivasan, *Anal. Chem*., 2011, 83, 2829–2833.

15. K. Aslan, J. R. Lakowicz and C. D. Geddes, *Anal. Chem*., 2005, 77, 2007–2014.

16. G. Blagoi, N. Rosenzweig and Z. Rosenzweig, *Anal. Chem*., 2005, 77, 393–399.

17. R. Ballerstadt and J. S. Schultz, *Anal. Chem*., 2000, 72, 4185– 4192.

18. C. Hou, Q. Xu, L. Yin and X. Hu, *Analyst*, 2012, 137, 5803–5808.

19. X.-C. Dong, H. Xu, X.-W. Wang, Y.-X. Huang, M. B. Chan- Park, H. Zhang, L.-H. Wang, W. Huang and P. Chen, *ACS Nano*, 2012, 6, 3206–3213.

20. D. Zhai, B. Liu, Y. Shi, L. Pan, Y. Wang, W. Li, R. Zhang and G. Yu, ACS Nano, 2013, 7, 3540–3546.

21. L. Cao, J. Ye, L. Tong and B. Tang, *Chem.–Eur. J*., 2008, 14, 9633–9640.

22. H. Yao, Y. Zhang, F. Xiao, Z. Xia and J. Rao, *Angew. Chem.*, Int. Ed., 2007, 46, 4346–4349.

23. F. Patolsky, R. Gill, Y. Weizmann, T. Mokari, U. Banin and I. Willner, *J. Am. Chem. Soc*., 2003, 125, 13918–13919.

24. I. L. Medintz, A. R. Clapp, F. M. Brunel, T. Tiefenbrunn, H. Tetsuo Uyeda, E. L. Chang, J. R. Deschamps, P. E. Dawson and H. Mattoussi, *Nat. Mater*., 2006, 5, 581– 589.

25. P. T. Snee, R. C. Somers, G. Nair, J. P. Zimmer, M. G. Bawendi and D. G. Nocera, *J. Am. Chem. Soc.*, 2006, 128, 13320–13321.

26. I. Karube, A. P. F. Turner and G. S. Wilson, Theory and application of calorimetric sensors in biosensors, Oxford University Press, New York, 1987.

27. T. Fang, K. Ma, L. Ma, J. Bai, X. Li, H. Song and H. Guo, *J. Phys. Chem. C*, 2012, 116, 12346–12352.

28 S. Singh and M. McShane, Biosens. Bioelectron., 2011, 26, 2478–2483.

CHAPTER 4 (b)

A Development of highly efficient, specific and rapid fluorescence based sensor for Cholesterol sensing

Water-soluble quantum dots (QDs) are extensively used for molecular sensing because of the flexibility they offer in terms of modification of the QDs surface with a variety of functional groups using thiol chemistry and monitoring by fluorescence intensity. We describe a simple assay that allows the photoluminescence (PL) detection of cholesterol in aqueous samples and demonstrate its applicability by estimating cholesterol in blood. To enable the cholesterol detection, we functionalized the 3-mercaptopropanoic acid (MPA) capped CdTe QDs with cholesterol oxidase (ChOx), the enzyme specific to cholesterol using carbodiimide chemistry. The fluorescence of the ChOx functionalized CdTe QDs was quenched on the interaction with cholesterol.

4A1. Introduction

As per available literature people with risk of cholesterol related cardiovascular disease (death)in India are estimated to be 1.25 million and Global estimate amount to 10.00 million deaths [WHO data, 2012]. The present lifestyle and food habits contribute towards the increase in cholesterol levels. This problem would inflate in the forth coming decades thus creating a major concern for human health. An easy, fast and accurate method for determination of cholesterol will assist in monitoring cholesterol levels. Cholesterol assessment is vital in diagnostics and management of hypercholesterolemia, associated with pathological conditions like atherosclerosis, cardiovascular diseases, coronary artery diseases and transient ischemic heart attacks [Hwang et al., 2012]. This has directed research in developing various cholesterol biosensors. These biosensors are principled on either enzymatic and non-enzymatic reaction of cholesterol with the sensor. [Arya et al., 2007; Solanki et al., 2009; Brahim et al., 2001; Srivastava et al., 2000]. The underlying principle for enzymatic biosensors is derived from traditional spectrophotmetric detection of cholesterol. Cholesterol oxidase (ChOx) is used as a biosensing element during fabrication of these biosensors. The enzyme oxidizes cholesterol to cholest-4en-3one and H_2O_2 [Ahn and Sampson, 2004]. The amount of H_2O_2 released is sensed to estimate the cholesterol level

$$\text{Cholesterol} + O_2 \xrightarrow{\text{Cholesterol Oxidase}} \text{cholest-4en-3one} + H_2O_2$$

In amperometric system, the electro oxidation current of hydrogen peroxide is measured after application of suitable potential to the system [Trukarslan et al.,2009]. The glitch with this system is overestimation of the response current due to inferring molecules like ascorbic and uric acid [Sean et al., 2001; Hooda and Pundir, 2008]. Also other electrochemically active species present in the sample will get oxidized due to the application of high anodic potential supplied to the system, leading to amplification of the signals [Saxena et al., 2011]. Another concern with these sensors is the immobilization of ChOx. The Immobilization techniques is prone to microbial attack, reduction in substrate and enzyme interaction due to steric hindrance, leaching of enzymes, long response time, metabolite interference and low storage stability [Hooda et al., 2009]. Also during immobilization process of the catalytic activity reduces due random orientation and partial denaturation of ChOx [Sarma et al., 2009].

In recent years, quantum dots with tremendous luminescent properties have received augmented interest because of their application in several sectors of fundamental and scientific significance [Bruchez et al., 1998; chen et al., 2000]. Guifen et al., 2007 has developed a CdS nanoparticle based electrochemiluminescence (ECL) sensor for detection of Low Density Lipoprotein (LDL). In this technique, quenching of ECL signals occur by binding of LDL to the sensor. It acts as a barrier for transfer of electrons between solution species and the electrode. The fabrication of the electrode is complex and bulky. In this paper, we explore the relevance of controlling the photophysical properties of QDs by H_2O_2 [Yue et al., 2012; Gill et al., 2008; Tang et al., 2008] to provide a new and versatile method for faster, simple and efficient detection of cholesterol. We demonstrate a simple CdTe QDs based fluorescent tool for sensitive and selective H_2O_2 and cholesterol sensing. This is carried out by the conjugation of ChOx enzyme onto 3-mercaptopropionic acid (MPA) capped water soluble CdTe QDs, using carbodiimide chemistry for photoluminescence detection.

4A.2 Materials and Methods

4A.2.a Reagents

Cadmium chloride ($CdCl_2$), tellurium powder (Te) and sodium borohydride ($NaBH_4$) (SD Fine Chemicals Limited, India), 3-mercaptopropanoic acid (MPA) (Sigma Aldrich, India), ammonium hydroxide (NH_4OH) (Merck Laboratories, India), hydrogen peroxide (50% w/v) (Merck Laboratories, India) and Cholesterol oxidase (ChOx) (Sigma Aldrich, India), 1- ethyl-3-(3-dimethylaminopropyl)carbodiimide (EDC) (Spectrochem Private Limited India), N-hydroxysuccinimide (NHS) (Sisco Research Laboratories India), were used as obtained. Isopropanol and acetone (Merck Laboratories, India) were used as received. Deionized water was acquired from a Millipore Milli-Q system.

4A.2.b Preparation of water soluble MPA capped CdTe QDs (CdTe–MPA)

3-Mercaptopropanoic acid stabilized CdTe QDs were synthesized using an organometallic route.27 In brief, NaHTe was prepared just before starting the CdTe QDs synthesis by reacting NaBH4 and Te powder in a molar ratio of 3 : 1. A round bottom flask was flushed with N_2 and then 0.5 mL N_2 purged water was added to it, through a syringe. Te powder (3.0 mmol) was mixed with $NaBH_4$ in water under nitrogen saturated conditions. The reaction was carried out at

room temperature under a nitrogen flow with the magnetic stirring of 150 rpm for 25–30 min. The reaction was stopped when the black Te powder was completely reduced and the solution turned transparent pink in color. This freshly prepared NaHTe solution was hot injected (100^0 C) to a N_2 saturated solution of $CdCl_2$ (15 mM) and MPA (36 mM) at pH 9. This solution was then refluxed under a nitrogen flow for 2 h at 100 C. The CdTe QDs solution was cooled to room temperature and precipitated with acetone and washed with water to remove Na^+ ions and unbound MPA. The solution was centrifuged at 10000 rpm for 10 min at room temperature. The pellet was collected, which was comprised of CdTe QDs and was dried with a rotary evaporator. The resulting solid CdTe QDs were readily redispersed in water, resulting in a clear solution.

4A.2.c. Conjugation of ChOx on MPA capped CdTe QDs (CdTe–ChOx QDs)

The conjugation of CdTe QDs with ChOx was done on the basis of EDC/NHS chemistry via the formation of an amide linkage between the carboxyl groups of the MPA and the primary amine groups of the ChOx. The thiolated CdTe QDs (100 mg in 20 mL of distilled water) were activated with 5 mL of a mixture of 0.26 mmol (40 mg) EDC and 0.05 mmol (8 mg) NHS in distilled water at pH 7.0 by incubating the mixture at room temperature for 30 min. Then, 4 mg of a ChOx solution (4 mg mL^{-1} of water) was added to the above mixture and then kept overnight at 4^0 C. Acetone was used to precipitate the CdTe–ChOx QDs. The precipitate was washed with water and reprecipitated with acetone. After centrifugation at 10 000 rpm, the GOx immobilized CdTe QDs (CdTe–ChOx) were suspended in 10 mL of distilled water and kept at 4^0 C until use.

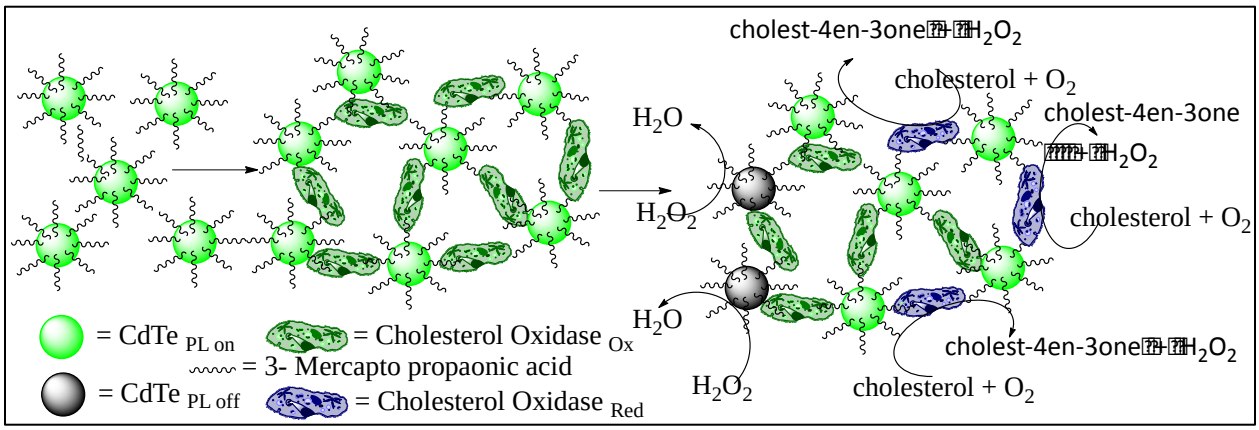

Scheme 1. Synthetic route for the conjugation of ChOx on MPA–CdTe QDs and reaction mechanism of CdTe–ChOx QDs on interaction with Cholesterol

4A.3. Photoluminescence spectroscopy study (PL)

The photoluminescence measurements were performed on a Perkin-Elmer LS 55 spectrophotometer. All the samples were prepared in distilled water, as well as PBS (pH 7.4). The initial concentration of the CdTe–ChOx for all the experiments was kept constant i.e. 1 $mgmL^{-1}$.

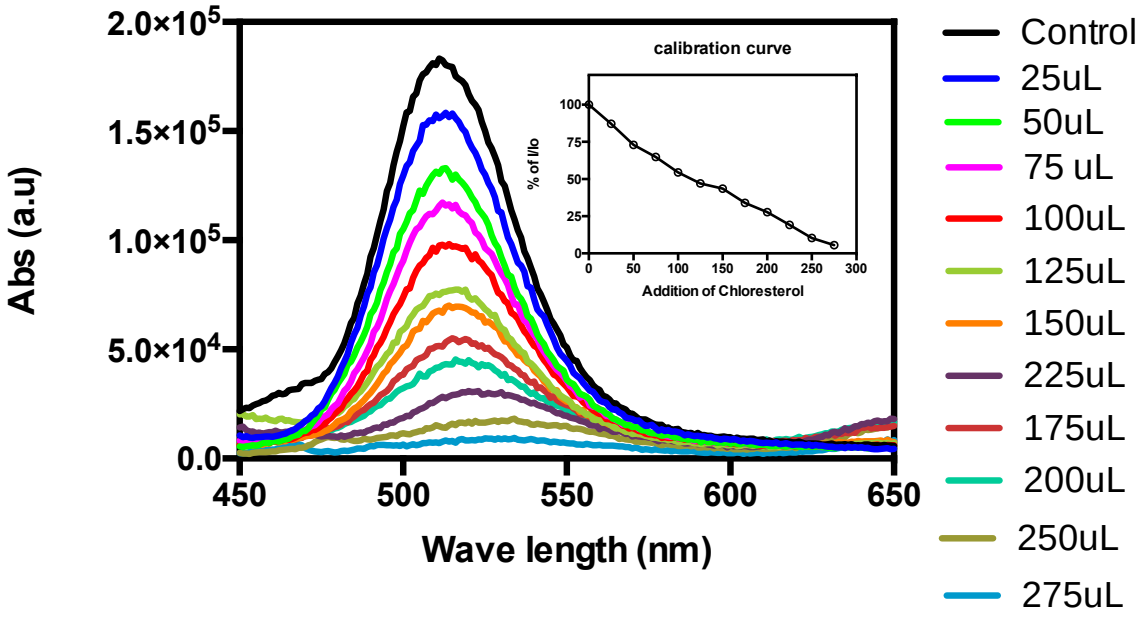

Figure.4A.1 *Photoluminescence spectra of ChOx conjugated CdTe with increasing concentration Cholesterol; inset is the corresponding calibration curve (intensity Vs Cholesterol concentration.*

4A.4. Transmission electron microscopy (TEM)

The transmission electron microscopy (TEM) images were obtained on a model JEOL 1200 EX. The CdTe–MPA QDs colloid and CdTe–ChOx QDs colloid were diluted 1000-fold with distilled H_2O, deposited onto a 200 mesh copper grid coated with a Formvar film and were dried overnight.

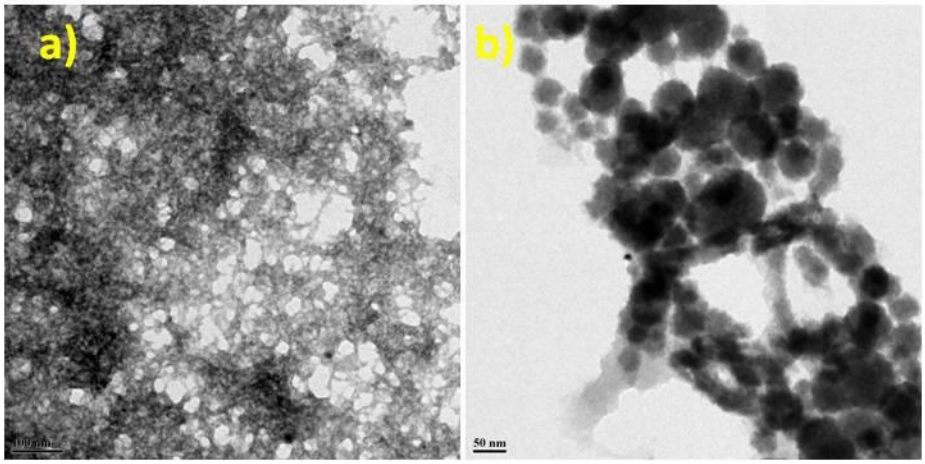

Figure.4A.2 TEM of (a) CdTe–MPA-ChOx (b) CdTe–MPA-ChOx with 4 mg mL^{-1} of cholesterol

4A.5. Hydrodynamic size and zeta potential determination

The technique of dynamic light scattering was used to determine the hydrodynamic radii of the conjugate nanoparticles, as well as in the presence of different concentrations of glucose. The hydrodynamic radii were measured on a Brookhaven Instrument (BIC – Brookhaven Instrument Corporation) 90 Plus particle size analyzer at a 90° angle using 100 mg mL^{-1} water based particle suspensions. All the measurements were performed at a fixed angle of 90^{O} at 25 ^{O} C. The zeta potential as a function of the magnitude of the electric potential and the stability of the nanoparticles dispersed in water, were measured using a Zetasizer model 3000HS, Malvern, UK. The zeta potential of a particle is the overall surface charge that the particle acquires in a particular medium and was also measured using the same instrument at 25 ^{O}C.

4A.6. Atomic force microscopy (AFM)

For a further validation of the morphology of the CdTe–ChOx QDs, with and without cholesterol, the CdTe–ChOx QDs were dissolved in distilled water and were drop cast onto a clean silica substrate for atomic force microscopy (AFM) analysis. The samples were air-dried overnight and were imaged in the contact mode with a PPP-NCH probe atomic force microscope. AFM with a RHK Technology, USA (SPM 100) was employed for the surface characterization. The AFM images were quantified using the Picoview software (version 1.2.4) provided with the microscope.

4A.7. Selectivity of the method

The selectivity of the method was investigated by checking the PL absorption maxima of the CdTe–ChOx QDs on their interaction with dopamine, ascorbic acid, uric acid, bile salts and bilirubin in the range 20–100 mg mL^{-1}. To confirm the precision and recovery of the probe, each set of experiments were carried out in triplicate, and similar results within a maximum error of 2–3% were obtained.

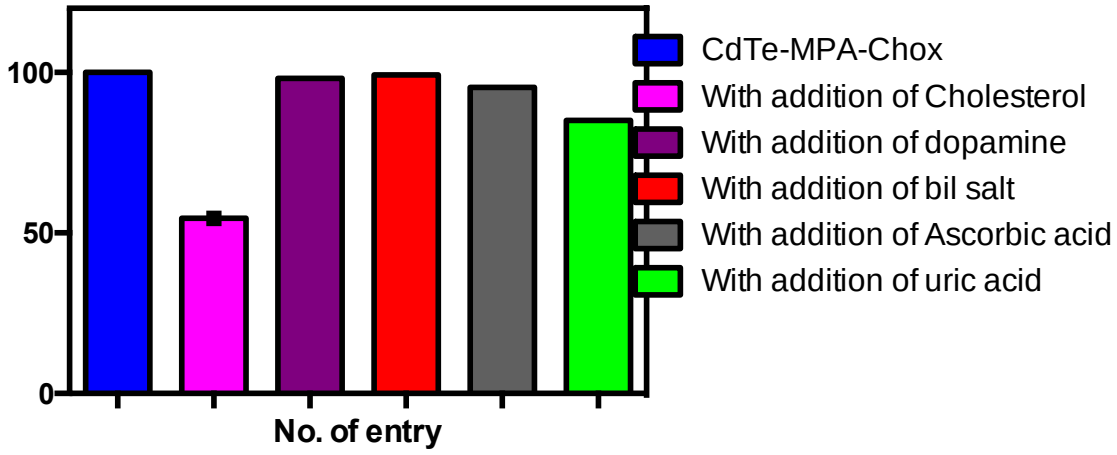

Figure.4A.3. Photoluminescence spectra of ChOx conjugated CdTe QDs with increasing concentration of Cholesterol, dopamine, bile salt, ascorbic acid and uric acid

Conclusion

We have devised a simple method for the detection of cholesterol in aqueous solvent using ChOx functionalized CdTe QDs. The color of the solution was found to change from red to brown in the presence of 4 mg mL^{-1} of cholesterol in water. The fluorescence intensity was quenched with the addition of cholesterol and the same result was observed when the CdTe–ChOx QDs were incorporated in an agarose gel and then exposed to a cholesterol solution. This showed the feasibility of the method for the quantitative measurement of Cholesterol in blood. The color change observable with the naked eye which may be used for a preliminary screening at home, ahead of referral for more focused investigations.

CHAPTER 4 (c)

Sensitive and selective detection of Bilirubin in blood using water soluble CdTe-quantum dot based bilirubin biosensor

We describe a simple assay that allows the photoluminescence (PL) detection of bilirubin in aqueous samples and demonstrate its applicability by estimating bilirubin in blood. To enable the bilirubin detection, we functionalized the 3-mercaptopropanoic acid (MPA) capped CdTe QDs with bilirubin oxidase (BiOx), the enzyme specific to bilirubin, using carbodiimide chemistry. The fluorescence of the BiOx-functionalized CdTe QDs was quenched on the interaction with bilirubin.

4B.1 Introduction

Bilirubin is an endogenous yellow colored waste material which is produced from the breakdown of hemoglobin molecules while clearing the old RBCs (red blood cells). Bilirubin is excreted from the body through bile and urine. Elevated amounts of bilirubin serves as a diagnostic markers of liver and blood disorders in adults as well as in newborn infants which causes hepatic disease, permanent damage to brain in severe cases which even results in death. [1, 2]

Bilirubin occurs as two major forms in human serum; conjugated bilirubin (Bc) and unconjugated bilirubin (Bu). Bc is non-covalently attached to serum albumin which gets dissociated on treatment with an organic solvent or detergent. It is a nonpolar, water insoluble molecule. In contrast, bilirubin conjugated with glucuronate is a polar, water-soluble compound that exists in plasma not bound to any protein.

Senescent RBCs are constantly processed in the macrophages of the liver and in the RES (reticulo-endothelial system) of spleen and bone marrow. Bilirubin is actually derived from heme present in hemoglobin which is released from the breakdown of RBCs. The heme is first converted to biliverdin which is further reduced to from bilirubin. Since bilirubin is extremely insoluble in water, when they are released in the blood from macrophages, they are bound to albumin, which reduces the concentration of free bilirubin (neurotoxic). Bilirubin enters into hepatocyte through hepatocyte cell membrane after dissociation from albumin. Inside hepatocyte, bilirubin is conjugated with glucuronic acid (bilirubin mono and di- glucuronide) with the aid of transferase in endoplasmic reticulum. This conjugated bilirubin (water soluble) then easily diffuses through cytoplasm and secreted into bile duct which is further excreted into the intestine with bile. [3].

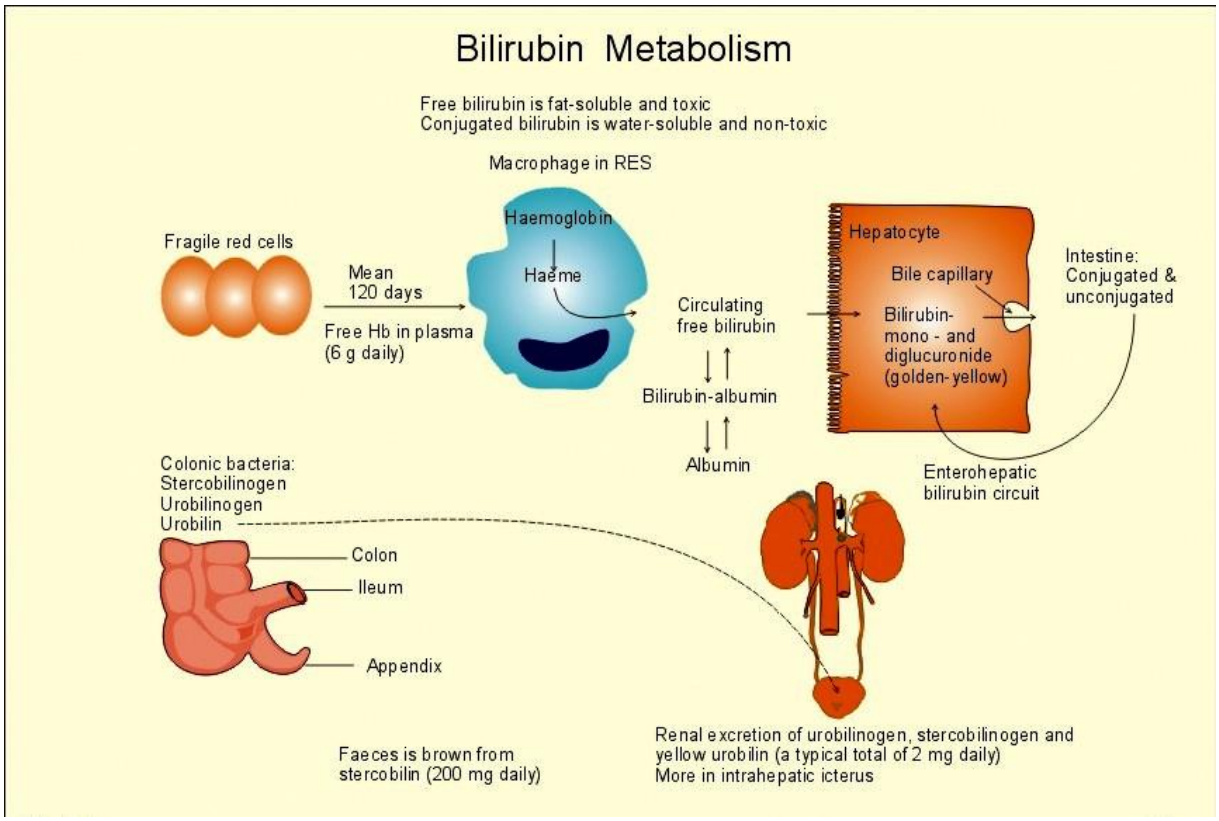

Figure.4B.1 Production and fate of bilirubin in human system

4B.2. Preparation of water soluble MPA capped CdTe QDs (CdTe–MPA)

3-Mercaptopropanoic acid stabilized CdTe QDs were synthesized using an organometallic route.27 In brief, NaHTe was prepared just before starting the CdTe QDs synthesis by reacting NaBH4 and Te powder in a molar ratio of 3 : 1. A round bottom flask was flushed with N_2 and then 0.5 mL N_2 purged water was added to it, through a syringe. Te powder (3.0 mmol) was mixed with $NaBH_4$ in water under nitrogen saturated conditions. The reaction was carried out at room temperature under a nitrogen flow with the magnetic stirring of 150 rpm for 25–30 min. The reaction was stopped when the black Te powder was completely reduced and the solution turned transparent pink in color. This freshly prepared NaHTe solution was hot injected (100^0 C) to a N_2 saturated solution of $CdCl_2$ (15 mM) and MPA (36 mM) at pH 9. This solution was then refluxed under a nitrogen flow for 2 h at 100 C. The CdTe QDs solution was cooled to room temperature and precipitated with acetone and washed with water to remove Na^+ ions and unbound MPA. The solution was centrifuged at 10000 rpm for 10 min at room temperature. The

pellet was collected, which was comprised of CdTe QDs and was dried with a rotary evaporator. The resulting solid CdTe QDs were readily redispersed in water, resulting in a clear solution.

4B.2.1. Conjugation of BiOx on MPA capped CdTe QDs (CdTe–BiOx QDs)

The conjugation of CdTe QDs with BiOx was done on the basis of EDC/NHS chemistry via the formation of an amide linkage between the carboxyl groups of the MPA and the primary amine groups of the BiOx. The thiolated CdTe QDs (100 mg in 20 mL of distilled water) were activated with 5 mL of a mixture of 0.26 mmol (40 mg) EDC and 0.05 mmol (8 mg) NHS in distilled water at pH 7.0 by incubating the mixture at room temperature for 30 min. Then, 4 mg of a BiOx solution (4 mg mL^{-1} of water) was added to the above mixture and then kept overnight at 4^0 C. Acetone was used to precipitate the CdTe–BiOx QDs. The precipitate was washed with water and reprecipitated with acetone. After centrifugation at 10 000 rpm, the GOx immobilized CdTe QDs (CdTe–BiOx) were suspended in 10 mL of distilled water and kept at 4^0 C until use.

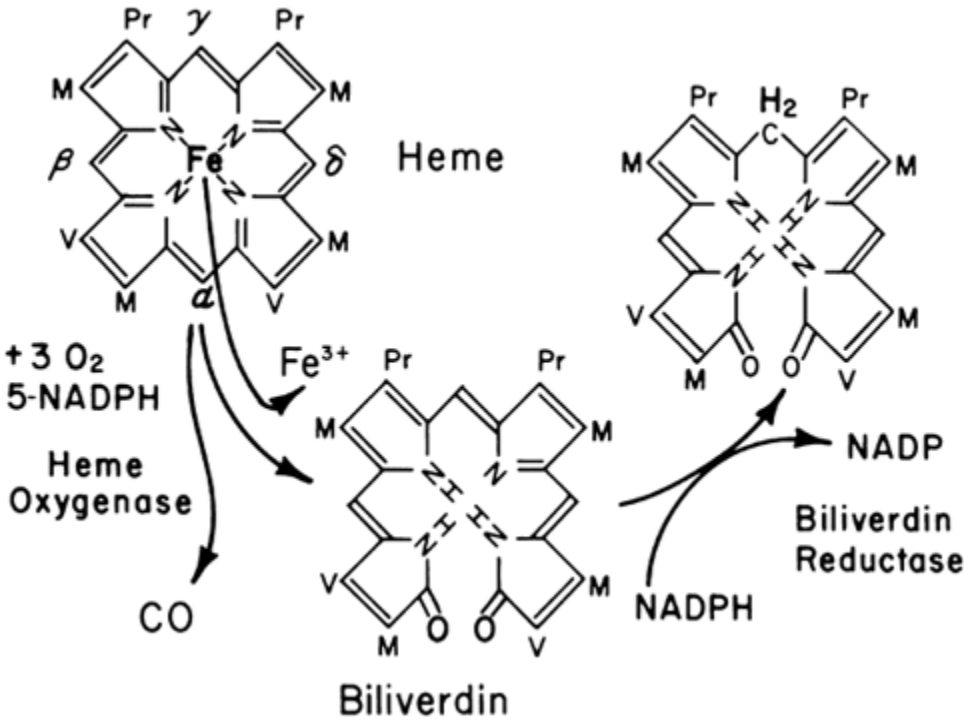

Figure.4B.2. Formation of Bilirubin

4A.4. Transmission electron microscopy (TEM)

The transmission electron microscopy (TEM) images were obtained on a model JEOL 1200 EX. The CdTe–MPA QDs colloid and CdTe–ChOx QDs colloid were diluted 1000-fold with distilled H_2O, deposited onto a 200 mesh copper grid coated with a Formvar film and were dried overnight.

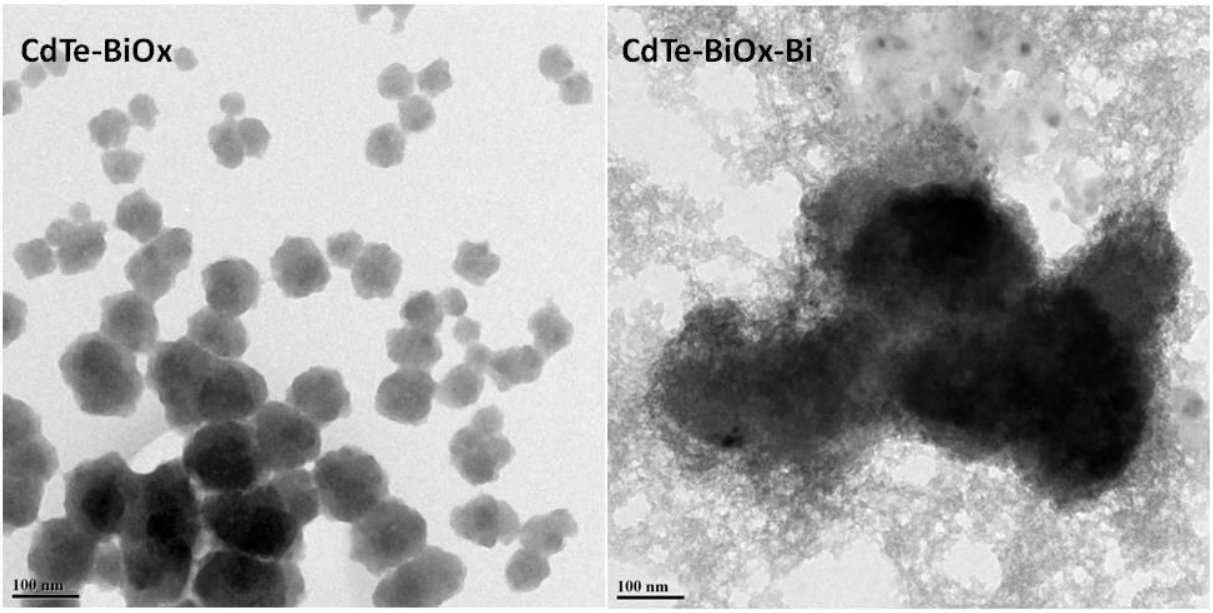

Figure.4B.3 *TEM of (a) CdTe–MPA-ChOx (b) CdTe–MPA-BiOx with 4 mg mL^{-1} of bilirubin.*

4B.3. Photoluminescence spectroscopy study (PL)

The photoluminescence measurements were performed on a Perkin-Elmer LS 55 spectrophotometer. All the samples were prepared in distilled water. The initial concentration of the CdTe–BiOx for all the experiments was kept constant i.e. 4 mg/mL^{-}

4b.4. Selectivity of the method

The selectivity of the method was investigated by checking the PL absorption maxima of the CdTe–BiOx QDs on their interaction with dopamine, ascorbic acid, uric acid, bile salts and dopamine in the range 20–100 mg mL^{-1}. To confirm the precision and recovery of the probe, each set of experiments were carried out in triplicate, and similar results within a maximum error of 2–3% were obtained

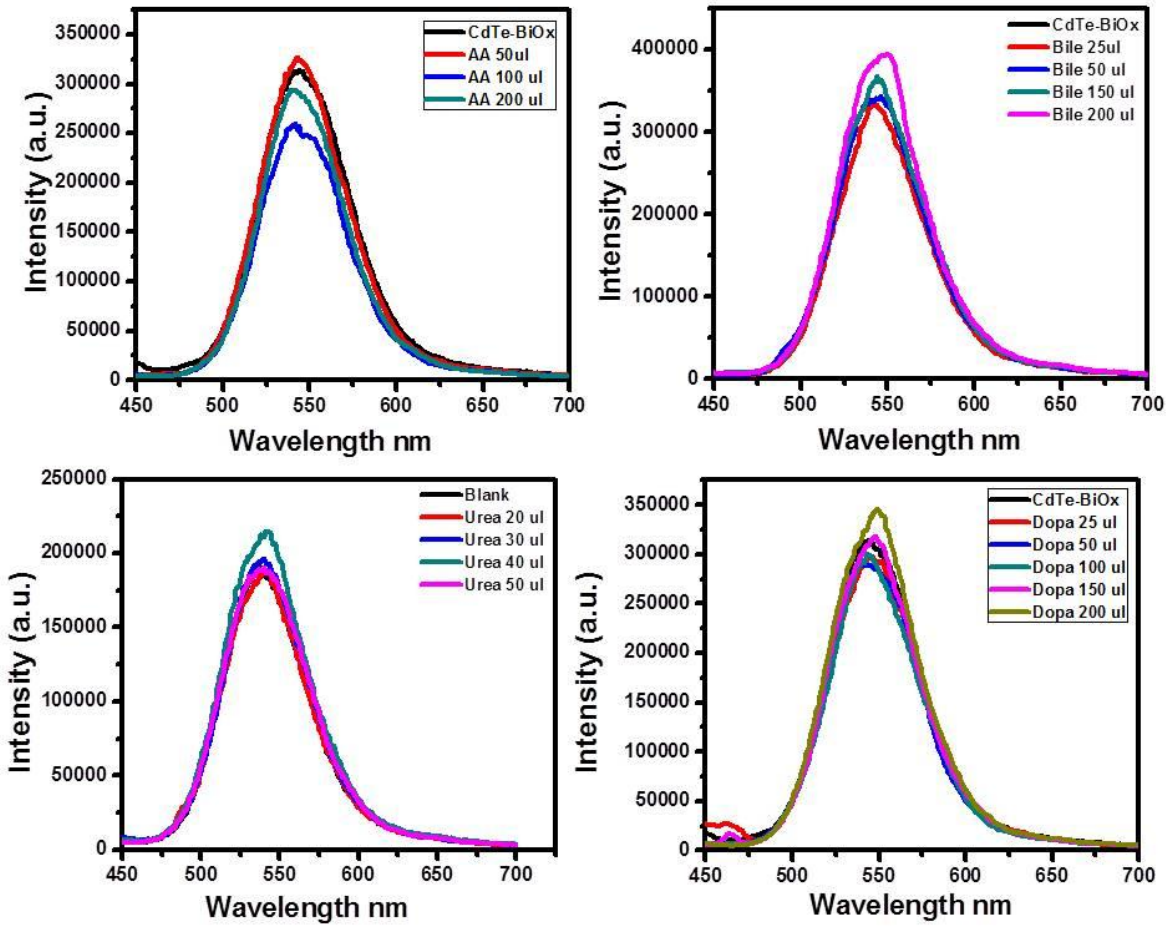

Figure.4B.4 *Photoluminescence spectra of BiOx conjugated CdTe QDs with increasing concentration of Ascorbic acid, Bile salts and Urea for selectivity test.*

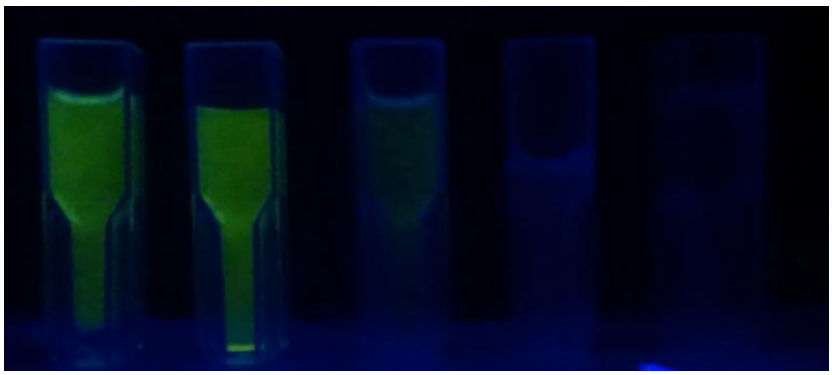

Figure. 4B.5. *Under UV light pictures (a) CdTe–MPA QDs, (b) CdTe–BiOx QDs, c) CdTe-BiOx on reacting with Bi.*

Conclusion

We have devised a simple method for the detection of Bilirubin in aqueous solvent using BiOx functionalized CdTe QDs. The color of the solution was found to change from red to grey in the presence of 4 mg mL^{-1} of bilirubin in water. The fluorescence intensity was quenched with the addition of Bilirubin. This showed the feasibility of the method for the quantitative measurement of Bilirubin in serum. The color change observable with the naked eye which may be used for a preliminary screening at home, ahead of referral for more focused investigations.

References

1. Marcos Roberto de Oliveira, Doumit Camilios-Neto, Cristiani Baldo, Agnes Magri, Maria Antonia Pedrine Colabone Celligoi, *International Journal of scientific and technology research* **2014**, 3, 133-146.

2. Fevery J, *Liver Inter* **2008,** 5, 592-605.

3. Paulev Zuvieta, *New Human Physiology*

http://www.zuniv.net/physiology/book/chapter23.html

CHAPTER 5

A Simple Water Soluble Photoluminescence *On-Off-On* Probe for Speedy and Selective Detection of Fluoride Ions even in HF Vapor

A CdTe QDs based new type of switch on-off-on photoluminescence (PL) sensor has been developed for the specific detection of fluoride ions (F-). Europium (Eu^{3+}) ions have been stabilized by the carboxylic groups of 3-mercaptopropanoic acid (MPA) capped CdTe QDs and this results in quenching of PL (switch off) of QDs. PL is regained (switch on) with the addition of F- ions due to the formation of EuF_3 as Eu^{3+} has higher bonding affinity with F- rather than carboxylic acid groups. The quenching of the PL property of CdTe-MPA QDs with Eu^{3+} and its regeneration in the presence of F- is highly selective, sensitive and speedy. Time of less than 15 s is required for PL recovery after addition of fluoride ions. The detection of HF vapor has also been carried out successfully and it is observed that PL off-on property of CdTe-MPA-Eu QDs remains unaffected even in presence of HF vapors whereas no PL intensity change is

5.1 Introduction

Colloidal semiconductor quantum dots (QDs), with radii 4 nm, have unique photoluminescence (PL) properties due to the quantum confinement effect of the charge carriers aided by surface functionalization effects[1]. QDs possess higher PL quantum efficiency, tunable luminescence depending on their size, wide band continuous absorption, narrower PL band, and higher photo stability over conventional organic fluorescent dyes[2]. Following the first use of hydrophilic QDs as fluorescence probes in cellular labeling in 1998[3,4], QDs have continued to attract widespread attention from the fields of biology and medicine, and have made remarkable inroads in biomedical application domain[5-7]. Additionally, sensing schemes based on fluorescence resonant energy transfer (FRET) or photo induced electron transfer (PET) have also been developed for detecting small molecules, and for tracing bio-recognition events or bio-catalytic transformations[8,9].

Chen and Rosenzweig reported the first practical use of CdS QDs as chemical sensors to determine Zn (II) and Cu (II) ions in aqueous media[10]. Recently, great attention has been paid to the applications of QDs as metal ion probes because of the environmental and biological importance of such ions[11,12]. Depending on the nature of QDs as well as surface coatings, a number of QDs-based probes were developed for transition metal ions, including Hg^{2+}, Cu^{2+}, Ag^{+}, and Pb^{2+}[13-15]. Nevertheless, relatively very little attention has been paid to the fluorescence behavior of QDs in the presence of various chemical species; mainly anionic pollutants[16-19]. Li and Han reported that cyclodextrin modified CdSe/ ZnS QDs allow a highly sensitive determination of environmental pollutant phenols[20]. Recently, Zhang and Johnson have developed a single QD-based aptameric sensor that is capable of sensing the presence of cocaine[17]. Owing to the sustained interest of selective chemosensor in environmental monitoring, the design of sensing devices based on QDs is a topic of great interest[21,22].

Amongst various ionic species the fluoride anion has unique chemical and physiological properties, and it is also associated with systems such as nerve gases, drinking water, and the refinement of uranium[23-25]. Therefore, it is necessary from the environmental and biological standpoint to develop effective fluorescent sensors, which could selectively detect the fluoride ion. Although a variety of organic molecule based fluorescent sensors for fluoride detection have

been presented in the literature[26-30], to the best of our knowledge, it is the first time that we demonstrate herein the capability of water soluble MPA capped CdTe QDs (one step synthesis) as speedy, efficient and most importantly a selective photoluminescence *on-off-on* probe for fluoride ions. The principle of our F^- sensing concept is shown in Scheme 1. Along with solution form we have also immobilized the CdTe-MPA QDs into agarose to get a highly fluorescent hydrogel which also acts as a PL based sensor, i.e PL switch off with addition of Eu^{3+} ions in solution followed by PL switch on with addition of F^- ions. We have extended the PL sensing mechanism further to detect HF vapors, which is important from the industrial point of view.

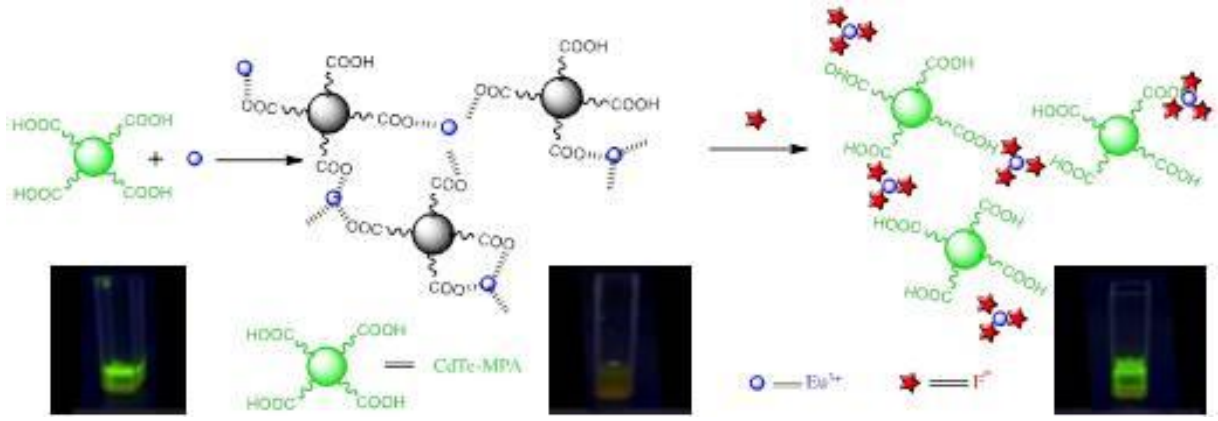

Scheme 1. Schematic illustration of F^- detection based on the competition of F^- with carboxylate groups on the CdTe –MPA QDs surface for Eu^{3+} ions.

5.2 Experimental

5.2.1 Reagents

Cadmium chloride ($CdCl_2$) and tellurium powder (Te) (SD Fine Chemicals), 3-mercaptopropanoicacid (MPA) (SRL Chemicals) and ammonium hydroxide (NH_4OH) (Merck Laboratories), sodium borohydride ($NaBH_4$) (30% w/v) (Merck Laboratories) and europium nitrate were obtained from Sigma Aldrich, India and used as obtained. Isopropanol and acetone (Merck Laboratories) was used as received. Deionized water was acquired from Millipore milli-Q system.

5.3. Preparation of water soluble MPA capped CdTe QDs

MPA stabilised CdTe QDs were synthesised using organometallic route[31-33]. In brief, NaHTe was prepared just before starting the CdTe QDs synthesis by reacting $NaBH_4$ and Te powder in molar ratio of 3:1. Round bottom flask was flushed with N_2 and then 0.5 ml N_2 purged water was added into it through a syringe. Te powder (3.0 mmol) was mixed with $NaBH_4$ in water under nitrogen saturated condition. The reaction was carried out at room temperature under nitrogen flow with the magnetic stirring of 150 rpm for 25-30 min. The reaction was stopped when the black Te powder was completely reduced and the solution turned to be absolutely transparent pink in color. This freshly prepared NaHTe solution was hot injected (100^oC) to the N_2 saturated solution of $CdCl_2$ (15mM) and MPA (36mM) at pH 9. This solution was then refluxed under nitrogen flow for 2 h at 100 C. The CdTe solution was cooled to room temperature and precipitated with acetone and washed with water to get rid of Na^+ ions and unbound MPA. The solution was centifuged at 10.000 rpm for 10 min at room temperature. The pellet was collected which comprised of CdTe QDs and was dried with a rotary evaporator. The resulting solid CdTe QDs are readily redispersed in water resulting in a clear solution.

5.4. Conjugation of Eu^{3+} on MPA capped CdTe QDs (CdTe-Eu^{3+} QDs)

Conjugation of CdTe QDs with Eu^{3+} was done simply by mixing Europium nitrate salt solution in the aqueous solution of MPA capped CdTe QDs.

5.5. Immobilization of CdTe- Eu^{3+} QDs into agarose

1 ml CdTe-Eu^{3+} QDs solution was mixed with 10 mg agarose powder and heated to 45^oC to get a clear homogeneous solution. The solution was then cooled to room temperature to obtain the CdTe- Eu^{3+} QD immobilized agarose hydrogel.

5.6. Photoluminescence Spectroscopy study (PL)

Photoluminescence measurements were performed on a PerkinElmer LS 55 spectrophotometer. All the samples were prepared in distilled water. The initial concentration of CdTe-Eu^{+3} in all the experiments was kept constant i.e. 2mg/mL. The sample shows a fluorescent green luminescence in the visible, when excited in UV light (365 nm). The photo luminescence (PL)

emission is broad over a range of 500–600 nm in the visible spectrum, typical of CdTe nanostructures but the maximum emission is achieved at 535 nm. The slit width for both excitation and emission was kept constant i.e. 2 nm.

5.7. Selectivity of the Method

The selectivity of the method was investigated by checking PL absorption maxima of CdTe-Eu^{+3}QDs on interaction with various other salts such as sodium thiosulphate, sodium chloride, sodium sulphate, sodium nitrate, sodium nitrite, sodium triphosphate, potassium per-sulphate, potassium bromide, ammonium dichromate, each at concentration of 20 -100 µg/ ml. To confirm the precision and recovery of the probe, each set of experiments was carried out in triplicate, and similar results were obtained within the maximum error of 2-3%.

5.8. Result and Discussion

MPA capped water soluble CdTe QDs were synthesized as reported earlier[31]. The quantum yield of the as-synthesized CdTe-MPA in water was 21% taking Rhodamine B as a reference. The PL intensity of CdTe-MPA QDs (*switch on*) quenched instantly with the addition of $Eu(NO_3)_3$, as initially the Eu^{3+} ions coordinate to the free carboxylate groups of MPA on the surface of the CdTe QDs. This results in a bridge for the induction of CdTe QD aggregation as shown in Scheme 1. As a consequence, the PL of CdTe QDs is quenched (*switch off*) through energy-transfer or electron-transfer processes. Then, such non-fluorescent CdTe-MPA-Eu^{3+} QD aggregates get dissociated after the introduction of F^- because Eu^{3+} ions display a higher affinity for small fluoride anion than for the carboxylate groups existing on the CdTe-MPA QD surface. In this case, the subsequent redistribution of QDs results in the restoration of PL (*switch on*).

Titration of Eu^{3+} ions into the CdTe-MPA solution results in PL quenching of CdTe-MPA as shown in Figure. 5.1. It shows the PL quenching of CdTe-MPA with increasing Eu^{3+} concentration in Millipore water and its corresponding calibration curve. It is observed that the PL intensity at 560 nm decreases as the concentration of Eu^{3+}ions increases. Over 90 % of the PL of CdTe-MPA (2mg/mL) is quenched by the addition of 0.213 mg/mL Eu^{3+} ions. To reveal the response time of PL quenching, time-resolved PL spectra were recorded and the result revealed the reaction time for PL quenching to be less than 45 sec. (Figure 5.10). Similar PL quenching of CdTe-MPA with Eu^{3+} addition was observed also in PBS buffer (pH-7.2) solution (Figure 5.8).

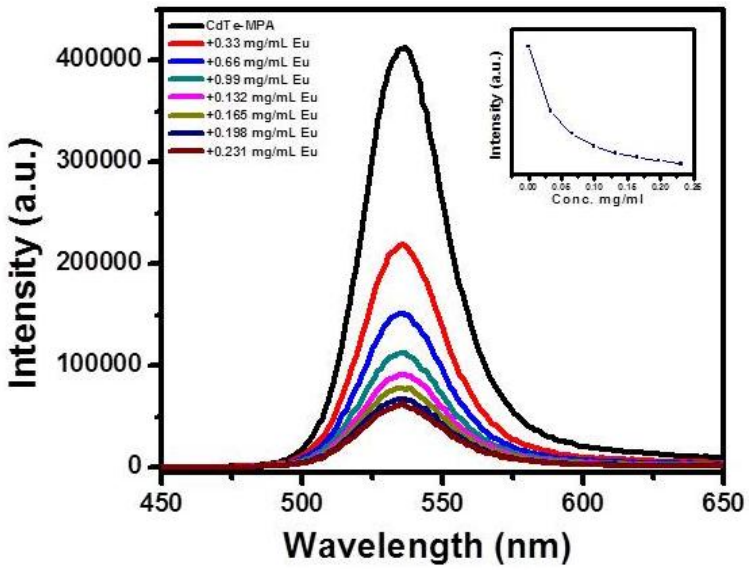

Figure.5.1. Photoluminescence spectra of CdTe-MPA with increasing concentration of Eu^{3+} ions carried out in water. The inset shows the respective graphical relationship of the PL intensity against an increasing concentration of Eu^{3+} ions.

The addition of F- to CdTe-MPA-Eu3+nanocomposite aggregates leads to the recovery of PL emission due to the desorption of Eu3+ from the surface of the CdTe-MPA-Eu3+ as a result of the competition for Eu^{3+} ions between the F^- and those from the carboxylate groups on the MPA on the CdTe QDs surface. Figure 3 shows the PL recovery with the addition of F^- ions and corresponding calibration curve. A linear relationship between the enhanced PL intensity of CdTe-MPA-Eu^{3+} and the concentration of F^- added is observed in Figure 5.3(b). The response time to recover PL is less than 10 sec (Figure 5.12). Similar result was also observed in a PBS buffer solution at pH- 7.2 (Figure 5.10).

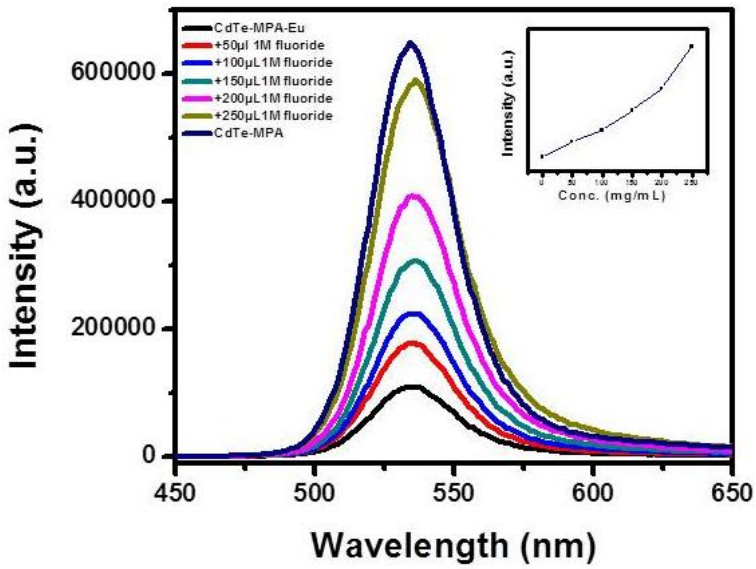

Figure 5.2. Photoluminescence spectra of CdTe-MPA-Eu3+ with increasing concentration of Fluoride ions carried out in water. The inset shows the respective graphical relationship of the PL intensity against an increasing concentration of Fluoride ion.

To determine possible selective sensing of HF vapors, a PBS buffer solution and hydrogels of CdTe-MPA-Eu^{3+}(*Switch off*) were kept under vapors of different acids and bases (HCl, HF, NHO_3, NH_3, NH_2NH_2). The PL recovery was observed only in the case of HF vapors whereas all other cases no change was observed in PL. The PL recovery phenomena are shown in Figure 5.3.

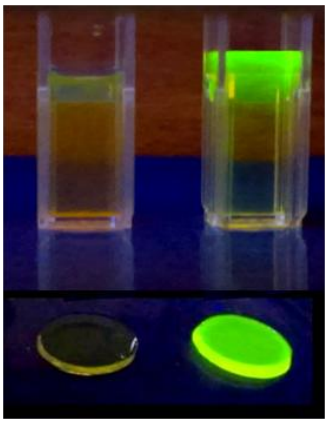

Figure 5.3. Pictures of CdTe-MPA-Eu^{3+}in PBS buffer pH-7.2 and agarose gels before (left) and after (right) contact with HF fumes in UV light.

Transmission electron microscopy (TEM) was used to study the change in the morphology of CdTe-MPA QDs, to identify the formation of aggregates on interaction with Eu^{3+} and their eventual disruption of aggregates when comes in contact with F^-. TEM micrographs of CdTe QDs show nearly monodispersed spherical morphology with an average diameter of 5±1 nm (Figure 5.4 (a)) which gets changed with the addition of Eu^{3+} due to the formation of agglomerates (Figure 5.4(c)). When F^- ions are introduced, Eu^{3+} induced larger agglomerates get disrupted and redispersed back to the original QDs of size 5±1 nm (Figure 5.4(e)). The corresponding HRTEM images of CdTe-MPA, CdTe-MPA-Eu^{3+} and CdTe-MPA-Eu-F systems are shown in Figure 5.4 (b), (d) and (f), respectively. In all the cases the lattice fringes with a d-line spacing of 0.37 nm, which correspond to the (111) plane of a face centered cubic phase of the CdTe QDs, are observed.

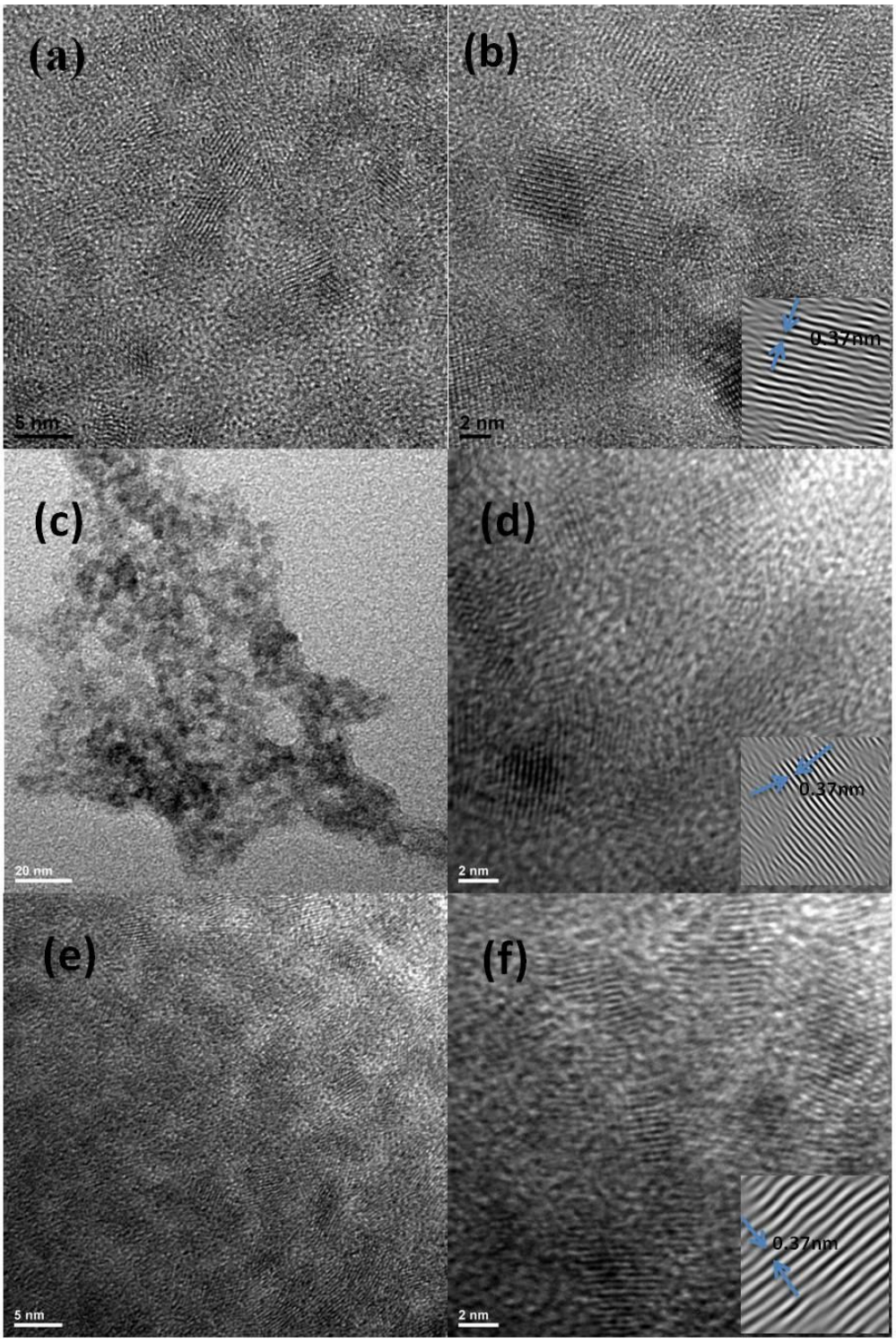

Figure.5.4. TEM and HRTEM images of CdTe-MPA a) and b); CdTe-MPA-Eu c) and d); and CdTe-MPA with Eu-F e) and f)

Field emission scanning electron microscopy (FESEM) images were also recorded to further validate TEM image based analyses. These show particle features of 2 types; one monodispersed and another in aggregated form. The formation of agglomerates of CdTe-MPA-Eu complex and their further disruption with the addition of F^- ions is also verified by the FESEM analysis of the CdTe-MPA sample. Fig. 5.5 (a) shows the presence of 5 nm monodispersed particles, which on addition of Eu^{3+} salt start forming clear 1-2μm sized spherical aggregates due to the formation of CdTe-MPA-Eu^{3+} complex as shown in scheme 1. With the introduction of F- into the solution of CdTe-MPA-Eu, Eu forms EuF_3 leaving the carboxylic group free of CdTe-MPA QDs. This leads to the disruption of the CdTe-MPA-Eu aggregate and recovery of pristine CdTe-MPA QDs as shown in fig 5.5 (c). The corresponding elemental mapping of CdTe-MPA, Eu, EuF was also done which clearly shows the presence of all the expected elements, as shown in the Figure 5.6 (a),(b) and (c).

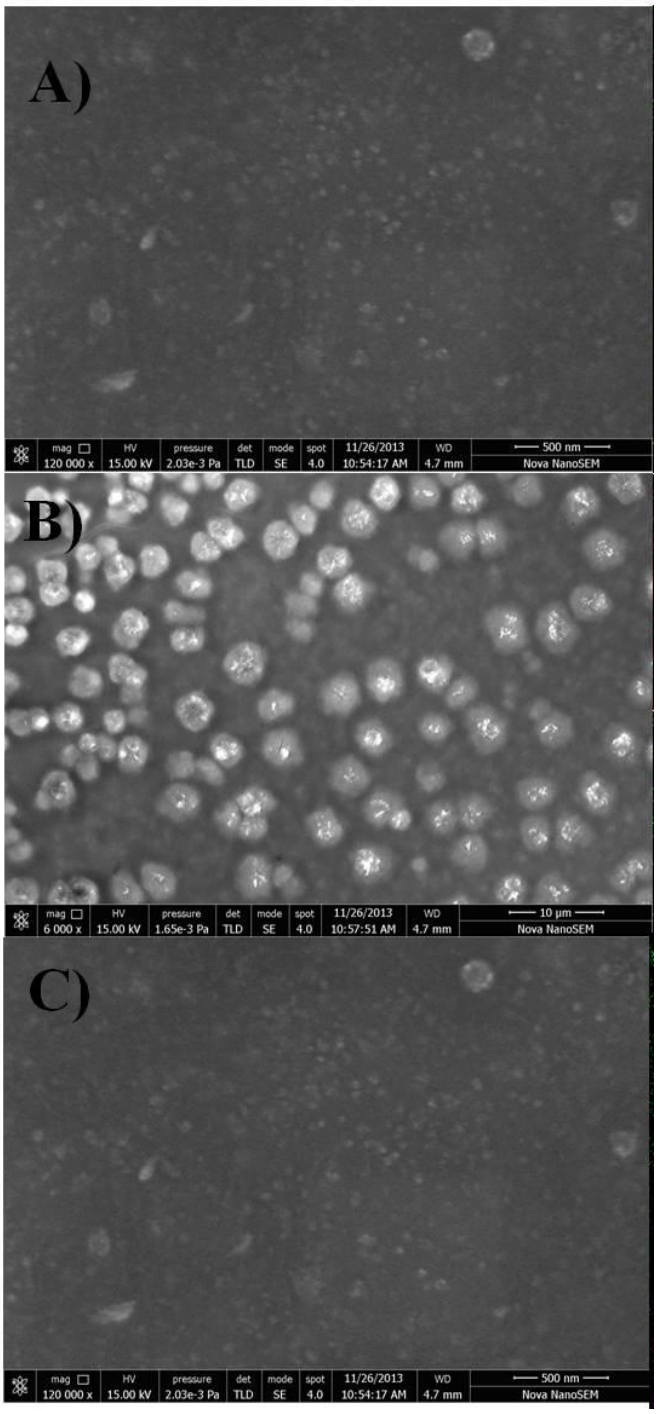

Figure 5.5. FESEM of A) CdTe-MPA, B) CdTe-MPA-Eu and C) CdTe-MPA-Eu-F respectively

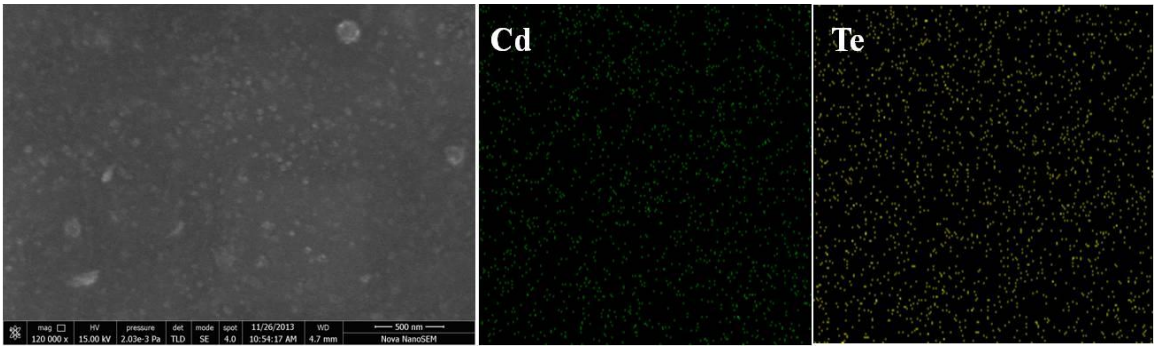

Figure 5.6 (a) FESEM and the corresponding elemental mapping data of CdTe-MPA QDs

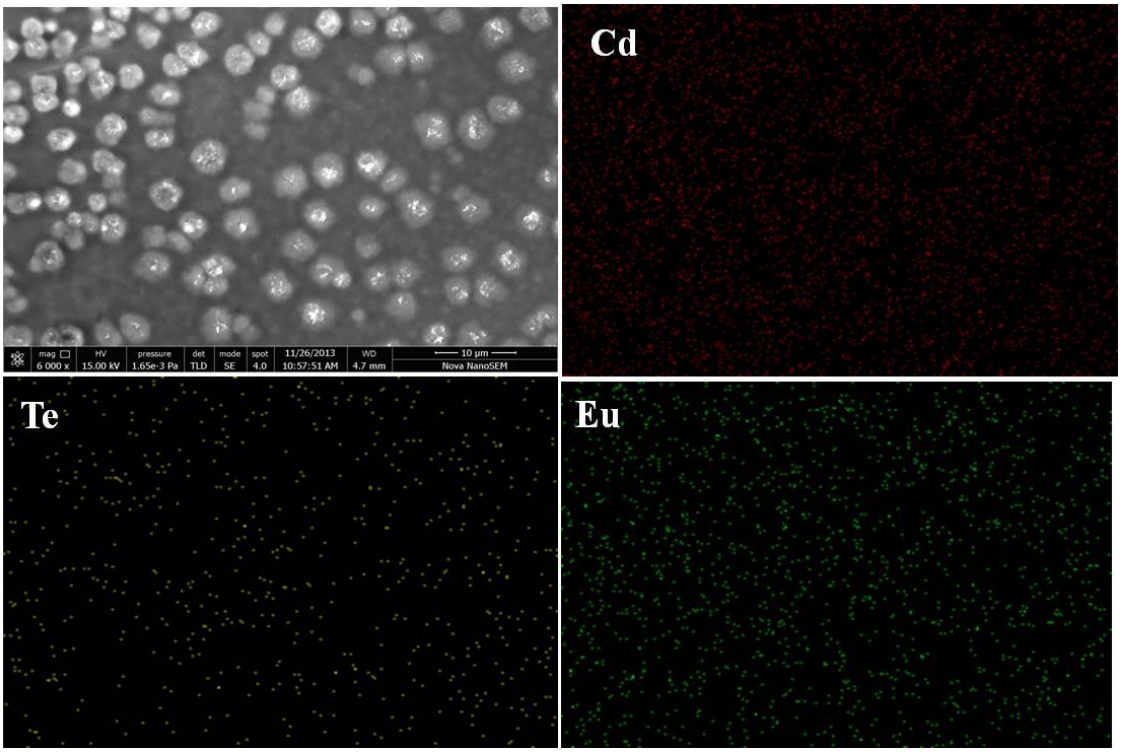

Figure 5.6 (b) FESEM and the corresponding elemental mapping data of CdTe-MPA-Eu

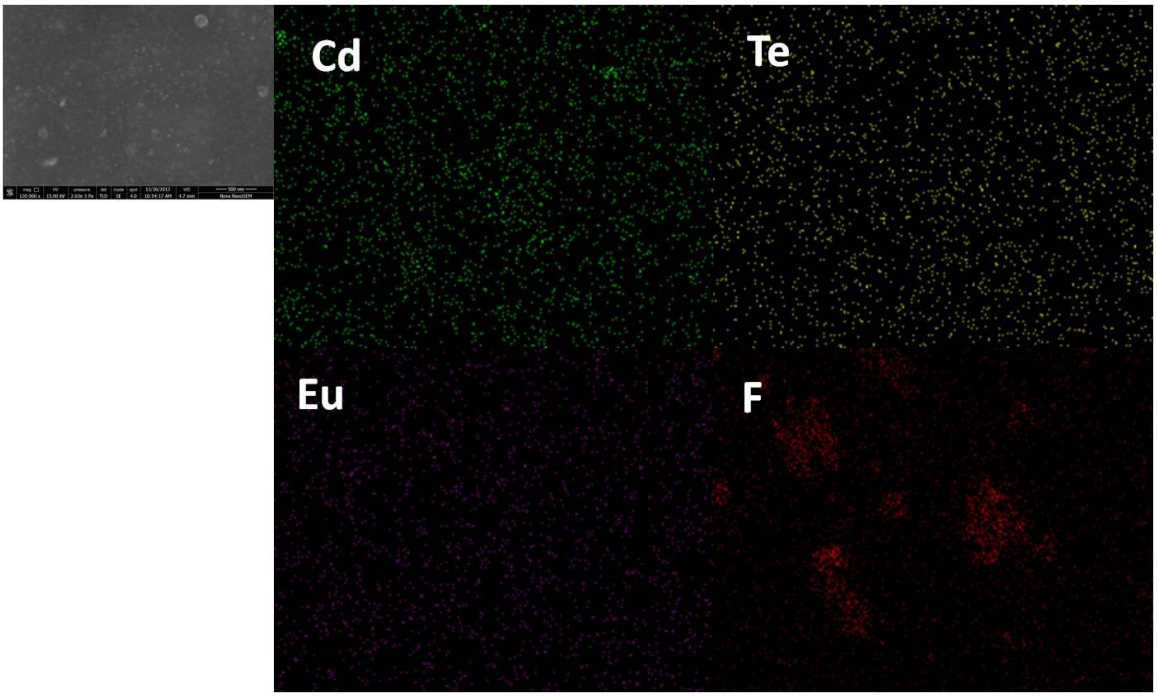

Figure 5.6 (c) FESEM and the corresponding elemental mapping data of CdTe-MPA-Eu-F

Considering the promise of the CdTe-MPA-Eu^{3+}nanocomposite as a PL sensor system for application in biological and environmental fields, the selectivity of the photoluminescent sensor for F^- was evaluated. This was achieved by monitoring the PL responses of the CdTe-MPA-Eu^{3+}nanocomposite complex upon addition of F^- and some coexisting substances, including anions such as thiosulphate, chloride, $S_2O_8^{2-}$, phosphate, bromide, sulphate, nitrite, nitrate, iodide, dichromate and cations such as nickel, iron (II), iron (III) and amino acids such as proline (Pro), serine (Ser), alanine (Ala), and histidine (His), all of which were kept at a concentration fifty times higher than that of F^-. As shown in Figure 5.7, F^- can significantly restore the PL intensity of the CdTe-MPA-Eu^{3+}nanocomposite in the presence of all potential competitors tested. In contrast, no clear enhancement is observed with any other ions or amino acids. This result demonstrates that this *on-off-on* PL probe is highly selective for F^-, to which it is several times more sensitive as compared to all the other substances tested. This high specificity could be attributed to the specific and robust affinity between Eu^{3+} ions and F^-, and the *off–on* nature of the assay presented. The bar diagram of PL quenching and recovery with all the tested samples are shown in Figure.5. 8. It clearly establishes that our PL based optical sensor is highly selective for the detection of fluoride ions.

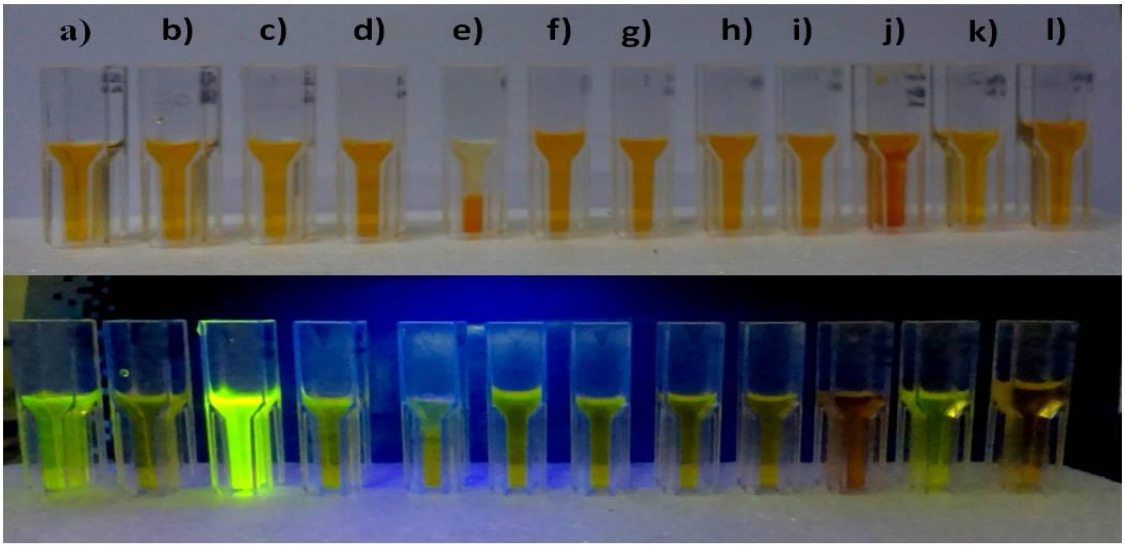

Figure 5.7. Visual and UV light pictures of a) CdTe-MPA-Eu-Fluoride b) CdTe-MPA-Eu, c) CdTe-MPA,d) CdTe-MPA-Eu-thiosulfate, e) CdTe-MPA-Eu-NaCl, f) CdTe-MPA-Eu-potassium per sulfate, g) CdTe-MPA-Eu-sodium sulfate, h) CdTe-MPA-Eu-Kbr, i) CdTe-MPA-Eu-sodium nitrite, j) CdTe-MPA-Eu-ammonium di chromate, k) CdTe-MPA-Eu-sodium tri phosphate, l) CdTe-MPA-Eu-sodium nitrate.

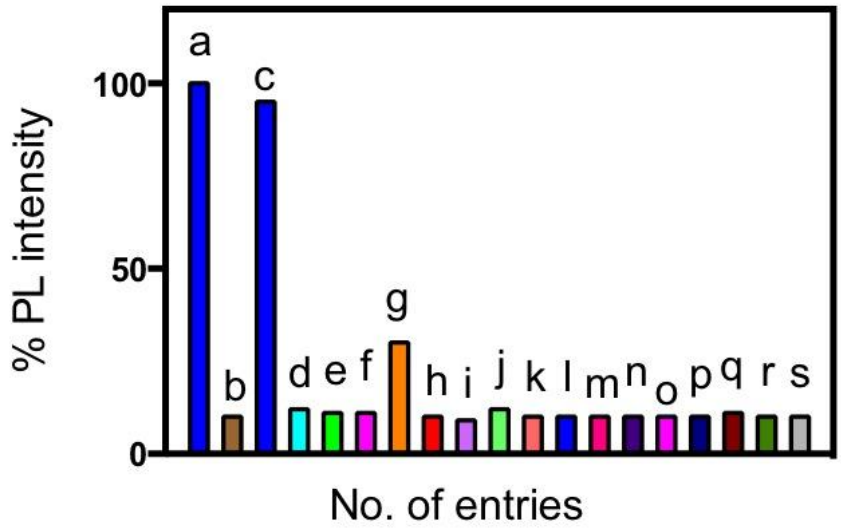

Figure 5.8. Bar diagram for the selectivity test results obtained with the addition of different anions, cations and aminoacids into CdTe-MPA-Eu sysyem:a) CdTe-MPA, b) CdTe-MPA-Eu^{3+}, c)CdTe-MPA-Eu-F^-, d) CdTe-MPA-Eu-thiosulfate, e) CdTe-MPA-Eu-Cl, f) CdTe-MPA-Eu-potassium per sulfate, g) CdTe-MPA-Eu- SO_4^{2-}, h) CdTe-MPA-Eu-Br^-, i) CdTe-MPA-Eu- NO_3^-, j) CdTe-MPA-Eu-$Cr_2O_7^{2-}$, k) CdTe-MPA-Eu-sodium tri phosphate, l) CdTe-MPA-Eu-NO_2^-, m) CdTe-MPA-Eu-Ni^{2+}, n) CdTe-MPA-Eu-Fe^{2+}, o) CdTe-MPA-Eu-Fe^{3+}, p) CdTe-MPA-Eu-Proline, q) CdTe-MPA-Eu-Serine, r) CdTe-MPA-Eu-Alanine, s) CdTe-MPA-Eu-Histidine.

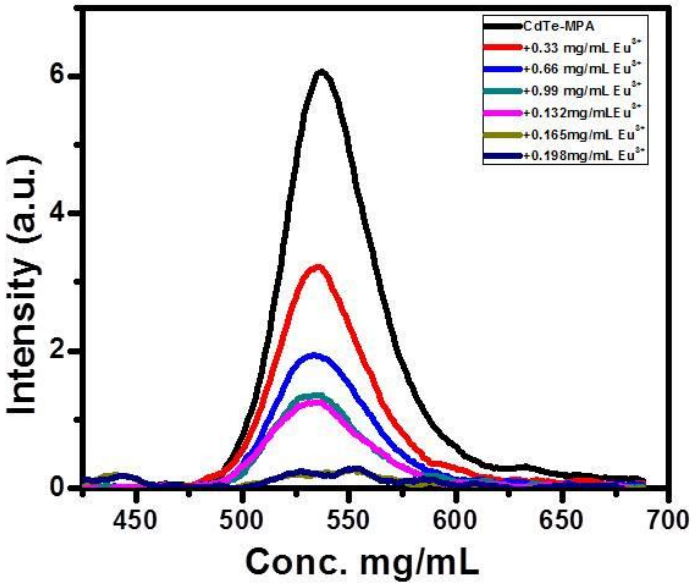

Figure 5.9. Photoluminescence spectra of CdTe-MPA with increasing concentration of Eu^{3+} ions carried out in PBS buffer (pH-7.2)

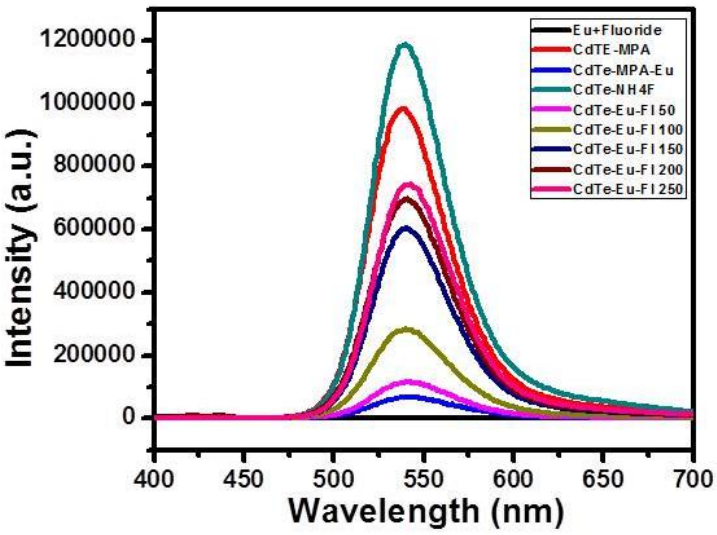

Figure 5.10. Photoluminescence spectra of CdTe-MPA-Eu^{3+} with increasing concentration of Fluoride ions carried out in PBS buffer pH (7.2)

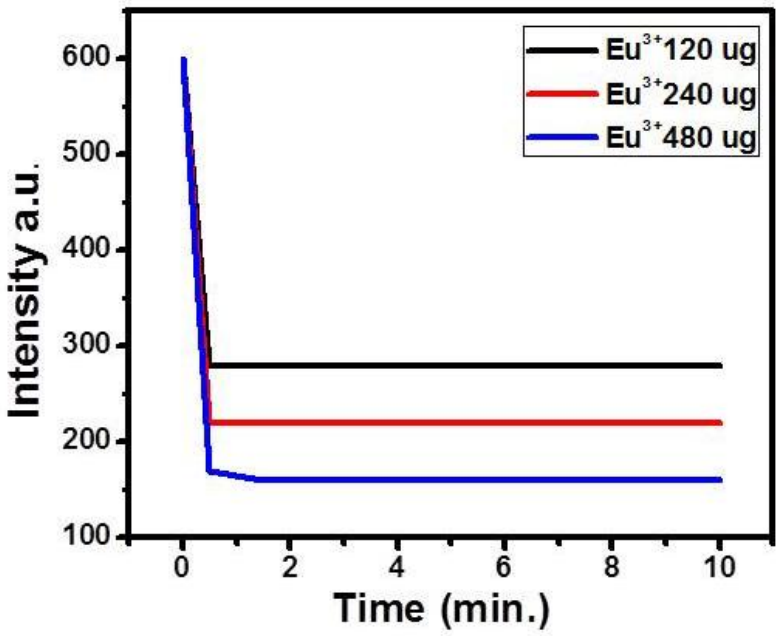

Figure 5.11. Response time of PL quenching of CdTe-MPA QDs (*switch off)* with increasing concentration of Eu^{3+} ions

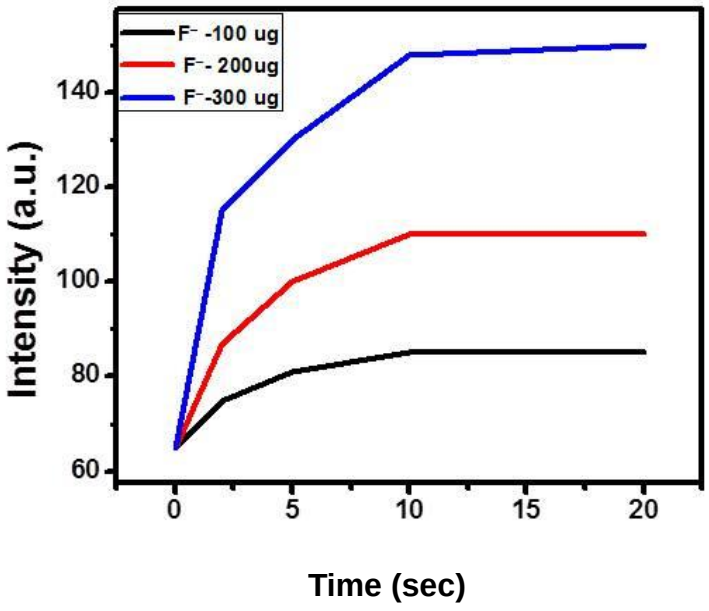

Figure 5.12 Response time of PL recovery of CdTe-MPA-Eu QDs (switch on) with increasing concentration of F^- ions.

Conclusion

In conclusion, we have demonstrated a new type of rapid, sensitive, and specific PL *on-off-on* assay for the detection of fluoride ions. Furthermore, the assay allows the selective detection of F^- from vapor generated by hydrofluoric acid. To the best of our knowledge, this is the first report for the use of easily synthesized one step procedure for water soluble CdTe-MPA QDs as PL probe for speedy and specific F^- ion photochemical sensing. The selectivity and sensitivity of PL quenching only for F^- ions suggests wide use of CdTe-MPA-Eu^{3+} as versatile probes in the fields of analytical determination, water treatment and biotechnology in the future.

References

1. Murray, C. B.; Kagan, C. R.; Bawendi, M. G. *Annual Review of Materials Science* **2000**, *30*, 545-610.

2. Qu, L.; Peng, X. *Journal of the American Chemical Society* **2002**, *124*, 2049-2055.

3. Chan, W. C. W.; Nie, S. *Science* **1998**, *281*, 2016-2018.

4. Bruchez, M.; Moronne, M.; Gin, P.; Weiss, S.; Alivisatos, A. P. *Science* **1998**, *281*, 2013-2016.

5. Ma, J.; Chen, J.-Y.; Zhang, Y.; Wang, P.-N.; Guo, J.; Yang, W.-L.; Wang, C.-C. *The Journal of Physical Chemistry B* **2007**, *111*, 12012-12016.

6. Thanh, N. T.; Green, L. A. *Nano Today* **2010**, *5*, 213-230.

7. Selvan, S.; Patra, P. K.; Ang, C. Y.; Ying, J. Y. *Angewandte Chemie* **2007**, *119*, 2500-2504.

8. Yildiz, I.; Tomasulo, M.; Raymo, F. ß. M. *Proceedings of the National Academy of Sciences* **2006**, *103*, 11457-11460.

9. Chan, Y.-H.; Ye, F.; Gallina, M. E.; Zhang, X.; Jin, Y.; Wu, I. C.; Chiu, D. T. *Journal of the American Chemical Society* **2012**, *134*, 7309-7312.

10. Chen, Y.; Rosenzweig, Z. *Analytical Chemistry* **2002**, *74*, 5132-5138.

11. Chen, C.-Y.; Cheng, C.-T.; Lai, C.-W.; Wu, P.-W.; Wu, K.-C.; Chou, P.-T.; Chou, Y.-H.; Chiu, H.-T. *Chemical Communications* **2006**, 263-265.

12. Freeman, R.; Finder, T.; Bahshi, L.; Willner, I. *Nano Letters* **2009**, *9*, 2073-2076.

13. Chen, J.; Gao, Y.; Xu, Z.; Wu, G.; Chen, Y.; Zhu, C. *Analytica Chimica Acta* **2006**, *577*, 77-84.

14. Gattas-Asfura, K. M.; Leblanc, R. M. *Chemical Communications* **2003**, 2684-2685.

15. Hosseini, M. S.; Pirouz, A. *Luminescence* **2014**.

16. Jin, W. J.; Costa-Fernández, J. M.; Pereiro, R.; Sanz-Medel, A. *Analytica chimica acta* **2004**, *522*, 1-8.

17. Zhang, C.-y.; Johnson, L. W. *Analytical Chemistry* **2009**, *81*, 3051-3055.

18. Wu, P.; Zhang, J.; Wang, S.; Zhu, A.; Hou, X. *Chemistry-A European Journal* **2014**, *20*, 952-956.

19. Zhou, Y.; Zhang, J. F.; Yoon, J. *Chemical reviews* **2014**.

20. Li, H.; Han, C. *Chemistry of Materials* **2008**, *20*, 6053-6059.

21. Basabe-Desmonts, L.; Reinhoudt, D. N.; Crego-Calama, M. *Chemical Society Reviews* **2007**, *36*, 993-1017.

22. Li, H.; Li, Y.; Cheng, J. *Chemistry of Materials* **2010**, *22*, 2451-2457.

23. Kimura, E.; Koike, T. *Chemical Society Reviews* **1998**, *27*, 179-184.

24. Yang, C.; Zheng, M.; Li, Y.; Zhang, B.; Li, J.; Bu, L.; Liu, W.; Sun, M.; Zhang, H.; Tao, Y.; Xue, S.; Yang, W. *Journal of Materials Chemistry A* **2013**, *1*, 5172-5178.

25. McDonagh, C.; Burke, C. S.; MacCraith, B. D. *Chemical Reviews* **2008**, *108*, 400-422.

26. Sui, B.; Kim, B.; Zhang, Y.; Frazer, A.; Belfield, K. D. *ACS Applied Materials & Interfaces* **2013**, *5*, 2920-2923.

27. Xu, G.; Tarr, M. A. *Chemical Communications* **2004**, 1050-1051.

28. Melaimi, M.; Gabbaï, F. P. *Journal of the American Chemical Society* **2005**, *127*, 9680-9681.

29. Hu, R.; Feng, J.; Hu, D.; Wang, S.; Li, S.; Li, Y.; Yang, G. *Angewandte Chemie International Edition* **2010**, *49*, 4915-4918.

30. Jose, D. A.; Kumar, D. K.; Ganguly, B.; Das, A. *Organic letters* **2004**, *6*, 3445-3448.

31. Singh, P.; Joshi, K.; Guin, D.; Prabhune, A. A. *RSC Advances* **2013**, *3*, 22319-22325.

32. Rogach, A. L.; Franzl, T.; Klar, T. A.; Feldmann, J.; Gaponik, N.; Lesnyak, V.; Shavel, A.; Eychmüller, A.; Rakovich, Y. P.; Donegan, J. F. *The Journal of Physical Chemistry C* **2007**, *111*, 14628-14637.

33. Singh, P.; Prabhune, A. A.; Ogale, S. B.; Guin, D. *Journal of Materials Chemistry B* **2013**, *1*, 6538-6543.

Chapter 6

Mercapto-propionic acid Assisted Supramolecular Assembly of Sophorolipids: A Potential Drug Delivery Vehicle

Herein, a novel nano-architecture was developed by simple mixing of glycolipid surfactant-sophorolipid (SL) and 3-mercaptopropanoic acid (3-MPA) at ambient temperature which holds promising potential as a drug carrier for the targeted delivery system. It is observed that SLs, which doesn't have any distinguishable, or specific nano/micro structure, forms spherical and porous nanostructure on interaction with MPA molecules. The detailed study on the effect of relative molar ratio of SL and MPA, presence of functional groups like thiol, carboxylic acids of MPA was successfully carried out and the obtained experimental results is also further supported by the theoretical studies. Along with toxicity studies in normal and cancer cell lines, antibacterial activity, drug loading and release studies of synthesized nanocomposite is also carried out at different pH and time interval.

6.1 Introduction

Recently, there has been a flurry of experimental work which has been carried out on understanding the supramolecular assemblies that are formed when lipids are mixed with some small molecules. Self assembled biological materials has been receiving special attention due to their widespread suitability because of their structural simplicity and tunability, functional versatility and cost effectiveness. [1]. Self assembly in biological systems is efficiently governed by non-covalent bond interactions such as hydrogen bonds, hydrophobic interactions, electrostatic interactions as well as π-π stacking interactions. Self- assembled biological compounds find various interesting applications in biomedical science.

Sophorolipids are a group of biosurfactants produced by *Candida* species. The biosurfactant consist of a dimeric sugar (sophorose) and a hydroxyl fatty acid, linked by a α-glycosidic bond. Glycolipid under different pH and solvent tend to form unexpectedly different structures due to the complexity of interactions involved. [2,3] Sophorolipid when dissolved in water, they form micelle like structures. Few research group have also reported the supramolecular assemblies of sophorolipids such as helical fibers/tubules/ribbons, rigid rods and even form vesicles under various parameters. [4-7]

In this Chapter, we have used Sophorolipid, as they are easily synthesised by non- pathogenic yeast using a cost effective resources. Sophorolipid are amphiphilic molecules which contain both the hydrophilic (polar) as well as hydrophobic (non-polar) group. This feature allows them to reduce surface tension and interfacial energies in order to form emulsions.

In this part of thesis, we have developed a nanospheres assembly by simple mixing of SL and MPA. It is observed that the morphology of nanospheres are highly dependent on relative molar ratio of reactants, thiol groups of MPA. Antibacterial assay was performed to see the bactericidal activity on both gram positive and gram negative bacteria. MTT assay was done to validate the anticancer property of the achieved nanostructures. Drug loading and drug release study was also carried out under different pH conditions in order to validated to be used as a targeted drug delivery vehicle. Sophorolipid used for nano-assemblies is FDA approved and allowable limit for human uptake is 5 ml/kg of body weight. For nano-assemblies, we have hardly used few milli grams. So there is no negative effect on the body system if administered by any route.

In our experiments, we have used three different types of sophorolipid- crude, acidic and lactonic. Physical characterizations and microscopic studies were performed for all the three type of samples under same conditions. When the lactonic and acidic sophorolipid was mixed with MPA in different ratios, we could not get the desired structures which could be utilized for our desired biomedical applications. But when we proceeded with crude sophorolipid with MPA, we obtained porous nanostructures of desired sizes. These nanostructures can easily be loaded with desired drugs and can be used for drug delivery vehicle.

6.2 Materials and methods

6.2.1 Chemicals

Media composition for the synthesis of Sophorolipid (SL) such as malt extract, glucose, yeast extract and peptone used were purchase from Hi-media, India, Oleic acid was purchased from Sigma-Aldrich USA, Sodium sulfate was purchased from Merck India, Organic solvents such as ethyl acetate and n-hexane used were of analytical grade and were purchased from Rankem, 3-mercaptopropanoic acid (MPA) was purchased from Sigma Aldrich, India, propionic acid was purchased from Sisco Research Laboratories, India, mercaptoundecanoic acid was purchased from Sigma Aldrich, India, Cefalexin and 6-aminopimellic acid was obtained from USP. Deionized water was acquired from a Millipore Milli-Q system.

6.2.2 Microorganism

A yeast, *Candida bombicola* (ATCC 2214) was used for the synthesis of sophorolipid. It was obtained from American type culture collection (ATCC)) USA.

6.3 Biosynthesis of Sophorolipid

Candida bombicola was first grown for 48 hrs at 28 °C on agar slants containing; 0.3% malt extract, 2.0% glucose, 0.3% yeast extract, 0.5% peptone, 2.0% agar. Before proceeding with the production of Sophorolipid, C. bombicola inoculum was developed by transferring a loopful of cells from slants to MGYP broth medium (0.3 % malt extract, 2.0% glucose, 0.3% yeast extract, 0.5% peptone) and incubated for 24 hrs at 28 °C with 180 rpm orbital shaking.

Production of Sophorolipid was performed in 1000 ml Erlenmeyer flasks containing 200 ml

MGYP medium. The fermentative production of SLs was initiated by transferring the inoculum (10%, v/v) into 200 ml of medium followed by incubation at 28 °C with the same 180 rpm orbital shaking condition. MGYP was supplemented with 1 mL oleic acid dispersed in equal volume of ethanol. The fermented broths were examined for the production of SL at regular intervals of 12, 24, 48, 72 and 96 hrs. [8]

Sophorolipid of oleic acid was prepared by resting cell method. In the first step adequate cell mass was harvested by growing *Candida bombicola* (ATCC 2214) in MGYP medium. Then the cells were redispersed in production medium containing 10% glucose. This production medium is supplemented with hydrophobic secondary carbon source (oleic acid) in absolute alcohol. Incubation of yeast biomass with glucose and fatty acid at 28 °C and 180 rpm orbital shaking for 96 to 120 hrs, a brown and viscous crude SL could be seen at the bottom of the flask. After incubation period, cells were separated from the broth by centrifugation at 5000 rpm for 20 min at 10 °C. Extraction of SL from supernatant was done with ethyl acetate. To the ethyl acetate phase, anhydrous sodium sulfate was added to remove residual water, filtered and then ethyl acetate was removed under vaccum. The unconverted fatty acid was removed by washing with n-hexane. Extraction of Sophorolipid was possible only with solvent extraction. Sophorolipids can also be synthesised with other lipophilic carbon materials substrate with carbon chain length of C (14-18). The most interesting molecule is Lactonic sophorolipid which is getting lot of attention by researcher due to its single structure form the diacetylated lactone. This particular form of Sophorolipid has biological importance because of its potential to be exploited in various biomedical applications like cancer therapeutics.

6.4. Synthesis of SL-MPA composite nanostructures

Sophorolipid nanoparticles were formed due to the supramolecular assembly with mercaptopropanoic acid which were very adept for biomedical applications. Different concentrations of MPA was added to a fixed concentration of sophorolipid in water (3mg/ ml). SL solution was prepared by mixing in deionized water completely until the solution becomes slightly milky colored. MPA was then slowly added into the solution and was vortexed for the proper mixing. The reaction mixture was then allowed to react by keeping on rotospin wheel at 50 rpm for 5 hrs at room temperature. TEM image of these solution were taken and was found that different morphologies are forming with different concentrations. The hydrodynamic radii

was also measured for the as-prepared nanoparticles in aqueous solution and it was found that different concentrations lead to the particles of different sizes. The particles were further checked for the properties like biocompatibility, cell viability as well as antimicrobial activity in order to optimize which is the most adept composition. taken and was found that different morphologies are forming with different concentrations.

6.5. Physical Characterization:

The particle size characteristics were investigated by Transmission Electron Microscopy (TEM), model JEOL 1200 EX, on a carbon coated TEM copper grid. HRTEM analysis was done on an FEI Tecnai300 system operated at 300 kV. Field emission scanning electron microscopy images were acquired on FEI QUANTA 200microscope, equipped with a tungsten filament gun, operating at WD 10.6 mm and 20 kV. 10 µL aliquots of all the sample solution were placed on a silicon wafer and these were fixed on copper stubs with the help of carbon tape. The samples were dried at room temperature overnight and images were recorded with gold coating. The zeta potential as a function of the magnitude of the electric potential and the stability of the nanoparticles dispersed in water were measured using a Zetasizer model 3000HS, Malvern, UK. Hydrodynamic radii were measured on a Brookhaven Instrument (BIC-Brookhaven Instrument Corporation) 90 Plus particle size analyzer at a 90° angle using 100 mg mL^{-1} water based particle suspensions.

Dynamic light scattering study was done to investigate the hydrodynamic radii of the nanocomposite obtained in the aqueous solvent. TEM and SEM study was also done to know the size and morphology of the SL-MPA nanocomposite. We prepared nanocomposite with different ratio of SL molecule and MPA molecule.

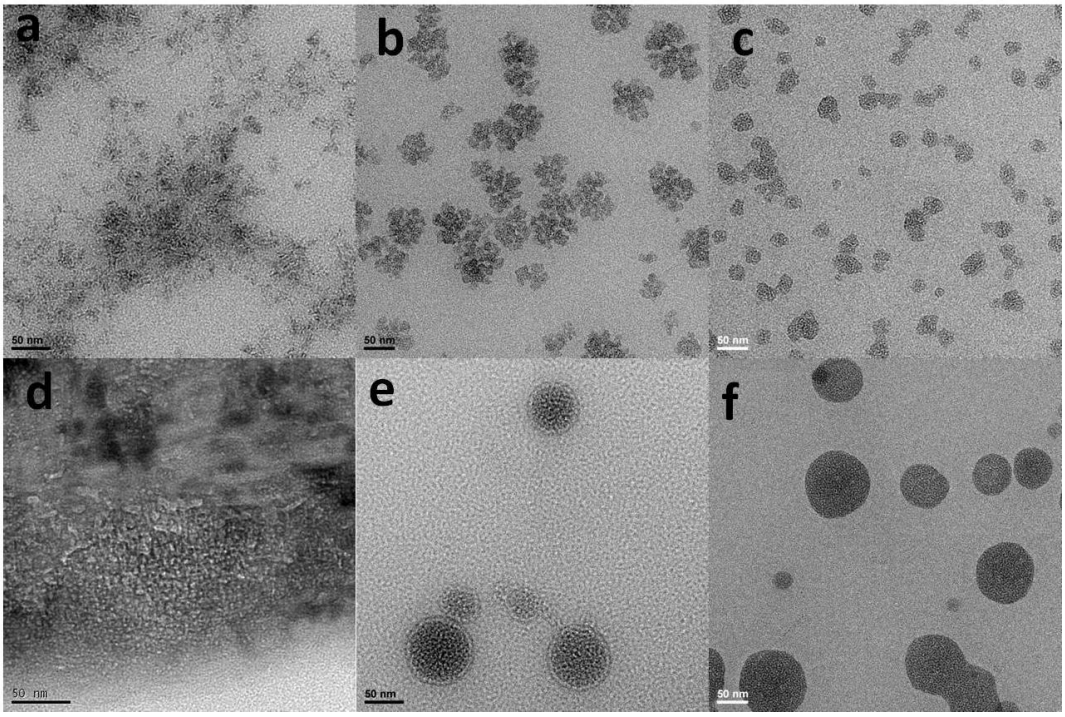

Figure 6.1. TEM of SL-MPA nanocomposite of different SL;MPA molecular ratio a) 1:1, b) 1:2, c) 1:3, d) 1:0, e) 3:1, f) 2:1.

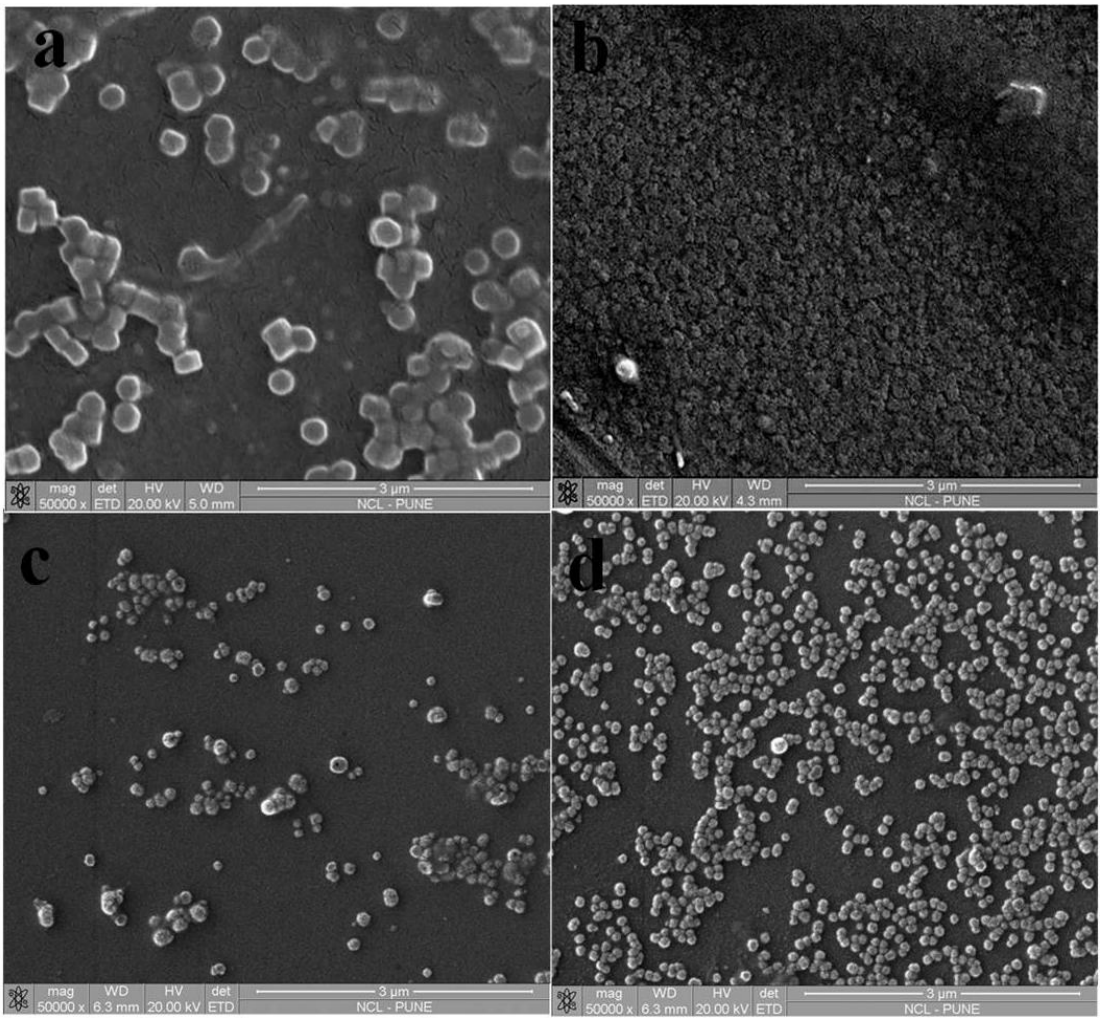

Figure. 6.2. SEM of SL-MPA nanocomposite of different SL;MPA molecular ratio a) 1:1, b) 1:2, c) 3:1, d) 2:1

We also correlate the data obtained from Hydrodynamic -radii, Zeta-sizer and TEM for further validation by making a correlation graph.

In order to investigate the interaction of SL and MPA on the basis of functional groups, we tested other similar molecules like, propionic acid and mercaptoundecanoic acid under same conditions. TEM was done to understand the morphology of the nanocomposite obtained with PA and MUA respectively. We observed that with MUA, we obtained similar morphology as MPA but not with propionic acid, so here we can conclude that thiol(-SH) group must have a role to play with the formation of these desired nanocomposites.

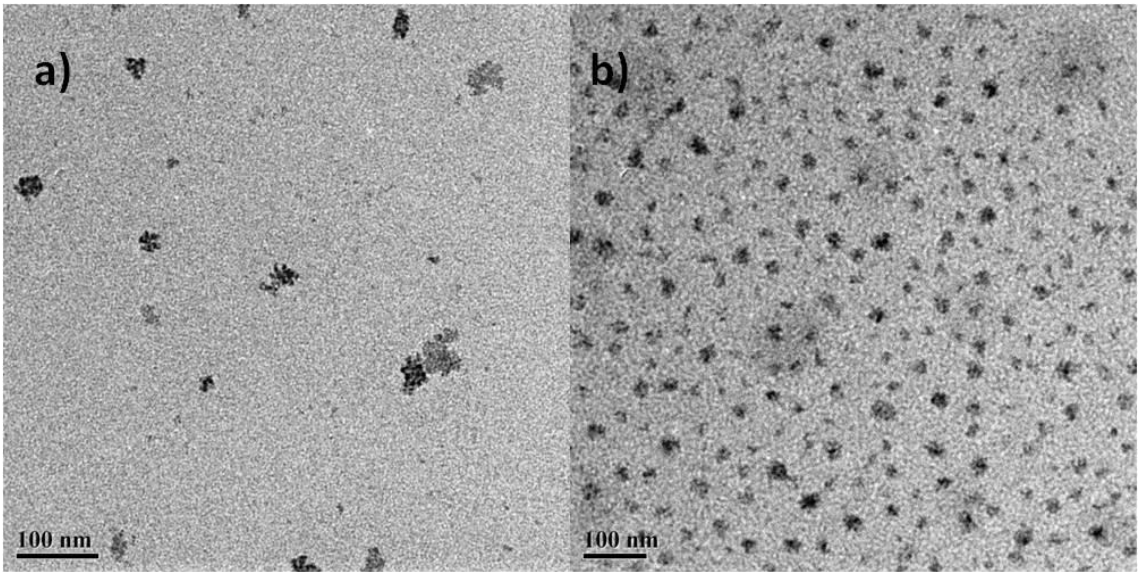

Figure. 6.3 TEM of a) SL-propionic acid nanocomposite and b) SL-Mercaptoundecanoic acid.

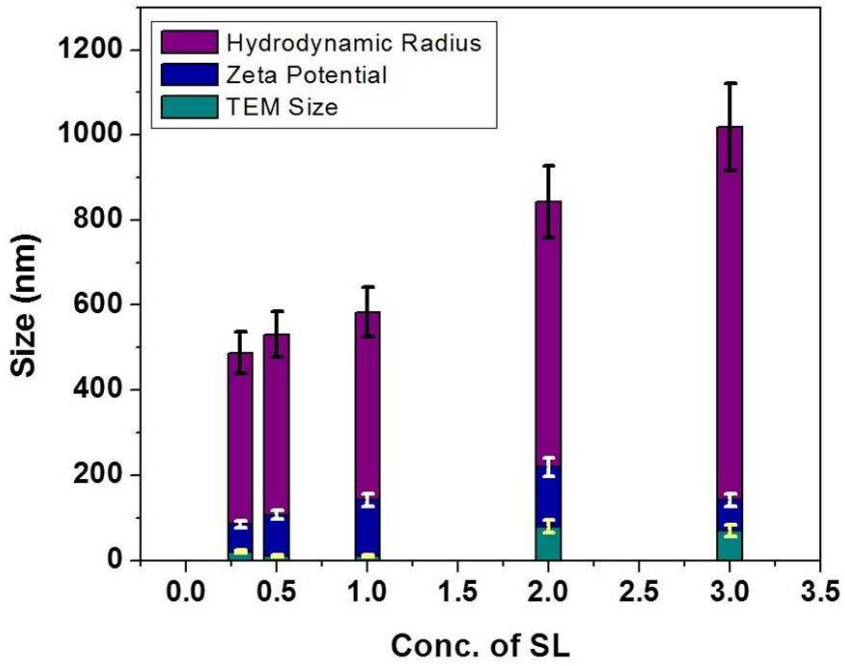

Figure. 6.4 Correlation graph of Hydrodynamic radii, zeta potential and size calculated from TEM images.

6.6. Cell culture studies

MCF-7 (human breast adeno carcinoma cell line) cells were grown in Eagle's Minimum essential Medium (MEM Gibco, Carlsbad, CA, USA) supplemented with 10% Fetal Bovine serum and penicillin/streptomycin, under 5% CO2 atmosphere at 37° C. NIH3T3 (Mouse Embryonic fibroblast cell line) cells were grown in Dulbecco's Modified Eagle's medium (DMEM, Gibco, Carlsbad, CA, USA) medium supplemented with bovine calf serum to a final concentration of 10% and penicillin/streptomycin under 5% CO2 atmosphere at 37 °C.

6.6.1. Cytotoxicity assay

The cytotoxicity of sophorolipid, MPA and SL-MPA nanocomposite on MCF-7 and NIH3T3 was assessed by MTT (3-(4,5-dimethylthiazol-2-yl)-2,5-diphenyltetrazolium bromide) assay. For MTT assay, cells were seeded at the density of 10^4 cells/ well in 96 well plates and incubated for 12-16 hs at 37º C before starting the treatment. Cells were treated with increasing concentration of SL-MPA nanocomposites capped (in the range of 0.01µg/ ml to 10µg/ ml) and incubated for 48 hs. At the end of incubation period, MTT solution was added to a final concentration of 0.05mg/ mL^{-1} to each well and incubated in dark at 37 °C for 4 h. Formazan crystals were dissolved by adding 100 µL DMSO to each well and the optical absorbance was measured at 540 nm on a plate reader. The readings in untreated cells were considered to be 100% viable as shown in Fig. 10. The cells were also exposed to only SL(3mg/mL) and only MPA (20µl/mL) with increasing concentration for comparison with SL-MPA nanocomposite.

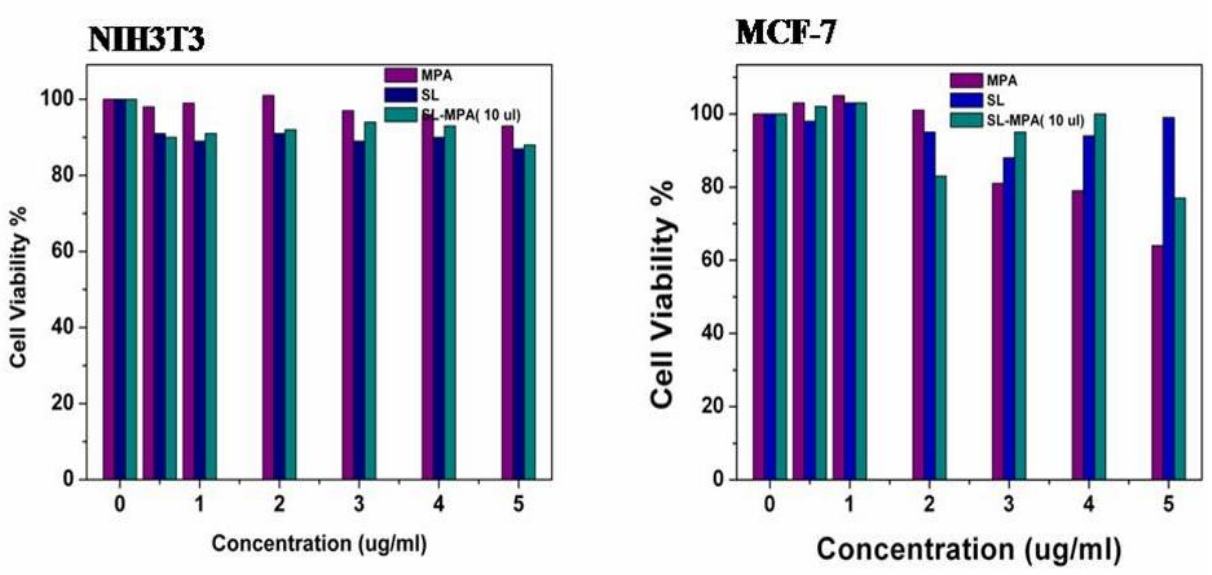

Figure. 6.5. MTT assay of SL-MPA nanocomposite on NIH3T3 and MCF-7 cell lines respectively.

6.7 Drug loading studies

SL nanocomposite (system 3) was 3mg/ ml was prepared. 1.5 mg drug was added into the nanocomposite solution and was kept on rotospin wheel for 20 hrs at room temperature.

6.7.1 *In vitro* drug release studies

Drug release from SL-MPA nanostructure was studied using dialysis method. Dialysis bags were soaked in DI water overnight before use in order to remove the preservative which was followed by rinsing thoroughly in distilled water. The release of doxorubicin was carried out in buffer at 3 different pH i.e. pH 3.0, pH 4.0 and pH 7.0. *In vitro* release of doxorubicin from the Dox loaded SL-MPA nanocomposite was performed by dialysis in dialysis bags (14000 MW cut off) dipped in 20 ml buffer at room temperature Experiment was done separately for 3 different pHs. Sampling was done after 0.5 hrs, 1hrs, 3 hrs, 5 hrs, 7 hrs and UV study was done to analyse the release of drug in the buffer solution.

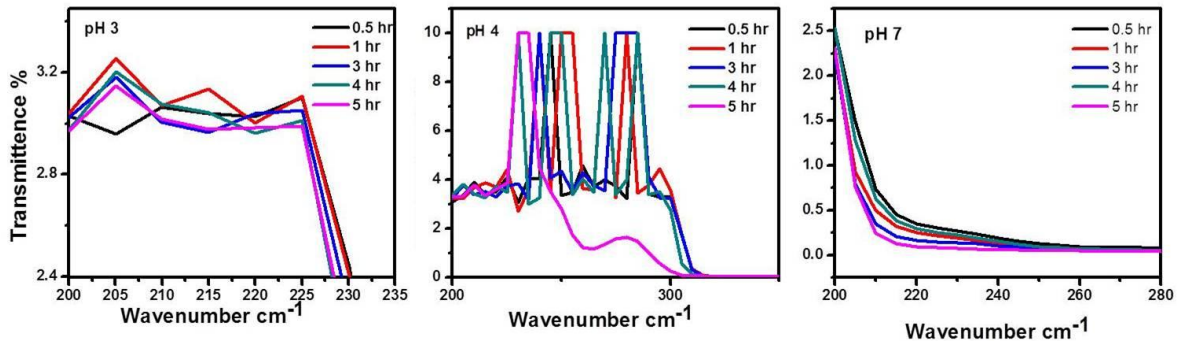

Fig 6.6. Drug Release profile of Dox loaded SL-MPA nanocomposite at a) pH 3.0. b) pH 4.0 and c) pH 7.0.

We also did MTT assay of different concentration SL-MPA nanocomposite loaded with doxorubicin drug on MCF-7 cell line and we have observed that our composite is quiet efficient (viability of only 5%) as compared to composite without any drug molecule.

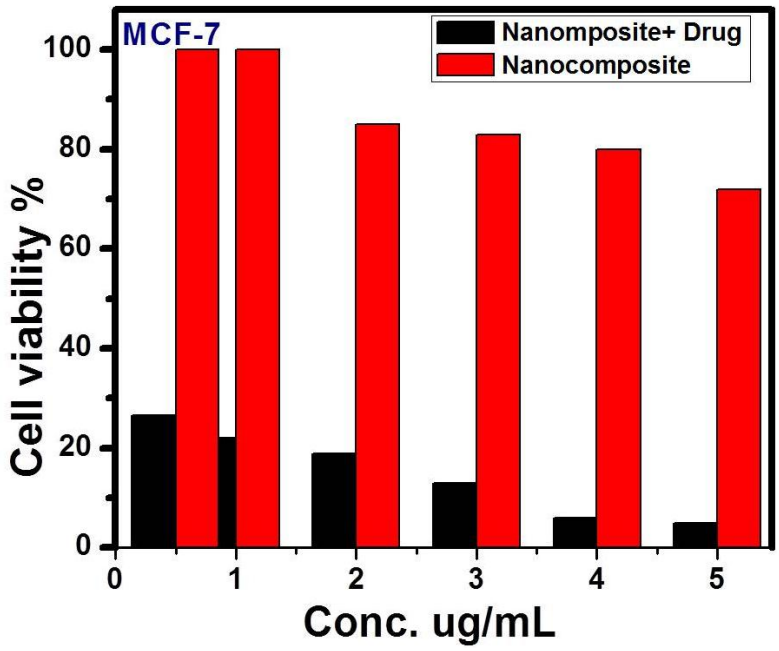

Figure. 6.7 . MTT assay of SL-MPA nanocomposite and Dox loaded SL-MPA nanocomposites on MCF-7 cell lines

We also did theoretical modeling to validate for the porous SL-MPA nanocomposite for the ratio of SL;MPA- 1:18 and 1:3, and we found that in case of 1:3, we found more porous structures as shown in Figure 6.10.and 6.11.

We also did antibacterial assay for the SL-MPA nanocomposite for both gram positive and gram negative bacteria. We used SL:MPA (1:3) nanocomposite and exposed *Staphylococcus aureus*, *Escherichia coli and Pseudomonas aeruginosa* and *Bacillus subtilis* for 0 hr, 2 hr and 4hr. After 0, 2 and 4 hrs each of the bacterial inoculum is spread on plate and kept on incubation for 12 hrs. We found almost 100% killing in all the cases, only *B. subtilis* showed growth in the presence of nanocomposite.

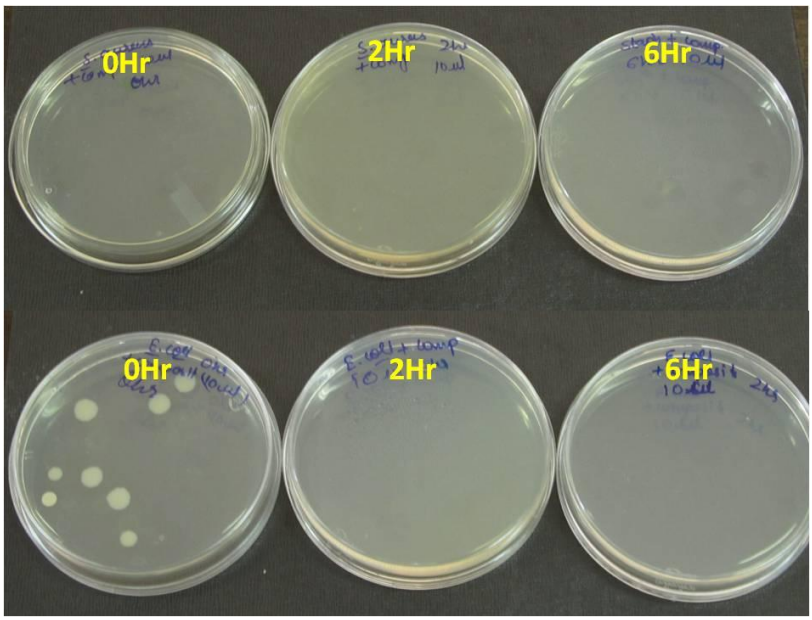

Figure.6.8. Antibacterial assay of SL:MPA, Row 1; **S. aureus** at 0hr, 2 hr and 4 hr, Row 2;E. coli at 0hr, 2 hr and 4 hr.

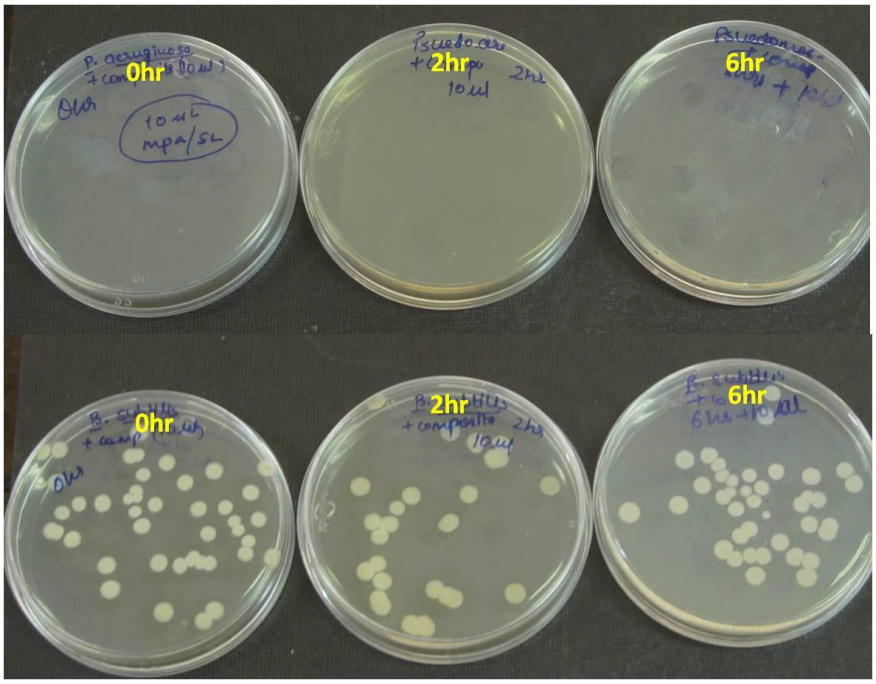

Figure.6.9. *Antibacterial assay of SL:MPA, Row 1;* ***P. aeruginosa*** *at 0hr, 2 hr and 4 hr, Row 2;* ***B. subtilis*** *at 0hr, 2 hr and 4 hr.*

6.8. Theoretical calculation

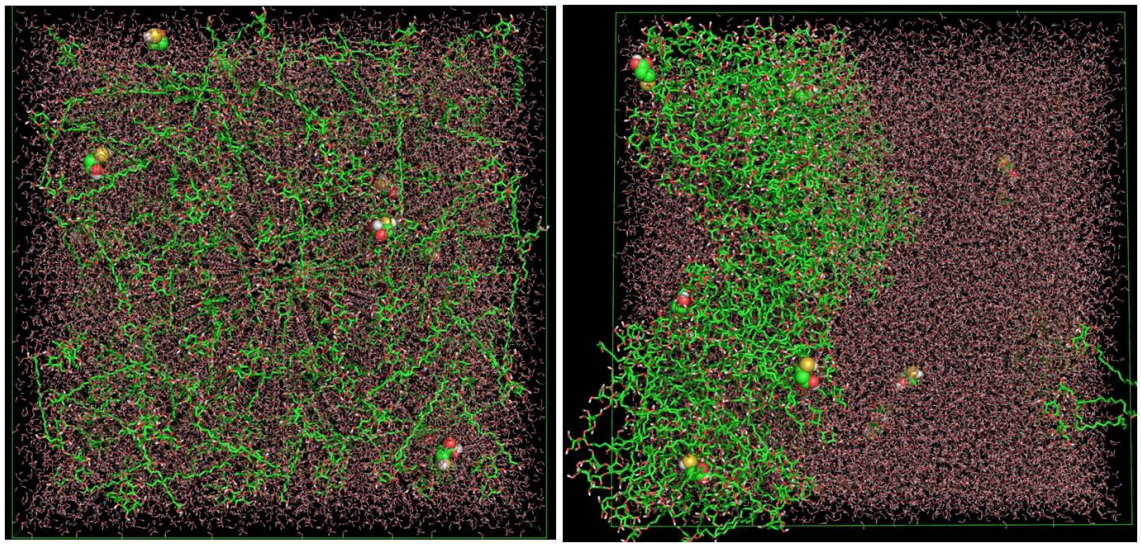

Fig 6.10. Molecular modeling of SL-MPA nanocomposite at 1:18 MPA: SL molecular ratio.

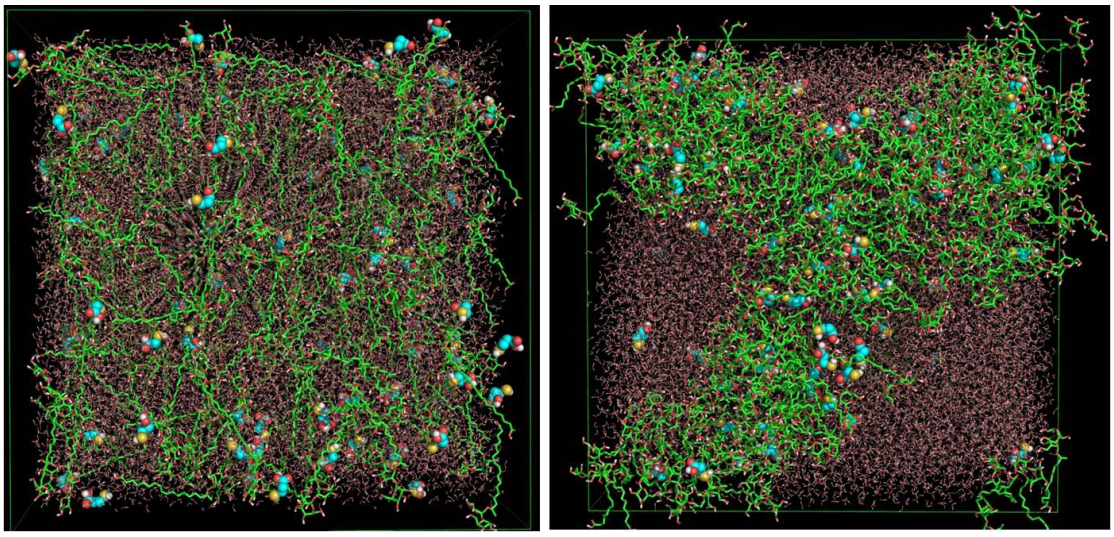

Fig 6.11. Molecular modeling of SL-MPA nanocomposite at 1:3 MPA: SL molecular ratio.

Summary

We have made porous nanocomposite using Sophorolipid and MPA molecule which can accommodate large amount of drugs and thus have great potential as dug delivery agents. This has a huge advantage over metal based nanoparticles as they are completely biodegradable as well as biocompatible. We have explored its loading and release efficiency using anticancer drug, Doxorubicin at different pH and time interval. We have also tested the nanocomposite loaded with anticancer drug on MCF-7 (breast cancer cell line), which showed significant killing of the cancer cell lines.

References;

1. M. Grzelczak, L M.Liz-Marza'n, *ACS nano*, 2010, VOL.4,NO.7, 3591-3605, http://en.wikipedia.org/wiki/liposome

2. Vill V, Hashim R. Carbohydrate liquid Crystals: structure-property relationship of thermotropic and lyotropic glycolipids. *Current Opinion in Colloid and Interface Science*, 2002; 7: 395–409.

3. Milkereit G, Garamus VM, Yamashita J, Hato M, Morr M, Vill V. Comparison of the supramolecular structures of two glycolipids with chiral and nonchiral methyl branched alkyl chains from natural source. *J Phys Chem B,* 2005; 109: 1599–608.

4. D. Kitamoto, T. Morita, T. Fukuoka, M. Monishi, T. Imura, *Current Opinion in Colloid and Interface Science*, 2009; 14: 315.

5. S. Zhou, C.Xu, J. Wang, W. Gao, R Akhverdiyeva, V. Shah, R. Gross, *Langmuir* 2004, 20, 7926.

6. E. Zini, M Gazzano, M. Scandola, *Macromolecules* 2008, 41, 7463

7. J. Penfold, M. Chen, R.K. Thomas, C. Dong, T J. P. Smyth, A. Perfumo, R. Marchant, I.M Banat, P Stevenson, A. Parry, I. Tucker, I. Grillo, *Langmuir* 2011, 27, 8867-8877.

8. R. Weisledder, *Science* 2006, 312,1168.

Summary and future outlook

The brief summary of the present work

Simple and improved strategy is used to synthesize CdTe-MPA quantum dots. QDs is further conjugated with a bio-molecule, Sophorolipid in order to achieve a nanocomposite which has both the properties of CdTe and Sophorolipid molecule. All the physical, chemical, biological characterizations are performed to validate the functionality of the nanocomposite constructed. The nanocomposite remains dispersed in water for long duration increases its suitability with most of the biological systems. It shows both diagnostic (fluorescence) and therapeutics (Sophorolipid) properties and henceforth can be used for theranostic applications in biomedical sciences.

CdTe-MPA is further conjugated with various oxidase molecule in order to make CdTe based sensors. CdTe is chemically conjugated with glucose oxidase, Cholesterol oxidase and Bilirubin oxidase independently to make glucose sensor, cholesterol sensor and bilirubin sensor respectively.

CdTe-MPA is further used to make a simple water soluble photoluminescence On-Off-On Probe for Speedy and selective detection of fluoride ions even HF fumes which is an immediate requirement for the regions where fluorosis is prevalent**.**

MPA (mercaptopropionic acid) assisted Supramolecular architecture is constructed in order to achieve a porous nanocomposite which can hold or accommodate hydrophobic drugs for the cancer treatment. This nanocomposite tends to be promising as they are absolutely biocompatible along with additional anticancer properties.

Future outlook

CdTe QDs and their nanocomposites are promising materials and needs more efforts to make it compatible in clinical diagnostics, therapeutics, drug delivery etc. Multifunctional QD-based nanocomposites in drug delivery scenario represent an extremely useful means for drug loading, targeting and controlled release of drug. Individual QDs, having high surface to volume ratio and surface functionalization chemistry, provide a suitable platform for the engineering of smaller targeted and traceable drug delivery vehicles and requires sustained efforts. SL-MPA

nanocomposite can be further used for such molecule which are hydrophobic in nature and require bioavailability and gradual release. In future these nanocomposites can be used for treating other disease like Parkinson's, Alzheimer etc.

List of Publications

1. ***Chemically conjugated sophorolipids on CdTe QDs: a biocompatible photoluminescence nanocomposite for theranostic applications***, **Pooja Singh,** Kasturi Joshi, Debanjan Guin and Asmita A. Prabhune, ***RSC Adv., 2013, 3, 22319.***

2. Glucose oxidase conjugated H2O2 sensitive CdTe QDs: an effective fluorescence tool for glucose sensing, **Pooja Singh,** Asmita A. Prabhune, Satishchandra B. Ogale and Debanjan Guin, **J. Mater. Chem. B, 2013, 1, 6538.**

3. ***Water Soluble Photoluminescence On-Off-On Probe for Speedy and Selective Detection of Fluoride Ions*** **Pooja Singh**, Asmita A Prabhune and Debanjan Guin, ***ACS Sustainable Chem. Eng., 2017, 5 (1), pp 982–987***

4. ***Mercapto-propionic acid Assisted Supramolecular Assembly of Sophorolipids: A Potential Drug Delivery Vehicle,*** **Pooja Singh,** Asmita A Prabhune, Satishchandra B Ogale and Debanjan Guin (manuscript under preparation)

5. ***Nanoparticle-loaded multifunctional natural seed gel bits for efficient water purification*** *Mandakini Biswal, Kirti Bhardwaj, Pradeep K Singh,* ***Pooja Singh****, Prasad Yadav, Asmita Prabhune, Chandrashekhar Rode and Satishchandra Ogale ,* ***RSC Advances, 2013, 3, 2288***

6. ***Blue Luminescent Graphene Quantum Dots by Photochemical Stitching of Small Aromatic Molecules: Fluorescent Nanoprobes in Cellular Imaging***, Rohan Gokhale * and **Pooja Singh,** ***Part. Part. Syst. Charact. 2013***

Patent

1. Novel assay for detection of floride ions; A Simple Water Soluble Photoluminescence On-Off-On Probe for Speedy and selective detection of floride ions even HF fumes.